2018

Wireless In-Vivo Dosimetry of High Dose Rate Brachytherapy for Prostate Cancer using MOSkin Detectors

Iliana Peters
University of Wollongong

UNIVERSITY
OF WOLLONGONG
AUSTRALIA

Wireless *In-Vivo* Dosimetry of High Dose Rate Brachytherapy for Prostate Cancer using MO*Skin* Detectors

Iliana Peters

This thesis is presented as part of the requirements for the conferral of the degree:

Masters of Philosophy (Medical Radiation Physics)

Supervisors:
Professor D. Cutajar & Dr. A. Rozenfeld

The University of Wollongong
School of Physics,
Centre of Medical and Radiation Physics,
Faculty of Engineering and Information Science

October, 2018

This research has been conducted with the support of an Australian Government Research Training Program Scholarship.

Declaration

I, *Iliana Peters*, declare that this thesis is submitted in partial fulfilment of the requirements for the conferral of the degree *Masters of Philosophy (Medical Radiation Physics)*, from the University of Wollongong, is wholly my own work unless otherwise referenced or acknowledged. This document has not been submitted for qualifications at any other academic institution.

Iliana Peters

October 19, 2018

Abstract

High Dose Rate brachytherapy is an effective treatment modality for prostate cancer due to the radio-sensitivity of the tumour and short treatment time. This procedure has strong radiation concentration and a steep dose gradient but no acceptable dose verification method to ensure prescribed dose is delivered to minimise damage to tumour-adjacent organs. With radiation emitted directly into the tumour, the most effective monitoring method is *in-vivo* dosimetry. A new MO*Skin*$^{\text{TM}}$ readout system, OneTouch, has been developed to provide real time dosimetric readouts and temperature variation compensation during *in-vivo* dosimetry. Through the additional of detectors to the rectal ultrasound probes used during brachytherapy, dosimetric and anatomical data can be transmitted. Two generations of MO*Skin*$^{\text{TM}}$ detectors were analysed through angular and sensitivity testing; the circular gate version proved superior normalised angular dose response of $\pm 1.5\%$ and sensitivity drift of -8.41$\pm$0.67%, compared to -28.24$\pm$1.19% with the parallel gate design. MO*Skin*$^{\text{TM}}$ detectors are an accurate *in-vivo* dosimeter, with normalised agreement to the treatment plan of 1.06$\pm$0.1 compared to radiochromic film normalised agreement of 1.10$\pm$0.01. The OneTouch and MO*Skin*$^{\text{TM}}$ system proved clinically viable and will further improve the safety of prostate cancer treatment through HDR brachytherapy.

Acknowledgments

I would like to thank the many people who have helped me with support and help over the period of writing this thesis. I want thank my family for their encouragement and constant motivation, their positive attitude and help have been one of the most important things to me during my university career. I want to thank my supervisor, Dr. Dean Cutajar, for his support and guidance during this thesis. Thank you for organising the many clinical experiments, helping collect data and proof reading my thesis. I would like to thank Professor Anatoly Rozenfeld for his continual support of all research at the Centre for Medical Radiation Physics and this project. To the staff at St. George Cancer Centre, especially Andrew Howie, Ryan Brown and Joel Poder, thank you for allowing me to use the brachytherapy facilities and assistance during experimental collaborations.

Contents

List of Figures

List of Tables

List of Equations

Chapter 1

Introduction

Tumours developing in the prostate, either prostatic carcinoma or primary prostatic sarcoma, are of great medical concern due to the high percentage of men developing the cancer, especially over the age of 50 and the location of the prostate itself (1). The estimated number of diagnosed cases of prostate cancer in 2017 in Australia alone is 16,665, which is more than a fifth of all new diagnosed cases of cancer in males. However, the percentage of surviving 5 years after diagnosis has increased from 60% in 1980's to an estimated 95% in 2009 (2). There is currently no ideal treatment for prostate cancer and research into this treatment is very important.

There are currently multiple methods in practice for treating prostate cancer, such as hormonal therapy, radical prostatectomy, radiotherapy or in early stages surveillance (3). The prostate is located between the urethra and rectum, both important and sensitive organs that increase the difficulty due to their proximity to the prostate (4). There isn't a universally accepted method for treating prostate cancer but due to the unique characteristics of the prostate, radiation therapy is very effective at destroying prostate cancer. There have been many studies into the special characteristics that make prostate cancer suitable for radiation treatment, such as the slow proliferation of the cancer and the low alpha-beta ratio, which

relates to the radiation sensitivity of the tissue (5). One effective form of radiation treatment for prostate cancer is high dose rate (HDR) brachytherapy.

Brachytherapy is a form of radiotherapy that uses irradiated seeds to transmit a treatment dose directly into the cancer through implantation of needles. HDR irradiations uses temporary source of Iridium-192, which has a high dose rate output with a limited range, to deliver a prescription dose over a matter of minutes (1). This method of treatment for prostate cancer is very successful, however due to the high dose rate radiation toxicity to organs near the prostate is a high concern (6). There is currently no method to verify the treatment dose however there have been many studies into possible *in-vivo* dosimetry methods

In-vivo dosimetry is the recording of irradiation directly during treatment and is the ideal form of detection for brachytherapy treatments due to the determination of dose directly in or next to the treatment volume (7). The dosimeter investigated in this thesis is a type of MOSFET detector developed by the University of Wollongong, called the MO*Skin*$^{\text{TM}}$ detector. With a sensitive volume of 0.55μm and real-time readout capabilities, the MO*Skin*$^{\text{TM}}$ detectors are the most ideal to record dosimetric information in the steep dose gradient area throughout HDR brachytherapy procedures (8).

This thesis utilises a new readout system called the OneTouch System (development title) to wirelessly transmit real-time dose data to the control room during treatment. This system also uses a simplified dose calibration method and a method to determine a temperature compensation factor that minimises dose variation due to temperature change. Tests were completed to investigate the sensitivity, temperature compensation and anti-annealing capabilities, and to determine if the dose response was within an acceptable range. This system increases the feasibility of a dose validation procedures of HDR brachytherapy, which will increase the security of the treatments and highlight any errors that would go unnoticed during previous

methods.

Simulation phantom experiments were also completed in conjunction with a real-time ultrasound treatment planning system through creating a dual purpose probe that both transmitted ultrasound images for planning and dose recordings through the OneTouch Readout system. The real-time *In-Vivo* dosimetric response of the MO*Skin*^{TM} detector and OneTouch system were compared to other readout systems and clinical detectors to further establish the accuracy and validity of the verification system.

1.0.1 Aims of Thesis

The objective of this thesis was to investigate the new readout system, OneTouch, and determine its suitability for clinical verification during HDR prostate brachytherapy. The OneTouch System and the MO*Skin*^{TM} detectors used were developed by the Centre for Medical Radiation Physics at University of Wollongong. The experiments were completed at St. George Cancer Care Centre, Kogarah, utilising their HDR Ir^{192} brachytherapy source.

Fundamental aims of this thesis are as follows:

1. Characterise a newly developed circular gate MO*Skin*^{TM} in comparison with the traditional parallel gate electrons through angular and sensitivity testing

2. Complete characterisation experiments on the OneTouch system into it's clinical reproducibility and temperature compensation ability with MO*Skin*^{TM}.

3. Perform a clinical simulation treatment using the MO*Skin*^{TM} and OneTouch System with the clinical equipment used during HDR prostate brachytherapy treatments. Investigate the OneTouch Readout response compared to previous readout systems and the MO*Skin*^{TM} dosimetric properties compared to other clinical dosimeters.

Chapter 2

Literature Review

2.1 Prostate Cancer

One of the most common causes of male mortality in many parts of the world is prostate cancer with the average annual diagnosis in the United States being 190,000 men (9). The prostate gland is usually 4cm in diameter and is part of three accessory glands of the male reproductive system. The main function of the prostate is to produce seminal fluid to increase the fluid volume of sperm and aid in fertilisation (10). The prostate itself is located inferiorly to the bladder, with the urethra located in the centre ranging from the apex to the base of the prostate, and the rectum located directly posterior to the prostate. On average, 70% of cancers are located in the peripheral zone, or near the base and posterior wall of the prostate making the exact location of the urethra and rectum important in any treatment method (11). The main type of tumours affecting the prostate are either prostatic carcinoma or primary prostatic sarcoma while prostatic hyperplasia is the most common type of lesion affecting men over the age of 50. Both tumours and lesions are proliferative and usually require some kind of medical intervention, however malignant tumours are the most dangerous and will be the main focus of this thesis (10).

The symptoms of prostate cancer vary greatly depending on the severity of the tumour and are usually unnoticeable until later stages. Some symptoms include hematospermia, presence of blood in semen, to bone pain or rectal obstruction for higher severity cancers (5). The diagnosis and staging of prostate cancer involves many different procedures like a physical examination, measurements of prostate specific antigen (PSA), and Gleason score determined through an ultrasound-guided biopsy (9). Prostate cancer has been able to be detected earlier through abnormal PSA count within the blood stream since the 1990's when PSA was discovered as a possible indicator for prostate cancer. PSA is glycoprotein present within the blood that aids in the liquidification of semen and when a malignant tumour is present the thickness of the membrane walls decrease, which increasing the PSA count within the blood stream. Depending on the PSA concentration the patient is separated into favourable, intermediate or poor risk (5). For a normal healthy male, the PSA concentration is 2ng/mL or less and abnormal is usually seen to be above 4ng/mL. These specific values vary for different countries and clinics (10). However, PSA testing is not a true positive method of determining the presence of prostate cancer, with only 1 in 3 men having cancer after elevated PSA levels were detected (5). Other test are also performed to determine the existence of prostate cancer, the exact location and the severity of the disease.

Gleason score is based on the glandular structure of the tumour, rating the disease from 1 to 5 with increasing aggressiveness; most cancers are not homogenous in structure so there are usually varying grades within a single tumour. Each patient will receive a number score based on the two most common glandular structures grades present in the tumour and are added together ranging from a value of 5 to 10 (11). With a higher Gleason score the prognosis, for the patient worsens and the most appropriate type of treatment is usually dependent on the Gleason score (5). Prostate cancer can also be classified through tumour stage, which determines

the severity of the disease based on the spread to nodes and nearby organs. Stage 1 prostate cancer can usually be detected through a PSA test, while Stage 2-3 the cancer is present in a large part of the prostate and the seminal vesicles. In Stage 4 the cancer is present in other organs such as the bladder or rectum, making treatment very difficult and the chance of survival very poor (11).

Prostate cancer is unique from other types of cancers because it is very slow growing and is susceptible to high radiation dose fractionation due to it's slow proliferative characteristics and low tumour α/β ratio of 1.5-2 Gy (5). The linear quadratic formula is used to determine the dose needed for specific normal cell and tumour cell survival percentages.

$$S = exp(-(\alpha D + \beta D^2)) = exp(-nd(\alpha + \beta d)) \tag{2.1}$$

Equation 2.1 illustrates the typical linear quadratic equation, with D being the prescription dose, n and d relating to the number of fractions and fraction dose respectively, and S being the survival rate of the tissue. The value for α describes the cell death from a single radiation event and the β value describes cell death from multiple radiation events (12). The values for α and β change depending on the tissue and tumour type and are very important factors when deciding the ideal type of treatment.

The accepted value α/β ratio value for tumours is 10-12 Gy while late responding normal tissue has a ratio value of 2-4Gy, meaning most tumours are not very sensitive to radiation but the late responding normal tissue is and high doses can be potentially dangerous (13). The total prescription dose needs to be separated into smaller doses through fractionation, which reduce the effects of radiation on normal healthy tissue but also increases the treatment time to weeks or months. However due to the prostates low tumour α/β ratio it is susceptible to higher doses of radia-

tion similar to normal tissue and increases the tumour control with a smaller number of fractions (14). With an increase dose to the prostate, the tissue and organs surrounding the tumour have a greater chance of radiation damage. The effectiveness of radiation on the rectum and rectal wall can be determined from the unique α/β ratio and the linear quadratic equation can describe the amount of damage from a treatment regime.

Similar to the α/β for the prostate, the α/β for the rectum isn't an exact value and research has been completed using rectal toxicity data from clinical studies. D.J. Brenner proposed a value of 5.4±1.3 Gy for the prostate determined from multiple studies in 2004 (15). He used four different studies treating prostate cancer with a combination of conventional and hypo-fractional external beam treatment and fit the data for late rectal toxicity $\geq$ Grade 2, associated with rectal bleeding, to the linear quadratic formalisation. He hypothesised that the reaction of rectal tissue should be between late effect tissue, with α/β 1-3Gy, and late effect tissue, with α/β 8-10Gy. This value however was questioned due to the different treatment methods of the 4 studies used and the α/β is highly relative (16). In another study completed by Marzi et. al in 2009 the α/β ratio was determined from dose volume data from hypofractionation EBRT that was fitted to the Lyman-Kitcher-Burman (LKB) Normal Tissue Complication Probability (NTCP) formalisation (17). The α/β value for toxicity $\geq$ Grade 2 was determined to be 2.3 Gy specifically for the rectal wall for intermediate to high stage prostate cancer. Finally, in a study completed by Tucker et al. in 2011, which was more in depth research into Brenner's work in 2005, used a large study into dose escalation and the LKB NTCP formalisation to model rectal toxicity from individual dose volume histograms (18). The value for the α/β ratio was found to be 4.8 Gy for this study and commented that the ratio value must be an intermediate reaction value based on several other studies; the α/β ratio varied from 2.2-8Gy. Tucker's value is very similar to previous studies by Brenner and 4.8

Gy will be used throughout this thesis to determine the reaction of the rectum to a specific brachytherapy regime for prostate cancer treatment.

Prostate cancer also has a very low potential doubling time of approximately 60 days; other types of cancer can double in size after a couple of days since irradiation (12). Due to this feature, the treatment dose for prostate cancer with radiation therapy can be highly effective and can be delivered with a wide variety of options. The treatment options are based on the severity of the cancer as well as the cultural and social attitudes of the patient and the main treatment options are further.

2.2 Prostate Cancer Treatment Options

Depending on the severity and stage of the cancer as well as the available techniques, there are a large variety of treatment options available to treat prostate cancer. There is no ideal form of treatment accepted internationally and there are no accepted studies that compare different treatment modalities.

Low risk prostate cancer treatments range from surveillance of the tumour or lesion to hormonal therapy or high intensity ultrasound (9). Active surveillance is mostly used for patients with high severity cancer with a low chance of survival and is always an option for patients not wanting to undergo any form of treatment. The patient's PSA levels are monitored and prostate biopsies are completed to monitor progression of the cancer (19). For higher risk prostate cancer, radiotherapy or radical prostatectomy are usual forms of treatment and can be combined to give the best change of removing or killing of all the cancer cells.

One of the oldest techniques for treating prostate cancer is through surgery, removal of the cancerous part of the prostate was first performed in 1904 (20). The procedure has progressed from there but hasn't changed much in method since the 1980's and is one of the most common treatments for prostate cancer today (20).

However, like all treatments, there are restrictions based on severity and age that limits the use of radical prostatectomy. The most at risk age bracket for prostate cancer is usually over 65 years old and an invasive surgery can be impossible due to the age of the patient (5). For the highest chance of cancer free survival, patients undergoing radical prostatectomy usually have low grade, early stage cancer that have not spread to other parts of the body. To determine if the cancer has been removed entirely, the PSA is measured after a set period of time to determine if it is still above normal concentrations. Even though radical prostatectomy is one of the most common clinical treatments, there has not been an acceptable clinical study that determines surgery is the ideal option for eliminating prostate cancer (20).

Another common clinical treatment is the use of radiotherapy through external beam radiation or EBRT. There are multiple types of treatment options with EBRT that vary in fractionation amounts and dose, movement of the treatment angle, intensity of the beam and imaging modalities used during treatment. The three most common types of treatment are three dimensional conventional fractionations, intensity modulated radiotherapy and stereotactic radiotherapy (20). External beam is delivered using a linear accelerator, which produces a beam of high energy electrons or different energy range x-rays. The beam is optimised to give an appropriate dose and shape for the patient's tumour while being a non invasive procedure (21). There are no errors with EBRT regarding the implantation of sources, catheters or any other surgical requirements and linear accelerators are very common in hospitals, this type of treatment is widely available (6). However, due to the radiation beam passing through normal tissue to reach the target, the prescription dose given in a single treatment is greatly limited and fractionation is used for all external beam procedures. EBRT is usually given over 8-9 weeks with usually one fraction per day but the number of fractions per day could increase depending on the type of tumour, the patient and the facilities available at the hospital. The dose fraction

also varies between 1.8-2 Gy/fraction, however because prostate cancer is more sensitive to fractionation dose, the given range could be from 2.1-10 Gy/fraction (9). Increasing the dose per fraction is called hypo-fractionated EBRT and decreases the overall treatment time with the same total prescription dose as traditional EBRT treatments.

Brachytherapy is another modality of radiotherapy to treat prostate cancer through the implementation of radioactivity directly into the target area. Brachytherapy has greatly increased as a form of treatment in recent years; in 1995 the percentage of American men treated with brachytherapy was 2.2% and in 2004 this percentage had increased to 30% (22). This treatment is separated into two different methods, low dose rate (LDR) brachytherapy and high dose rate (HDR) brachytherapy. The different rates depend on the activity of the source and length of time within the patient, for example LDR implants lower dose sources permanently into the target area giving doses ranging from 100-160 Gy over several months (9). The type of radioactive sources used in LDR are Iodine-125, Palladium-103 or Cesium-131 delivering varying doses to give the equivalent dose to external beam radiation therapy. Iodine and palladium are common radioisotopes used in prostate brachytherapy while cesium is commonly used in gynecological brachytherapy (1). The usual dose given with I-125 radioactive sources are 144-145 Gy, 100 Gy for Pd-103 and 85 Gy for Cs-131 and with varying half-lives the total treatment times are very different depending on the isotope (20). The usual dose rate for LDR isotopes are between 0.4-2Gy/hr and can be administrated manually (23). Some of the disadvantages of this type of treatment are the difficulties with positioning the sources within the patient due to swelling and oedema, the movement of the radioactive sources within the patient and the radioactivity of the patient leading to increased risk to the public from this radiation (6). Radiation safety procedures need to be performed for each patient depending on the type of permanent radioactive source

implant and the dose rate of that specific isotope (20). With the changes in anatomy over the months of LDR treatment, it is very hard to predict were the sources are within the tumour volume and therefore the amount of dose given to the tumour volume as well as surrounding organs. Also with this form of treatment there is no possible verification method that can give a real time measurement of dose (9). The sources used in LDR are permanently implanted into the patient and therefore cannot be used in future treatments, increasing the cost of the entire treatment. Previous studies have shown the advantages of treating prostate cancer with higher amounts of radiation over a shorter amount of time, leading to high tumour control but more severe late effects to normal tissue (20). However due to the much lower radiation dose rate given in this form of brachytherapy the potential late effects are much less damaging than higher radiation dose given in HDR brachytherapy. LDR, similar to HDR, can be performed as a mono therapy or in combination with EBRT depending on the severity of the disease.

High Dose Rate (HDR) brachytherapy uses the same method of implanting radioactive sources as LDR brachytherapy but the type of source varies greatly. The isotope used in HDR is Iridium-192 that can give a dose rate of 20 cGy per minute with a treatment time of less than 10 minutes (9). This radioisotope has an average photon energy of 400keV, meaning the range of the emitted radiation is very short leading to a very steep dose gradient. Due to the steep dose gradient, small positioning errors in HDR brachytherapy can be very damaging and can cause severe damage to the rectum and urethra (19). The high dose given with this type of brachytherapy is ideal for prostate cancer, due to the very low alpha/beta ratio discussed in section 2.1. However, with higher dose rates the toxicity to organs at risk is also seen to increase and needs to be monitored after treatments for any late effects (6). This also highlights the importance of a procedure that monitors and reports the dose to the rectum, urethra and bladder to make sure it is below the

acceptable values. The advantages of HDR over LDR brachytherapy is the much higher dose rate given, approximately 1000 times higher, and the much shorter treatment time of both LDR brachytherapy and EBRT (20). There are no positioning errors due to source movement with high dose rate treatments and the patient is only radioactive during the very short treatment times. HDR brachytherapy can be given as a monotherapuetic treatment of up to three fractions given over two days with 6-8 Gy per fraction. It is completed under image guidance to ensure accurate placement of the catheters within the patient and there is no radioactive material left inside the patient during planning and in between fractions (9). There is a very specific treatment method for HDR brachytherapy that minimises any errors and takes advantage of the unique characteristics of prostate cancer to delivery the most effective treatment.

2.2.1 Prostate HDR Brachytherapy Treatment Technique

The current procedure for HDR brachytherapy has been optimised over the years to be the most efficient procedure possible however there is very little verification and data collection from the treatments compared to other forms of radiotherapy. The radiotherapy treatment time is between 6 to 10 minutes, depending on the prescription dose and activity of the source at the time of treatment. Hollow catheters are inserted into the target volume and surrounding areas and is completed under image guidance usually using transrectal ultrasound (TRUS) and gold fiducial markers indicating the apex and base of the prostate. The catheters used in HDR brachytherapy are usually between 12-22 and a treatment plan is created from a CT image taken after placement of catheters (20). For HDR brachytherapy, remote afterloaders are used to deliver the treatment, which are portable, lead-lined containers that are used for safe storage and administration of radiation dose without any manual operation. This allows for the safe and reusable administration of dose

through a treatment plan that position multiple sources along a catheter for set dwell times (23). The treatment plan then can be repeated for future treatments, eliminating any human reproducibility errors in position of the radioactive sources; the positioning of the catheters is still completed manually and might be a source of error. Depending on the activity and the type of source within the afterloader, HDR brachytherapy can be performed usually with Ir-192. The remote afterloader also allows for many patients to be treated using the same source, reducing the cost of HDR compared to LDR brachytherapy (4).

Brachytherapy is usually completed within a shielded room specifically designed for protecting against the high activity sources in HDR brachytherapy. CT and ultrasound images are frequently in brachytherapy planning as well as treatment. Ultrasound probes are used to deliver an image of the prostate through the rectum and contrast may be used to delivery a clearer picture (20). An initial TRUS image is taken and contours of the target regions are calculated along with desired positioning of the needles within the volume. A second image is taken after needle insertion, which is contoured again and used in treatment planning (24). Depending on the procedure of each hospital, the acceptable percentage dose to the critical tumour volume (CTV) and to the organs at risk (OAR) are determined through imaging and a treatment plan is created (19). For example, according to the radiation therapy oncology group number 0321 (RTOG 0321), the acceptable percentage of prescription dose to the urethra is 125% and to the rectum is 75% to 1mL (20). The toxicity to the urethra, rectum and bladder are the main concern with HDR brachytherapy due to the higher radiation dose given and the steep dose gradient of the sources used. Multiple CT images or MRI images are also used for preliminary imaging and treatment planning; multiple studies have shown for fractionated HDR brachytherapy treatments, additional treatment plans created directly before each fraction treatment gives a more accurate treatment with less toxicity to any organs

at risk (25). Dose escalation and dose optimisation can also be completed within HDR brachytherapy, especially with the use of remote afterloader. The usual treatment regime for fractionated HDR brachytherapy is completed over 2-4 days with catheters remaining within the patient for the entire treatment. Similar to EBRT the minimum time between fractions is 6 hours, which is the half life of repair of cancer cells and this time allows for the treatment to be the most effective (12).

After treatment is completed, either a monotherapy or as a combination with another form of radiotherapy, check up time is usually 6 weeks after completion and then every couple of months (19). Any errors in dose from the treatment can only be accessed after treatment and there is no validation method currently for real time dosimetry for brachytherapy. PSA and OAR toxicity is evaluated at the following check ups but these procedures are different for each clinic. Data bases and studies are being completed that look at the treatment plan for each individual and the survival rates and OAR toxicity as a comparison between different treatments. An example of a collective data base is the Surveillance, Epidemiology and End Results (SEER) data that contains information of prostate cancer patients with a minimum 6 years follow-up after HDR brachytherapy (26). However, each hospital might have an individual data base of treatments plans and follow up information that may be used as quality assurance for future treatments.

2.3 History of Brachytherapy Treatment

The concept of brachytherapy started in the early 1900's but due to the presents of live radiation sources and the lack of appropriate safety procedures and accurate implantation technique it wasn't seen as a favourable form of treatment until the 1980's (9). Radium was the first isotope used for medical purposes and was seen as an acceptable alternative for treating cancer compared to surgery (27). Radium

therapy was performed from the early 1910's and in the 1920's permanent radon source brachytherapy started to be used as a method of treating prostate cancer. At this time, the advantages of radon therapy over other methods of treatment were the lack of risks or deformations caused by surgery and the rapid cell death of cancerous tumours. By the 1950's, this treatment option was seen as less favourable due to the safety risks to staff and public from the radiation used as well as the late effects occurring after treatment (28). Other treatment options that became more popular were surgery and external beam therapy, however the cancer control decreases with these methods (27). Most of the implantations of radon sources during the early stages of brachytherapy were performed by hand and needles were positioned using a template but without any other form of image guidance (28). Manual insertion of radioactive sources had very limited tumour control and many dosimetric issues leading to late effects (9). Through the development of more sophisticated and safety methods of implantation, such as manual and remote afterloading, and the combination of imaging modalities during treatment planning and implantation, such as ultrasound, CT and MRI, brachytherapy was seen again as a very important tool for treating cancer.

The first improvement of brachytherapy technique started in the 1950's when doctors and staff would not perform radon therapy due to the severe consequences of radiation exposure. Afterloading removes live sources from being used in the surgery and the sources were implanted through handheld, manual applicators that were shielded to protect the clinical staff. The concept of afterloading radioactive sources using an applicator started in the 1910's but wasn't used in a medical capacity until the 1950's. Manual afterloading techniques initially consisted of threading through nylon strands or ribbon implanted with radioisotopes, mainly Au-198 and Ir-192, through implanted needles. Radon was eventually phased out medically because of its high emission energy that required more shielding than other effective isotopes.

The next development happened during the 1960's when permanent sources were inserted in the patient using nylon tubes containing one radioactive source placed inside the implanted needles. Later, an applicator was used to replace the manual insertion of the nylon tubes due to the frequent occurrence of sources dropping out before implantation. The sources used in this permanent afterloading technique, now called LDR brachytherapy, were Au-198, Co-60, Ir-192 and I-125, and used to treat head and neck tumours, prostate, breast, skin and penis cancer (27).

The remote afterloading system was first introduced in 1962 using a moveable trolley that stored the radioactive sources with a relaxable cable to transport the sources to the needles implanted in the patient, controlled by the set treatment plan. Using this system cut down the treatment time and made brachytherapy more affordable due to the multiple treatments used from one remote afterloader system. It was also a safer way of performing brachytherapy that allowed for higher dose treatments, such as HDR brachytherapy to be performed. HDR and LDR could be performed using a remote afterloader depending on the sources stored within; HDR brachytherapy was performed using Co-60 and Ir-192 sources while LDR used a combination of sources. In the 1980's, multiple channel devices were created, allowing sources to be inserted into more than one cable (27). During the 1980's, brachytherapy started to be performed more regularly with the addition of new imaging and planning systems incorporated into the treatment delivery.

Image guidance was a very important improvement for brachytherapy, especially in determining the prescription dose and an optimal treatment plan. During the 1970-80's, closed retropublic implant procedures for LDR brachytherapy were being performed, which were less invasive then previous methods. Around this time, preoperative CTs were being performed to determine the dose distribution with I-125 sources, giving an overall dose of 140-160 Gy (28). Contours and isodose curves could be calculated from the CT images to give each patient a treatment plan with

a target volume; early treatment plans didn't take into account damages to OARs near the tumour (9). The needles and sources were still implanted by hand but with fluoroscopic guidance, later with a manual afterloader applicator to reduce radiation exposure to staff. Transrectal transducers were created in 1974 and were attached to a stepper unit to accurately determine volumes within the patient (28). Using ultrasound, the prostate was able to be visualised and volumetric dose calculations could be determined using multiple ultrasound images (9). Ultrasound images were used to guide needle placement along with a template attached to the perineum of the patient. Images taken after implantation were used to calculate dosimetry information but this very limited (28). In the 1990's, transrectal ultrasound (TRUS) started to be used as common practice in brachytherapy planning and implantation, for both LDR and HDR brachytherapy, as well as being capable of real time imaging (28). Also around this time, planning and placement of needles were in the same procedure, eliminating any errors due to movement and different placement during the two procedures. With the improvement of computer-based planning dosimetric system, treatment plans could be optimised the distribution to the target and OAR could be determined in three dimensions (9). 3D imaging has allowed technicians to accurately determine the geometry of the entire treatment area and assess the changes to the volume throughout the treatment, adapting the dose to the changes in geometry (29). Even through the improvement of imaging and placement of radiation sources within the patient, this gives no information about the exact dose given during the treatment and currently there are no method of dose verification for brachytherapy.

2.4 Dosimetry for Prostate HDR Brachytherapy

High dose radiation brachytherapy uses a large amount of radiation, meaning the exact position of the catheter as well as anatomical organs is very important to determine the absorbed dose within the volume. Brachytherapy currently does not have a method of measuring the radiation dose during treatment as part of a routine and quality assurance of the treatment. The American Association of Physicist in Medicine (AAPM) Task Group 43 (TG-43) has determined a protocol of calculating the simulated dose specifically for brachytherapy and has been used in the treatment planning process for clinical brachytherapy. The equation takes into account several factors such as angular and distance dependence, scatter and attenuation corrections, activity of the source outside of the shell as well as differing calculations for line and point sources (22). The 2-dimensional TG-43 equation is shown in equation 2.2 and can also be used in the validation of experimental data from many radiation detectors.

$$\dot{D}(r,\theta) = S_K \cdot \Lambda \cdot \frac{G_L(r,\theta)}{G_L(r_0,\theta_0)} \cdot g_L(r) \cdot F(r,\theta) \tag{2.2}$$

From the equation, S_K, is the air kerma value that describes the apparent activity outside of the source at a reference point in air and Λ is the dose rate constant. The third value is a fraction, $\frac{G_L(r,\theta)}{G_L(r_0,\theta_0)}$, that describes the geometry of the source at different points in space and $g_L(r)$ is the radial dose function that takes into account scatter and attenuation in the medium. The final component in the equation F(r,θ) is the anisotropy function, that takes into account the dose dependence with angle around the source's shell (22). The TG-43 equation can be used to the dose of various sources used at different clinics but it cannot determine the exact *in vivo* dose during radiation treatment, which can vary due to external factors that are

not described in the calculation. Examples of external factors are oedema caused by the insertion of needles, filling and emptying of the bladder and rectum, or general movement of the patient can cause shifts in the dose coverage during treatment (30). Also, over long periods of time, either between insertion of needles and treatment or in-between fractions, movement of catheters within the patient due to these external factors can greatly change the geometry of the original treatment plan (25). This equation is very important when verifying the response of experimental detectors with quality assurance phantoms to determine their accuracy in clinical use.

An important source of error within brachytherapy treatment planning method is the changes to the patient and target volumes between treatment planning and actual treatment. There have been many studies into movement of needles within patients, comparing the physical differences between original scan and scan after treatment as well as the radiobiological effects of this movement (25) (31) (30). In a study in 2009 by Simnor et. al. (25), movement of catheters within prostate brachytherapy patients was seen due to internal organ movement, external movement due to transportation or patient movement, and the formation of oedema between the perineum and apex of the prostate. Patients in this study underwent 3 fractions of brachytherapy with a CT scan before and after each treatment, determining any needle shift and the treatment plan was updated based on these images. The mean movements between fraction 2 and 3 was 7.8mm, and 3.8mm between pretreatment and fraction 3 was seen. Even though the dose given wasn't studied, an improvement in treatment was seen for patients with the corrected plan that took into account to caudal movement of the catheters throughout the entire brachytherapy treatment. The primary tumour volume (PTV) was seen to decrease by 20% for treatment plans without change but a change of 5% was seen for treatment plans with the movement corrections included. Another study by Milickovic et. al. (31) in 2009 looked at needle movement and the effect it had on dose vol-

ume histograms (DVH) as well as radiological effects of patients undergoing a single treatment of HDR brachytherapy, by taking treatment planning, pre treatment and post treatment images. The contours of the treatment volume and organs at risk (OAR) volumes were calculated and compared. It was seen that the radiobiological and dose differences for the urethral volume were significantly different in pretreatment images and the post treatment images. The changes in volume were seen more between the treatment planning and post treatment images, suggesting the time between planning and treatment does affect the dose given, specifically to the OAR. Further dosimetric knowledge of HDR brachytherapy treatments would provide more knowledge on the exact effect of these changes and would also provide more radiobiological information on the amount of damage these dose changes would have on organs surrounding the target volume.

Dose given to critical organs during brachytherapy directly relates to any late effects or complications the patient might have after treatment. Since HDR brachytherapy uses sources with very high dose rate for a short amount of time, the position of the source and any changes to the patient's geometry can have large impacts on the dose distribution given. Errors separated into two categories: human error, which takes into account any miscalculations with planning or connection errors, patient identification, diagnosis, prescription of dose and data entry, and reconstruction errors, which includes any errors to equipment such as the afterloader or computer system (29). Some of these errors are taken into account and checked by the treatment planning system and imaging modalities used, there are many uncertainties remain between planning and treatment (32). These errors can lead to many different and unknown late effects to the patient, including rectal bleeding, proctitis or development of a fistula (8). With more knowledge and regulation of errors, these late effects can be reduced and prevented in future brachytherapy treatments.

There are currently some databases that record any known errors, such as SAFRON

or ACCIRAD, but most clinics only keep records of their own hospital data and most radiation effects occur after months of initial treatment (8). There currently is no regulated system that validates treatment plans or determines the type and occurrence of errors during the treatment, allowing brachytherapy errors within clinics to go unregulated. There have been many studies into the type of errors that occur in brachytherapy and hypothesised methods of correcting or monitoring these errors, however there is no accepted clinical practice of an independent verification system (29). *In vivo* dosimetry is the measuring of dose within the treatment volume or surround areas, which could be the key to having an acceptable dose verification method for brachytherapy within clinics. Many different studies have been completed to explain the reasoning behind *in vivo* dosimetry as well as determining the most ideal detector.

2.4.1 *In vivo* Dosimetry in Brachytherapy

Within most radiotherapy treatments there are verification and quality assurance checks that are completed during and before treatment, but with brachytherapy these checks are limited with many uncertainties present during treatment. *In vivo* dosimetry is the determination of dose during a radiotherapy treatment from within the patient and is very important for identifying errors and determining the exact dose given to the patient (33). Brachytherapy especially presents many problems when identifying an ideal dosimetry detector, such as the need for precise positioning within a high dose gradient field and movement of organs throughout the treatment. With the small dose range within brachytherapy, the detectors must be sensitive enough to record a large range of dose values and provides information on the dose throughout the treatment (32). The position of the detectors is usually within the areas of risk; for prostate cancer brachytherapy they are positioned in the urethral or rectal cavity and need to have good signal to noise ratio to accurately determine the

dose measurement. However, most detectors that could be used for verification purposes need to be calibrated beforehand, usually in a homogenous water-equivalent environment to minimising the large energy dependence that most common detectors experience (29). The sources used within brachytherapy also present challenges because of the low photon emission, especially with LDR brachytherapy with sources Pd-103, and high amount of dose given in HDR brachytherapy treatments, all within a heterogeneous material (32). Research into *in vivo* dosimetry is highly important to improving the safety and reliability of future clinical brachytherapy treatments.

From previous studies and experiments, it has been determined that the majority of errors within brachytherapy come from geometric variations from organ and equipment movement during treatment. A study into the internal movement during the planning and treatment of cervical brachytherapy determined that there was a 20-25% geometrical variation of dose to the treatment volume (29). Current quality assurance procedures for brachytherapy consist of utilising urethral catheters and rectal balloons to limit the movement of internal organs, but the requirement of *in vivo* dosimetry for brachytherapy in clinics is not mandatory and only performed occasionally. For general brachytherapy treatment, the most common type of treatment verification is completed using a rectal diode dosimeter, however this is subject to position error as well as measurement error with the steep dose gradient present in brachytherapy (34). Other options are less invasive with detectors on surface above the treatment area but these are subject to averaging and signal areas due to positioning errors of the detector and source. Due to this gradient the organs at risk (OAR) could be subject to great errors and need an accurate dosimetric method to determine the dose given (32). Much research has been dedicated to determining an ideal detector used in brachytherapy specifically for *in vivo* dosimetry to determine the dose in organs at risk during the treatment.

An *in vivo* dosimetry method would identify these uncertainties and identify

any variations of dose that differs from the treatment plan. An ideal system for brachytherapy would be easy to use with minimal training, be seamlessly implemented into current clinical practices and have an automatic readout (9). The system would also need to be able to be reproduced in other hospitals and clinics, making it commercially available for brachytherapy centres around the world. Each patient has different treatment plans and volumes therefore the position of the detector within the patient may be different for each treatment, but limit the invasive implantation to reduce infection or discomfort. Current commercial detectors are subject to volume averaging, dependencies on temperature and energy, self attenuation and nonlinear dose response (32). An ideal *in vivo* dosimeter would be tissue or water equivalent, small in size for *in vivo* measurements with a small sensitive volume for brachytherapy ranges, consistent read outs with minimal calibration requirements, real time readout system during treatment and safe to use by staff and patients (33). Below many available detectors are compared in terms of these properties to determine the most suitable dosimeter for *in vivo* measurements during HDR brachytherapy for prostate cancer.

2.4.2 Detector Options for Dose Verification

There are many different options for detectors to be used in brachytherapy and many different studies looking into the advantages and disadvantages of them. The detectors in this review are thermoluminescent detectors (TLDs), optical simulated luminescence (OSL) detectors, scintillation detectors, ionisation chambers, film detectors, and semiconductors including diodes and MOSFETs. The characteristics that are compared with each type of dosimeter are size, reproducibly, reusability, cost, ability to produce real time data, and ease of use in a clinical setting along side current brachytherapy practices.

Thermoluminescent detectors (TLDs) have been used previously for dose veri-

fication in other forms of radiotherapy and therefore are among the most common detectors that are being considered for brachytherapy (35). TLDs are made up of inorganic crystals that have a high concentration of traps within the band gap of material due to the addition of impurities. During irradiation, energy is absorbed by the crystal causing electron-hole pairs to be released. Electrons are raised to the conduction band however some electrons become trapped within the band gap; an analogous process happens with holes being trapped near the valence band (36). The number of trapped electrons is directly related to the amount of radiation exposure and can be determined after the irradiation has stopped (23). To determine the amount of dose absorbed the crystal is slowly heated and the trapped electrons become thermally excited enough to move to the conduction band. The electrons then recombine with the trapped holes near the valence band, releasing a photon that can be recorded. The light yield of the crystal is then converted into an electrical signal using a photomultiplier tube and analysed through a glow curve, which is a function of emitted photons and temperature. The area under the glow curve is proportional to the radiation absorbed by the TLD (36). The light released from the detector is very dependent on energy and temperature factors and the absorbed dose can only be determined from a calibrated detector irradiated with a known dose (23). This cannot give a real time dose readout and can only determine the dose to the overall volume, not to a specific area. TLDs also require a very lengthy preparation process consisting of 'annealing, individual calibration, careful handling, fading correction' for every detections and for each detector (32). The detectors can be reused multiple times through heating the crystals to high enough temperatures to remove all trapped electrons and holes (36). They detectors can be formed into varies shapes; the ideal shape to be used in brachytherapy would be small, thin rods that could be inserted into catheters to directly measure the average radiation dose within that area. They are also very available within clinics, have been studied greatly and

understood well in hospitals, and have an average sensitive volume of 1mm^3 thick (8). Overall, TLDs have good dose measurement properties with limited angular dependence but can only give readout after the detector has been irradiated.

An alternative to TLDs is optical simulated luminescence (OSL), which uses the same principle but with an external source of strong light to read out the data from the detector. Such external sources are light emitting diodes or lasers that shine light onto the source that is a different wavelength to the emitted light. Photomultiplier tubes along with optical cables are used to readout emitted light only, which can be converted into an absorbed dose value. They have very high sensitivity down to a few μGy and are currently replacing TLD personal radiation detectors (36). The detector can store information without degrading it or the crystal, can produce a fast read out and can be shaped into many sizes. OSL dosimetry can be used in brachytherapy with small detectors placed within the catheters in the patient. Through the study of OSL materials, it has been shown that they can read out dose data in real time through measuring data in radioluminescene (RL) mode. The real time output of an OSL crystal shows limited angular or energy dependence but have only recently become commercially available and have to be frequently calibrated (32). The use of OSL detectors in brachytherapy for dose verification is being studied greatly but there is limited data on its proposed use in a clinical setting.

Another type of detector system that is being studied for *in vivo* dosimetry are scintillator systems, which produce scintillator light that is proportional to the radiation dose. Scintillators can be made from organic or inorganic material and have differing properties depending on the crystal used. The main advantages of scintillator systems are the high spatial resolution, low energy dependence, water equivalency and linear proportional light response with dose (32). Radiation energy is absorbed by electrons within the crystal and the excited electrons are moved to a

higher energy state. Each crystal structure has a different time in which the electrons are de-excited, usually a few nanoseconds, and return to their normal energy state while emitting fluorescence as they decay. The light produced is proportional to the energy absorbed by the crystal and through converting the light produced into a current using a photomultiplier tube or photodiode, the dose absorbed can be determined (36). Two common scintillation systems that are being considered for *in vivo* dosimetry with brachytherapy are plastic scintillation detectors and fibre optical detectors.

Plastic scintillation systems are relatively inexpensive and are readily available in various sizes, which make them a popular choice for brachytherapy verification measurements. There has been studies on the degradation of scintillators with high amounts of radiation dose over time and possible temperature dependence of the detectors (32). The response of scintillation detectors has been studied and seen to decrease linearly with increase of temperature (29). Another option is fibre optic scintillation crystals that can be made as small as 0.5-1mm thick, giving a similar sensitive volume to TLDs (37). Due to the flexibility and small diameter of fibre cables, these detectors can be placed within needles or in urethral catheters to determine the irradiation dose in a specific position during brachytherapy. The interaction of radiation within the optical fibre can cause unwanted radiation called Cherenkov or stem light to appear and give inaccurate measurement of dose. This is caused by electrons moving through the material faster than the speed of light, leading to the creation of high energy photons (37). The removal of this excess radiation has been studied and there are many proposed methods to allow scintillation detectors to output the absorbed dose readings only, such as background subtraction or filtering (29). The position of the fibre optic detector is also important to achieve an accurate reading; the central axis must be perpendicular to the dose gradient for the entire treatment to minimise dose averaging. If the position of source change

throughout treatment or the detector moves, this can impact the data recorded (8). The detectors are capable of real time dose readout, which is essential for detectors to give dose verification in brachytherapy. They have very limited angular and energy dependence, as well as a user friendly calibration procedure but both types of scintillation detectors require additional invasive insertions to give an *in vivo* dose reading during brachytherapy treatments (32).

Another type of detector that has been used previously for dose verification in other radiotherapy modalities is film, either radiographic or radiochromic film. Film has very high spatial resolution, depth dose around 150μm, and comes in many sizes that can be molded to the shape of the body (8). An image is created through the interaction of radiation with the particles within the film, creating a latent image of the path of radiation that is proportional to the amount of dose absorbed by the film (36). Similarly to TLDs, this is a passive method of dose verification and cannot provide a real time dose readout during brachytherapy treatments (35). Radiographic film consists of a transparent base covered in an emulsion layer made of silver bromide crystals that interact with electrons to record a shadow image. The silver bromide crystals become silver during the developing process and the degree of silver on the image is proportional to the amount of radiation absorbed. This is determined through the net optical density of the film, through a the sensitometric curve (4). Radiographic films in particular have a complicated chemical developing procedure taking 24 hours while radiochromic films doesn't require any developing but does take the same amount of time to get an accurate dose reading (8). Radiochromic film is an alternative to radiographic film with characteristics like tissue equivalence, high spatial sensitivity and no sensitivity to visible light. The colourless film changes colour with irradiation due to polymerisation of radiation sensitive dye and the dose can be determined from the optical density of the film using a spectrophotometer with a limited wavelength (4). Radiochromic film is less

energy dependent but both forms of film are sensitive to temperature and need to be carefully calibrated beforehand (8). Radiographic film can only provide an average dose readout over an entire volume and radiochromic film is more suitable for brachytherapy dosimetry.

Finally, semiconductors have been strongly researched to develop an *in vivo* method within brachytherapy, specifically diodes and metal oxide semiconductor field effect transistors (MOSFETs). Semiconductors have been used previously in external beam treatment verifications due to their small sensitive volume size, real time readout capabilities, high sensitivity and small size. They show a high dependence on temperature, angle and position, energy and radiation damage (32). The disadvantages of semiconductors in brachytherapy dosimetry is the determination of position and angle and geometric changes over the delivered high dose. There has been a lot of research into compensating or eliminating these dependencies to allow semiconductors to be used for dose verification is small areas with steep dose gradients. Diodes and MOSFETs produce a current readout that is proportional to the dose absorbed by the detector with an easy to operate, real-time readout system (35). Diodes are a silicon p-n junction, created from p-type silicon doped with n-type material with a depletion zone in between making up the sensitive volume of the dosimeter. The sensitive volume is 0.2-0.3mm^3 and during irradiation electron-hole pairs are produced creating a current within the diode between the n and p regions. Due to the lower energy needed to create the electron-hole pairs, 3.5eV in Si compared to 34eV in air, silicon diodes are more sensitive to radiation but show a higher energy dependence due to the higher atomic number (36). Diodes are limited by their size as well as being severely directionally dependent with slight temperature dependence. They have been used for dosimetry purposed in brachytherapy within the rectum or bladder, using rectal probes with a diode array or a single diode implanted (29). Diodes are also very available commercially and are very easy

to operate due to being present in clinics for many years. Semiconductors, both diodes and MOSFETs, are also inexpensive to purchase and implement into clinical brachytherapy setting (32).

MOSFETs are seen as a more ideal semiconductor for *in vivo* dosimetry due to their small sensitive volume and smaller size that can be implemented in brachytherapy treatments. They have a smaller diameter than diodes and due to their submillimeter size can fit within catheters to give dose readout within target areas throughout a brachytherapy treatment. MOSFETs are non-tissue equivalent, miniature p or n type silicon semiconductors with a sensitive volume of a couple of microns (29). Due to size of the sensitive volume, they are ideal for recording absorbed dose in steep gradient fields through producing changes in electrical characteristics that is proportional to radiation dose(37). They can record absorbed dose uniformly in every direction but as the position of the source changes the recorded dose becomes non-linear. Due to the ever increasing threshold voltage of the MOSFET, it has a limited lifetime and is subject to some deterioration with long radiation exposure. As the detector is exposed to radiation, the sensitivity of the detector becomes less as the amount of threshold voltage increases towards saturation (38). Similar to diodes, they are also known to have several dependencies that limit their use within *in vivo* dosimetry, such as temperature, energy and angular dependence (32). Energy dependence can be compensated through individual calibration with the same treatment source and there are several methods to limit the temperature dependence of the detector (29). Traditional MOSFETs also have an epoxy resin covering the sensitive volume, which increases the effective depth dose of the detector, but without it produces unreliable results with many uncertainties. The thickness of the epoxy resin usually around 1mm minimum, which is a dome shape over the sensitive volume of the detector (8). The main advantages of MOSFETs for *in vivo* dosimetry are the capability of real time readout that is dose rate independent with no change

in the data with time and the dose readings can be permanently stored within the detector (9). Figure 2.1 shows an image of the structure of a p-type MOSFET or N channel MOSFET that is commonly used in brachytherapy experiments and the operation of the detector is described below.

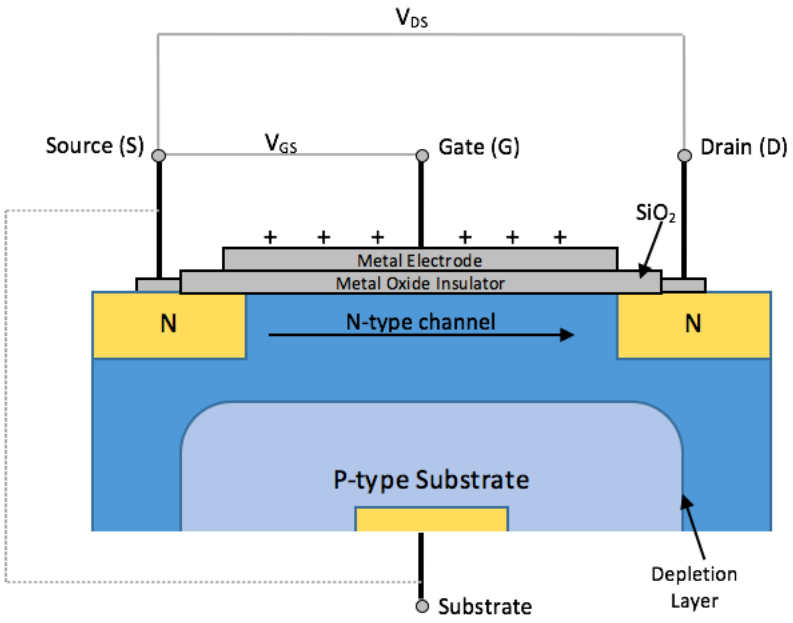

Figure 2.1: Structure of a MOSFET dosimeter, (1)(39)

A MOSFET consists of a substrate, making up the bulk of the detector, and a drain and source channels, made from a p-type or n-type semiconductor with two doped regions of opposing type. There is also an insulated electrode gate made from aluminum and silicon oxide grown in between the drain and source (40). The substrate is used as a grounding material and the induced n-type channel flowing from the source to drain, is proportional to the voltage inputted into the detector (39). Like most semiconductors, incoming radiation creates electron-hole pairs and in MOSFETs these are created within the silicon material of the gate of the detector. The holes or positive charges are attracted to the silicon substrate - silicon oxide insulator interface and are trapped, creating a build up of positive charge as the detector is irradiated (1). The build up of positive charge directly affects the

n-type regions and creates an inversion layer of moving electrons from the source to the drain, changing the voltage of the detector. This allows the transistor part of the MOSFET to be turned on and a flowing current forms. The resistance between the drain and source is directly related to the threshold voltage of the system; at low voltages between the gate and source the resistance is very high, not allowing current to flow. As the voltage increases past a certain point the resistance decreases significantly, allowing the transistor of the MOSFET to become operation and current to flow (39). To get a reading from the MOSFET the voltage created in the gate must be greater than the base threshold voltage (40). The readout of the MOSFET system is the voltage difference between the gate and source voltage and the drain and source voltage.

$$V_{GD} = V_{GS} - V_{DS} = V_{th} \tag{2.3}$$

The readout of the MOSFET system shows an increase of threshold voltage that is directly proportional to the radiation dose absorbed at the oxide gate. To determine the dose absorbed in the detector, a calibration factor is determined that relates the change in voltage to radiation delivered. Once the n-type dopped regions have reached saturation, the MOSFET no longer produces a linear response and cannot accurately measure dose. Therefore, the lifetime of the MOSFET is limited and the manufacturer sets a maximum voltage that the detector can be used up to for a reliable response (1). The limited use of the MOSFET is one of the main disadvantages of the detector system, however these detectors are very affordable and can be easily replaced in clinics. The Centre for Medical Radiation Physics (CMRP) at University of Wollongong has created a unique MOSFET design, MO*Skin*$^{\text{TM}}$, that address many of the disadvantages of traditional MOSFET designs, including the inadequate depth dose, angular dependence and temperature dependence. The

MO*Skin*^{TM} is based on the same electronic properties as MOSFETs but produces a more accurate readout system that is ideal for *in vivo* dosimetry for brachytherapy.

2.5 MO*Skin*^{TM} Detectors

The Centre of Medical Radiation Physics at University of Wollongong developed a uniquely designed MOSFET detector, MO*Skin*^{TM} , used for skin dosimetry and later in *in vivo* dosimetry measurements (41). As discussed previously, the MOSFET use within brachytherapy and skin measurements is limited due to the skin depth. Shown in figure 2.2, the MO*Skin*^{TM} design uses a thin-film encapsulating layer above the sensor that replaces the epoxy resin used in traditional MOSFET designs. Measurements of a water equivalent depth of 70μm are possible due to the small sensitive volume and size of the gate being 55μm (8). The dimensions of a MO*Skin*^{TM} detector are 2mm wide, 0.4mm thick and 330mm long, designed with the sensor in the tip and a long tail connected to a read out system (24).

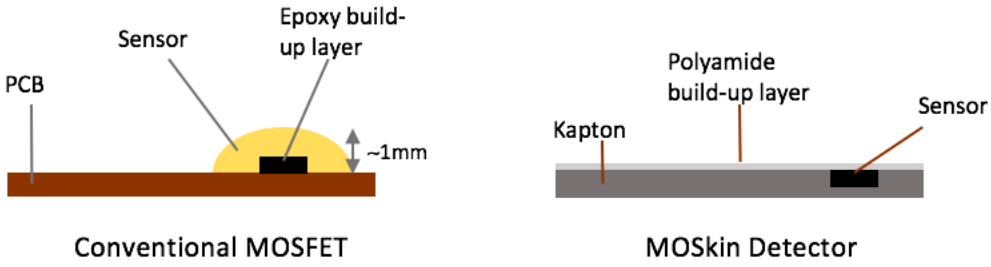

Figure 2.2: Comparison of original MOSFET and MO*Skin*^{TM} design (42)

MO*Skin*^{TM} detectors are ideal for brachytherapy *in vivo* measurements due to the sub-micron size sensitive volume, allowing dose to be determined accurately in steep dose gradients, and they are also capable of real time readouts. However similarly to MOSFETs, they have a maximum threshold voltage that the MO*Skin*^{TM} detector can be used up to, around 26V, for accurate results (43). A lot of research has been completed and still is being completed for characterising these detectors

in different environments to determine clinical protocols for dosimetry use.

2.5.1 Temperature Dependence of MO*Skin*™ Detectors

MOSFETs, including MO*Skin*™ s, are ideal to be used for *in vivo* dosimetry due to their size and sensitive volume however one major issue is the effect of temperature on the recorded dose, determined to affect the recorded dose up to 12% (38). The dose is determined from the changing threshold voltage readout but this is directly dependent on the temperature of the detector, especially when the detector is calibrated in a room temperature environment and data is collected from a body temperature environment (9). There have been many proposed methods for compensating or eliminating the affect of temperature on general MOSFET detectors and specially MO*Skin*™ that are used clinically. One proposed method was reading the irradiated dose from a thermostable current between the source and drain, which is when the threshold voltage is not affected by changes in temperature. This is usually at a very low current, which is very hard to achieve, and the detector needs to be the same temperature, even if the environment temperature changes, throughout the entire treatment (44). Another method is to place the detector inside the patient and wait for the detector to reach temperature equilibrium, about an hour after implantation. At that point the detector will be temperature independent with an accurate dose recording, but this increases the total treatment time dramatically (24). A final option is to use dual detectors during clinical irradiation to determine the impact of the temperature on the dose recorded and remove the dosimetric signal (29). Research completed by Garcia-Inza *et. al* in 2014 proposed a method with two detectors using the same silicon die, experiencing the same dependencies, with the dose determined from the difference in signal between transistors. The contribution of temperature to the readout signal through applying different gate voltages to each detector and mathematically determining the affect of temperature. This

study determined the sensitivity increased and the uncertainty decreased with the use of dual detectors to determine the dose, but there was a large amount of noise present. Further studies are being completed to determine the clinical suitability of this method to compensate for temperature during in vivo dosimetry (38). In this thesis a new method is proposed, using the internal properties of a single MO*Skin*™ detector to create a temperature compensation value to remove any dependence on the dose readout.

2.5.2 Previous Studies Using MO*Skin*™ Detectors

MO*Skin*™s have undergone many research studies to determine their ideal use within clinical radiotherapy. Even though MO*Skin*™s were originally designed for skin dosimetry, they have shown to be ideal for *in vivo* dosimetry for brachytherapy and the following studies describe different methods and results from research teams around the world.

Hardcastle et al. (44) in 2010 was one of the first teams to propose the use MO*Skin*™ in for *in vivo* dosimetry to determine the dose to the rectal wall during hypo-fractionation external beam radiotherapy. Due to the low alpha beta ratio of the prostate mentioned previously, high dose rates are more ideal for treating prostate cancer however the dose to organs at risk becomes greater. The study investigates rectal balloons, which immobilise the rectum throughout treatment and are fairly common clinically, with a MO*Skin*™ attached to the balloon to verify the dose to the OAR with real time output. Due to the air cavity within the rectal balloon, the dose gradient between the rectal wall and balloon is very steep; the MO*Skin*™ 's small sensitive volume is ideal for determining dose in this environment. A 'face-to-face dual MOSFET arrangement' was used to determine depth dose and correct for angular discrepancies. The phantom was irradiated with various

fractions of dose between 2-10 Gy and the sensitivity, reproducibility and angular dependence was looked at. The dose to the rectal wall compared to the treatment planning system used showed a lower dose reading, which agreed with previous research into treatment planning with rectal balloons due to the air cavity. There were some discrepancies due to temperature and positioning of the balloon that made this design difficult for clinical *in vivo* dosimetry. The temperature dependence was seen unless readout from a thermostable current, as described previously. Temperature independence was hypothesised with the use of an additional MOSFET detector or utilising the intrinsic properties of the MOSFET without additional detectors. Angular discrepancies were seen to be ±2.5% for the azimuth axis and between -2.5% and +4% for the polar axis for a single MOSFET, however the dual MOSFET showed an angular dependence of ±2.5%. Another issue with this study is for each fraction a new balloon and detector is used and therefore the position of the *in vivo* dosimetry system would change for each fraction in EBRT. The following study are researching dosimetry in brachytherapy, where ideally the dosimetry system would not be moved and used throughout treatment.

Another study using MO*Skin*™ detectors was performed by Kwan et al. in 2009, who investigated the the dose to the rectal wall during high dose rate (HDR) prostate brachytherapy (8). The dose to an empty air filled heterogeneous rectum was studied to determine the amount of backscatter delivered to the rectum during treatment using a rectal phantom with two MO*Skin*™ detectors. The dose recorded in the phantom tests were compared to treatment planning data. The phantom used in this study was made from solid, water-equivalent plastic made from slabs to alternate distances and a cylindrical air cavity to represent the rectum. The results of this study showed a measurement dependence on distance, with the difference between the treatment plan and detector readout increasing further away from the detector. Due to the assumptions of the treatment plan that the rectum is homogenous, the

dose is overestimated. It was also seen that due to the small sensitive volume in the MO*Skin*™ detectors, the orientation of the detector to the gradient of the dose was not significant on the dose recorded. This study recommended additional studies into the backscatter affects for different parts of the rectal anatomy and accounting for the heterogeneity of the rectal tissue within the treatment planning system.

In a study performed by Alnaghy et. al, in 2015 (45), the dose to the anterior rectal wall during prostate cancer treatment using hypo-fractionated stereotactic body radiotherapy (SBRT) delivered during tomotherapy. This type of radiotherapy takes advantage of the low alpha beta ratio of the prostate and in previous studies the toxicity to the OARs is relatively low. The aim was to create a monitoring system that incorporates organ deformation and variations in setup position for each fractional treatment to determine any issues with treatment as well as the real time dose. A rectal probe with similar dimensions as an TRUS probe was used with dual MO*Skin*™ detectors to complete *in vivo* dosimetry of the anterior rectal wall. The replica probe was constructed from Perspex with density of approximately 1.09-1.12g/cm^3, length of 200mm and a diameter of 20mm. Four detectors were placed at an angle descending from the head of the probe with the wires wrapping around the length. Each detector was calibrated in a solid water phantom, facing upwards and downwards, with an average calibration factor determined 30 seconds after irradiation. An IMRT Head and Torso Freepoint Phantom was used to complete clinical experiments and CT images were used to complete a tomotherapy treatment plan for comparison of dosimetric measurements. The results from this study showed that 75% of the recorded measurements coincided within ±5% of the treatment plan. The angular position of the detector showed errors at 180° and 90° position but was seen as less important as at 0° due to the lower doses and the CT doses were only at 0°. Due to the steep dose gradient, a large discrepancy was seen in between voxels on the CT treatment was seen highlighting the importance of dosimetric measurements

for small positional changes. The main issue with this study was the exact position of the detectors within the phantom, which is significant in steep dose gradient regions. It was also highlighted that the tomotherapy treatment in this study would only be used as a boost, averaging two fractions, and therefore the insertion of the probe for the entire treatment wouldn't cause increased discomfort for the patient compared to a full treatment lasting numerous fractions.

Finally, in a multi-paper study completed by Tenconi et. al. in 2014 (46) and Carrara et al. in 2016 (24), MO*Skin*™ detectors were investigated to be used for verification measurements during High Dose Rate prostate brachytherapy. Due to the common use of TRUS probes during brachytherapy to provide real time imaging during treatment, this study looks at including dosimetric detectors in the probe to give *in vivo* measurements as well as images. In the Tenconi et. al. study two MO*Skin*™ detectors were placed on a TRUS probe along the longitudinal axis with a silicon spacer separating the detector from the probe. The advantages of the longitudinal position are using a transversal ultrasound image the detector position can be located and the radial positional uncertainty is relatively small. These measurements were completed using a gel phantom with needle matrix template and cylindrical space for the probe. A treatment planning system was used to optimise the dose given and the probe was placed inside the phantom for the entire treatment. Three doses were recorded and averaged and the position of the detectors was determined using ultrasound images from the probe. The results from these measurements agreed with the TPS values within an acceptable range, recommending this procedure with a dual purpose TRUS probe as a method for dose verification. The angular and positional dependence didn't affect the measurements significantly. Further study was recommended to investigate the affect of organ movement or patient movement in-between the treatment planning images and the actual treatment.

In a continuation of this research, the study completed by Carrara et. al. in 2016

looked further into the incorporation of two MO*Skin*^{TM} detectors on an ultrasound probe during clinical prostate brachytherapy for 12 patients (24). The measurements were compared to treatment planning doses calculated from images taken before treatment and after treatment, to compare the movement of organs throughout treatment. The position of the detectors along the probe was determined through a reference structure and data was collected from 18 treatment sessions. During these sessions, a few detectors failed due to stress on the detector and a five detector probe has been suggested for more accurate dose recordings. The angular position of the detectors was within 70° with ±2% in the longitudinal direction and within 80° with ±3% in the transversal direction. An issue highlighted in this study was that the calibration was completed in a different temperature environment compared to the body temperature environment during dose recording. The study suggested that the dual purpose probe be implanted into the patient before calibration and once the detector has reach temperature equilibrium, averaging 1-hour prior, calibration should be completed. The study also concluded that uncertainties in treatment increases when the time difference between treatment planning images and treatment is greater than 1.5 hours. Through the results of this study, *in vivo* dosimetry using a MO*Skin*^{TM} dual purpose probe is a possible method to complete dose verification during treatment. Future research is required to form a clear clinical procedure for implementation in hospitals during HDR prostate brachytherapy.

2.6 Discussion

Through the research into MO*Skin*^{TM} detectors as a possible dose verification tool, this detector was chosen to be used in this thesis as part of a *in vivo* verification method during HDR prostate brachytherapy treatments. A new readout system created by the Centre for Medical Radiation Physics, University of Wollongong, incor-

porates compensations directly based on the dependencies of MO*Skin*$^{\text{TM}}$ detectors and will be used to wirelessly readout the treatment dose in real time. Characterisation of this new system and treatment simulation experiments were completed at the St. George Cancer Care Centre (SGCCC) with the medical physics team at the hospital.

Chapter 3

Circular Gate MO*Skin*$^{\text{TM}}$ Dosimeter and OneTouch Characterisation

3.1 Introduction

The MO*Skin*$^{\text{TM}}$ and OneTouch Readout System were investigated to determine the feasibility of producing a clinical dose verification system during HDR brachytherapy. Both a newly updated MO*Skin*$^{\text{TM}}$ detector with a circular gate and OneTouch system were compared to previous generations to determine the ideal equipment to be used clinically.

The circular gate MO*Skin*$^{\text{TM}}$ detector was designed and produced to remove the angular dependence and to increase sensitivity. The original MOSFET dosimeter had a thick epoxy resin layer that protects the sensor, however this extra thickness greatly decreases the accuracy of readouts in steep radiation gradient situations like HDR brachytherapy. (46) MO*Skin*s$^{\text{TM}}$ were designed to remove the epoxy resin to increase the effective depth of the sensitive volume to 55μm, however angular

dependence was still present with this design (47). The newer MO*Skin*^{TM} design was created to limit the angular dependence effecting the dose rate readout and the effectiveness of this new design was the focus of this initial experiment. The previous generation of MO*Skin*^{TM} utilised three straight electrode terminals, with the D, G and S symbolising the drain, gate, and source terminals shown in figure 3.1. The newer MO*Skin*^{TM} detector uses circular electrodes to minimises the effect of changes in angular position on the dose readout.

Figure 3.1: Detector design of previous parallel gate MO*Skin*^{TM} dosimeter and new circular gate MO*Skin*^{TM} dosimeter

The sensitive volume of the circular gate detector is also larger then previous generations, allowing for a probable increase of sensitivity of dose readouts. With the changed electrode design of the detector, the sensitivity and angular response was investigated to determine if the dose readout was acceptable. The angular dependence of the circular gate MO*Skin*^{TM} detector was investigated to determine the relationship between readout and source position with the new electrode design. A gelatine phantom and replica rectal probe were used in the angular tests to mimic HDR prostate brachytherapy. The estimated dose and experimental data was calculated and compared to determine the angular dependence of the circular gate MO*Skin*^{TM} dosimeters. The sensitivity of the parallel and circular gate versions were analysed through determining the dose readout over long irradiation periods. These tests highlighted the superior dosimetric capabilities of the circular gate MO*Skin*^{TM} detector and its ability to be used as a brachytherapy verification system.

A user-friendly system is essential for *in-vivo* dosimetry, for displaying the dose

recorded in real time throughout the treatment. A wireless readout system called OneTouch created by Centre for Medical Radiation Physics (CMRP) at University of Wollongong (UOW) allows dose information to be transmitted via Bluetooth or ultra-high frequency bandwidth as well as incorporating a temperature compensation factor and dose calibration. The OneTouch system allows the user to evaluate and store a temperature compensation factor and calibration factor, which can be used throughout the lifetime of each detector. The device is used in conjunction with the MO*Skin*™ detectors for HDR prostate brachytherapy measurements to demonstrate a suitable verification system for the treatment of cancer. The system was characterised to determine the reliability and accuracy to continually record MO*Skin*™ measurements as well as the ease of use in a clinical setting. Multiple tests were completed such as irradiating a single detector with the same dose multiple times until the maximum voltage had been reached, completion of a comparison test looking at the different algorithms used to compensate for radiation 'creep-up' or 'anti-annealing'(8)(48), and a temperature variation test to evaluate the temperature compensation factor. All these experiments were completed at St. George Hospital in the Brachytherapy suite with an Ir-192 source in a solid water phantom and at the Centre for Medical Radiation Physics in the University of Wollongong with a current controlled TE Technology® Peltier Cooling Plate (49).

3.2 OneTouch Design and Capabilities

Figure 3.2: The OneTouch Readout System designed by University of Wollongong

The OneTouch system is designed to transmit information from a maximum of six detectors through six ports located on the main transmitter device, shown in figure 3.2. The data is transmitted wirelessly to a computer through two types of USB receivers, either a Bluetooth or an ultra-high frequency (UHF) bandwidth. In Australia it illegal to use UHF bandwidth, therefore the Bluetooth receiver was only used in this thesis. In a clinical setting the transmitter device would be located next to the phantom or patient, connecting the *in-vivo* detector to the OneTouch system where dose data can be transmitted throughout the treatment giving a real-time dose response. The receiver USB is also placed within the room, out the way of equipment and staff and transmits received information through an extension cord to the connected computer system in the brachytherapy control room. In figure 3.3, showing the program associated with the OneTouch system, a target dose is inputted and 'Measured Dose' is shown as a percentage that slowly increases during

treatment to the total dose as well as a single Grey value. This allows for the dose readout to be completed as treatment progresses, creating a dose verification system to display any abnormalities in delivered dose.

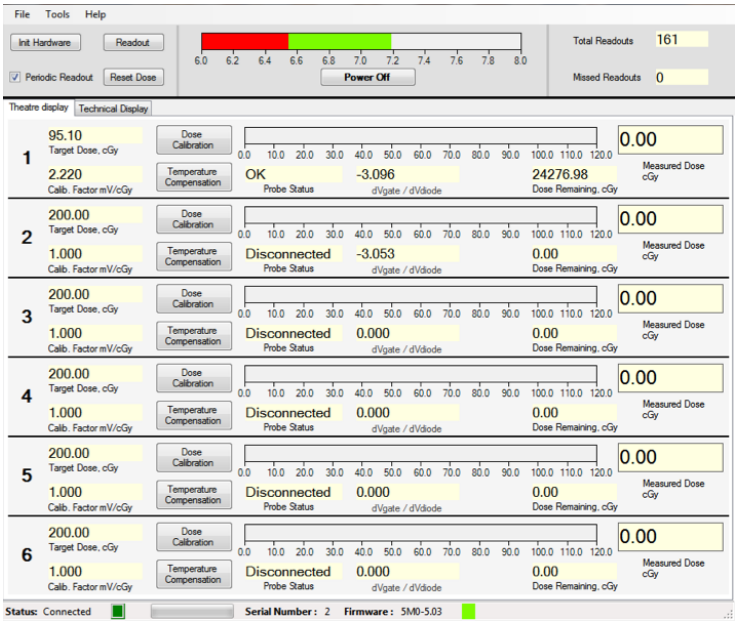

Figure 3.3: The OneTouch readout system program interface depicting calibration values and the dose recorded graphically

Another advantages of this system is the simple and precise method of determining a value that compensates for errors in data measurement due to temperature fluctuation and calculating a value that relates voltage output to absorbed dose. As previously mentioned, temperature can affect the dose measurement of MO*Skin*$^{\text{TM}}$ detectors, especially when calibration is performed in a separate environment to the treatment environment within the patient. With an increase or decrease in temperature, all MOSFETs, including MO*Skin*$^{\text{TM}}$ detectors, experience a change in threshold voltage; a decrease in threshold voltage when the temperature decreases and vice versa. The variations in threshold voltage with changing temperature is due to thermal energy being added or removed from the system, affecting the electrons being released in the semiconductor of the MOSFET detector. With more thermal energy the detector will simulate an increase in radiation due to an increase

in electron-hole pairs creating a higher threshold voltage value (40). The threshold voltage of the detector output is determined but with a temperature change the actual dose becomes unknown (38). Methods have been proposed to compensate for temperature dependence, including measuring radiation at a thermostable point only or allowing the detector to reach temperature equilibrium within the patient before calibration and measurement (29) (24). These methods however limit the detectors potential as well as taking a great deal of time to complete; the OneTouch temperature compensation method is completed within a couple of seconds and the compensation factor can be stored for the duration of treatment. The system uses the characteristic of the MO*Skin*™ detector that allows for two terminals of the MOSFET chip that act like a diode during temperature change.

3.2.1 Temperature Compensation Calculation

When the MO*Skin*™ detector is irradiated, a current is induced creating a voltage between the gate to the source. This voltage is a measurement of the amount of absorbed radiation during a single treatment. Due to the temperature dependent nature of MOSFET detectors, a voltage change is also created during a temperature change and mimics an irradiation readout with an increase in threshold voltage. As well as voltage between the gate and source there is also a reverse voltage created between the substrate or bulk and source during temperature change. This phenomenon creates a diode within the detector that can be used to determine how the detector will react during temperature change. The temperature calibration factor, C_T is calculated from the equation below, using a ratio of the two voltages discussed.

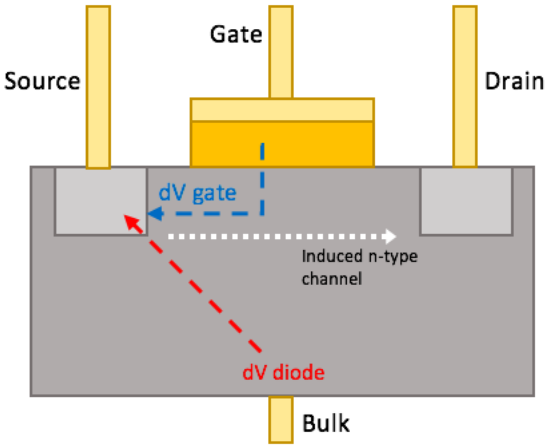

Figure 3.4: Schematic of MO*Skin*™ temperature dependence using reverse voltage from diode (dv diode in red) and voltage difference from MOSFET (dv gate in blue)

$$C_T = \frac{dV_{gate}}{dV_{diode}} = \frac{V_{gate}max - V_{gate}min}{V_{diode}max - V_{diode}min} \tag{3.1}$$

To initiate a temperature compensation calibration, the detector is heated for several seconds by placing a finger or an active heat plate end of the detector and the device calculates the value when a 'Temperature Compensation' button in pressed on the system interface, shown in figure 3.3. The aim of the OneTouch system is to determine how the dose readout after initial calibration will readout to any variation in detector temperature due to body heat. A difference in maximum and minimum voltage is determined from both the diode and gate voltage, shown in figure 3.4. This can be used with any MO*Skin*™ detector and the calibration value is intended be applicable to all dose measurements during the lifetime of the detector. From initial testing, the usual value for the compensation factor is approximately -3 due to the negative difference in reverse voltage between the substrate and gate during a change in temperature and is unit-less due to being a voltage ratio.

3.2.2 OneTouch Program Interface

The new OneTouch system also has more stable electronics than previous models with a lower bias voltage of approximately 9V compared to 15V used in previous models, increasing the lifetime of the MO*Skin*^{TM} detectors. Another key features of the OneTouch system includes the input of a target dose and a visual display of accumulated dose for up to six detectors, signal quality based on the missed readouts and total readouts, manual input of readout period, visual display of the battery level, the amount of noise present during measurement, and various threshold voltage levels of the detector. The device also allows for a calibration factor relating voltage to dose to be calculated in a similar manner to the temperature compensation value and stored throughout treatment. Previously, detectors needed to be calibrated manually from an average of multiple readings but the OneTouch system allows the factor to be determined by pressing 'Dose Calibration' button after a single irradiation, seen in figure 3.3. This is completed through inputting a target dose, calculationed using TG43 (22), and irradiating the detector before pressing the 'Dose Calibration' button.

The OneTouch system also includes multiple algorithms to compensate for the radiation 'creep-up' that is characteristic of all MOSFET detectors (48). The algorithms available in the OneTouch system include Standard, Min2, Average2, Medium3 and Medium4, and were compared as part of the system characterisation tests performed. The default setting of the system is Standard, which readouts the highest recorded value. Min2 algorithm looks at the current readout and the previous readout and identifies the lesser of the two values. Average2 algorithm takes the average of the current and previous value and compares this average to the previous average calculated. Medium3 and Medium4 perform the same medium calculation with the current value and previous 2 or 3 measurements. Through a comparison of the current readout value with the previously calculated one, the OneTouch system will stop

recording readouts when it is apparent radiation exposure has ceased, and account for the radiation creep present in the MO*Skin*™ detectors.

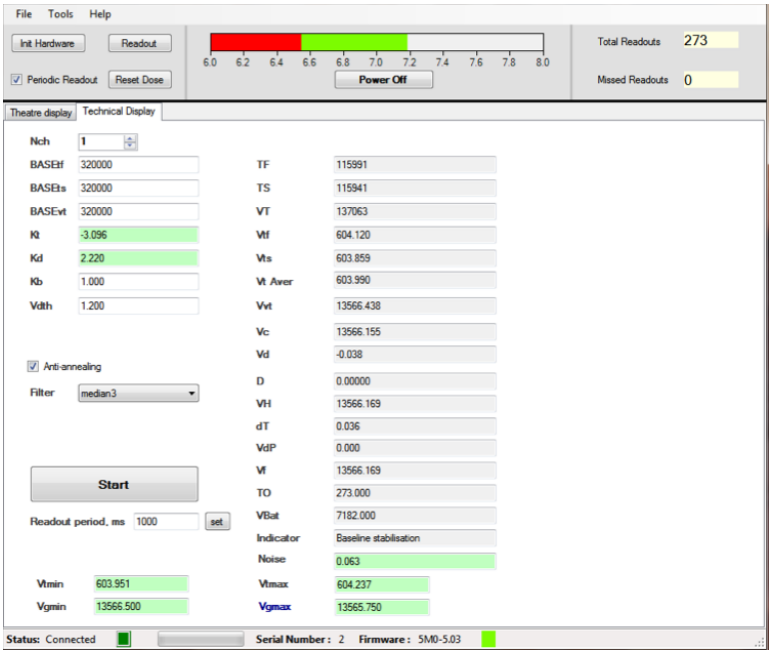

Figure 3.5: The OneTouch readout system interface depicting the technical display for each channel

In figure 3.5 the technical data is shown and it is through this data that the temperature corrected dose output is determined. MO*Skin*™ detector.

$$V_c = V_{vt} - (V_{Fdiode} - V_{Sdiode}) \times C_T \tag{3.2}$$

$$V_{temp} = (Vc - V_{vt}) \times C_T \tag{3.3}$$

Utilising the temperature correction factor, C_T, the voltage, the total threshold voltage output, V_{vt}, is corrected using the diode voltage within the detector. V_{Fdiode} or VTF on the OneTouch interface is the maximum diode voltage, V_{diode}max, with

V_{Sdiode} or VTS being the minimum diode voltage, V_{diode}min. The voltage from temperature variations only can be determined through equation 4.3 using the corrected voltage, V_c, and total output voltage with the compensation factor. The average of the diode voltages, Vtavg shown on the interface, accounts for overall changes in temperature from the initial calibration temperature. The effectiveness of the compensation factor will be investigated and discussed below.

3.3 Methodology

The characterisation of the new readout system was completed through three separate tests investigating the creep compensation algorithms, the sensitivity drift of the system through multiple irradiation exposures, and temperature calibration factor verification. The MO*Skin*™ experiment was separated into multiple individual test to determine suitability of the circular gate MO*Skin*™ design to be used clinically. The tests included calculating the calibration coefficient of the detector used, determine the angular dependence of the newly designed MO*Skin*™ detector, and investigate the sensitivity of both versions of detectors. The angular testing and calibration were completed using the Clinical Semiconductor Dosimetry System (CSDS), a battery operated readout device that is directly connected to the MO*Skin*™ detectors within the brachytherapy suite to the control room. The One-Touch system was used during the long irradiation tests to compare the sensitivity of the different electrode designed MO*Skin*™ detectors.

All tests performed in the brachytherapy suite in the Cancer Care Centre at St. George Hospital, Kogarah. The brachytherapy machine was a HDR Nucleon remote afterloader (Nucletron, Veenendaal, The Netherlands) with the Oncentra® Brachy Treatment Planning System used to plan the tests. As with most clinical high dose rate brachytherapy treatments the source used was Iridium-192 with an associated

source strength of 40.7 mGy/ hr m^2 (40700U). The associated source strength is not the true activity of the source, as it degrades over time, however the source dwell time for each treatment plan is adjusted to irradiate for a single associated source value. As the lifetime of the source increases so does the brachytherapy treatment period. The dose can then be directly calculated from the TG43 formulation shown in equation 2.2 (22). This allows for the treatment plan to be created hours before the actual treatment without having to re-plan directly before treatment.

3.3.1 MO*Skin*™ Comparison Tests

3.3.1.1 Circular Gate MO*Skin*™ Calibration

The dose calibration of each detector is essential before clinical use to accurately determine the proportional readout of absorbed dose. The MO*Skin*™ detectors were calibrated using a CIRS Plastic-Water® phantom at the Prostate Cancer Institute at St. George Hospital, Kogarah. The calibration value for the angular test was calculated using the CSDS, completed through manually reading out the current threshold voltage of the detector and using equation 3.3.1.1.

$$C_D = \frac{dV_{avg} \times 1000}{D_{TG43}} \tag{3.4}$$

Each MO*Skin*™ detector was placed in the plastic water phantom and a catheter was placed at the centre with a 15±1mm source to detector distance. There was additional water equivalent plastic placed above and below the catheter to simulate backscatter present in clinical treatments as well as blue tac that was used to secure the detector and catheter in place. The source was stationary at the distal end of the catheter, position 234±1mm, for the entire calibration test. The dosimeter was irradiated for 10 seconds and a voltage readout was taken before and 30 seconds

after irradiation with the CSDS model. This was completed five times and the average increase of threshold voltage was determined from the final four readings. The initial reading was ignored as a warm-up reading, as is usual practice for determining the calibration value clinically.

For the sensitivity tests the calibration value was automatically determined through a single irradiation and using the OneTouch interface, which use the same formalisation in equation 3.3.1.1. Each detector was calibrated using the OneTouch system over a 10 second dwell period at 15±0.5mm source to detector distance. The temperature compensation factor and compensation value for the parallel MO*Skin*™ detector was calculated to be -3.096 and 2.220±0.001mV/cGy, and -3.300 and 2.308±0.001mV/cGy for the circular MO*Skin*™ detector. The calibration and temperature compensation method with the new system will be further explained in Section 3.3.2.

3.3.1.2 MO*Skin*™ Angular Dependence Characterisation

Angular testing of the circular gate MO*Skin*™ was completed using a large gelatine prostate phantom, following the procedures to produce a radiotherapy bolus. The bolus was a gelatine-water mix created through mixing 5 tablespoons of gelatine in 100mL of boiling water until dissolved then adding an additional 400mL of cold water. The mixture was added to the phantom and repeated until the container was full, creating 1500mL of gelatine-water mix. The phantom was placed in the fridge overnight to solidify and was used the following day. The dimensions of the phantom are 150mmx170mmx140mm and the hollow experimental probe has multiple indentations near the apex of the probe to attach the MO*Skin*™ detectors (47). Above the probe entrance on the phantom is a template matrix at either end, size of 11x10, for the catheter insertion and the probe entrance is hollow at one entry point with a solid plastic stopper at the other end.

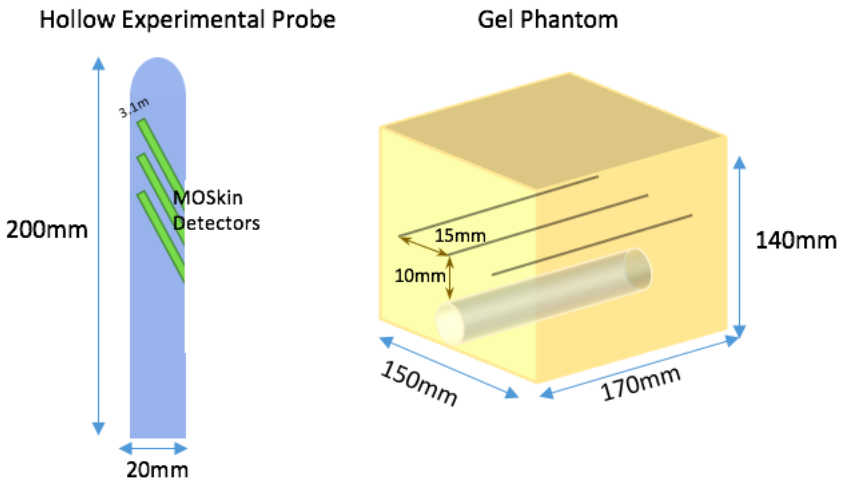

Figure 3.6: Experimental set-up for gelatine-water phantom angular dependence Test (47)

Seven positions were tested along the catheter in 23±1mm step increments from the posterior to the anterior of the phantom. The dwell times at each position increased further away from the detector to compensate for decrease in dose due to the inverse square law and radiation attenuation. The detector was taped to the hollow probe and situated at the centre of the phantom at 165±1mm. A single detector used for all tests and the results were recorded 30 seconds after irradiation with the CSDS. The calibration value was adjusted for gel phantom testing due to the sensitivity drift of the MO*Skin*™ detectors lifetime. Due to the differing temperature of the gel phantom, that was in a refrigerator until catheter insertion, the initial threshold voltage was lowered and there was no temperature compensation value used.

3.3.1.3 MO*Skin*™ Sensitivity Analysis

The sensitivity drift response of the two versions of detectors was characterised over a long irradiation period. This was completed with two separate tests with a single source and detector in the CIRS Plastic-Water® phantom using the new OneTouch Readout System. The first tests were completed over 900 second dwell period with

the parallel MO*Skin*™ detector 20±0.5mm from the source and a readout every second, and the second test was completed over an 800 second dwell period with the circular MO*Skin*™ detector 15±0.5mm from the source and a readout every 5 seconds. The response over the entire period was analysed for each test and the capability of the different versions of detectors to accurately monitor the radiation over a long period was established.

3.3.1.4 Sensitivity of Readout System

To determine the sensitivity of the OneTouch Readout System several irradiations were completed with a MO*Skin*™ detectors in a solid water phantom. The identical irradiation test was completed over the lifetime of a single MO*Skin*™ detector with a Ir^{192} HDR brachytherapy source at St. George Hospital Cancer Care Centre. The source underwent a 30 second dwell time, 20±0.5mm away from the source giving a target dose of 95.1cGy, calculated from TG43 (22). Using the OneTouch System, a temperature compensation value and calibration value were determined to be -2.839 and 2.220±0.001mV/cGy respectively. 35 irradiations were completed and the dose readout was analysed to calculate the sensitivity of the system.

3.3.2 OneTouch Characterisation Tests

3.3.2.1 Anti-Annealing Compensation

The first set of tests completed involved an in depth look at the algorithms available on the OneTouch system through identical irradiations using different creep compensations calculations. The creep was demonstrated through 5 identical readouts with a treatment equivalent to a 10 second source dwell time using a Ir^{192} HDR brachytherapy source utilised at St. George Hospital Cancer Care Centre. The radiation absorbed was displayed directly after irradiation and 30 seconds post-irradiation. This was completed in open air environment with an estimated source

to detector distance of 10±1mm and using the Median3 algorithm, set as such due to the initial factory settings of the OneTouch Readout system. A temperature compensation value for the detector was determined through the OneTouch method discussed previously. The calibration value was inputted manually to be 1mV/cGy as a simple way of demonstrating the typical creep seen from MO*Skin*™ detectors. Two algorithm comparison tests were completed to determine the ideal calculation method to be used in clinical treatments. The first test was completed in an open air environment with a dwell time of 10 seconds and a 2 second readout with the Ir^{192} HDR brachytherapy source. Two MO*Skin*™ detectors that were individually calibrated for temperature, -2.666 and -2.679, but with a manual calibration value of 1±0.001mV/cGy. The dose value was recorded using the Standard, Average2, Min2, Median3 and Median4 algorithms with 5 repetitions. A second comparison test was completed using a CIRS Plastic-Water® phantom with a source to detector distance of 35±0.5mm and a dwell irradiation time of 60 seconds Ir^{192} HDR brachytherapy source. Based on the dwell time of the source, the target dose was calculated to be 62.24cGy from the TG43 formulation, with a source strength of 40700U and 3.5mm Ir^{192} source length (22). A temperature compensation factor and calibration value was calculated by the OneTouch system for a single detector, -4.406 and 2.134±0.001mV/cGy respectively. The detector was irradiated three times for the Standard, Median3, Median4 and Average2 algorithms with readout every 2 seconds. The exact point of dose measurement cut-off was analysed and compared between all algorithms. The threshold voltage readouts after this point were also recorded and evaluated to determine the ideal algorithm for clinical use. The normalised average of the difference in threshold voltage of each algorithm in open air and solid water phantom was compared.

3.3.2.2 Temperature Dependence of the OneTouch Readout System

To determine the accuracy of the temperature compensation factor in minimising voltage variation with temperature, a varying temperature source was utilised during irradiation. A current controlled heat plate or Peltier Cooling Plate was sourced from TE Technology® and characterised using varying voltages to create a temperature range of 25°C to 41°C. This simulates clinical temperatures used in treatment using the heat dissipation side of the plate, from calibrating at room temperature to recording in vivo dosimetry within the patient. The heat plate was characterised at the Centre for Medical Radiation Physics Lab at University of Wollongong with a 30 second wait period for the plate to reach thermal equilibrium. Once the heat plate response was analysed, the OneTouch System was tested at the Cancer Care Centre at St. George Hospital to see the response of temperature variations.

At St. George Hospital, several identical irradiations were completed on a MO*Skin*™ 2015 detector at varying temperature with a Ir^{192} HDR brachytherapy source. The detector was placed directly onto the heat plate and was approximately 5±1mm from the source, however due thickness of the detector there was an error in the source to detector distance. For calibration the detector was irradiated for a dwell time of 5 seconds, giving a target dose of 242cGy calculated using the TG43 formulation (22). The readout from the OneTouch system was set to every second, the 'creep-up' algorithm was Standard, and temperature compensation factor and calibration value were -2.556 and 2.365±0.001mV/cGy respectively. To determine the temperature compensation factor, the MO*Skin*™ detector was heated up for several seconds through supplying 5V through the heat plate. An initial irradiation was completed to warm up the detector from room temperature to the maximum temperature tested. Three dose readouts were taken at an initial room temperature of 19±0.2°C, at 40±0.2°C, at 36.5±0.2°C, at 29.8±0.2°C, at 24.4±0.2°C and at final room temperature of 18.4±0.2°C. A readout was also taken during the tem-

perature increase from initial room temperature to 40±0.2°C and the dose readout at 36.5±0.2°C was completed to simulate body temperature during *in-vivo* dosimetry. The dose recorded and increasing threshold voltage of the detector were then analysed and compared.

3.4 Results

3.4.1 MO*Skin*™ Tests

The calibration factor of the circular gate MO*Skin*™ detector using the CSDS readout, with four readings taken and the difference between initial and finial voltage threshold was calculated, is shown in Table 3.1.

Initial (V)	Final (V)	Difference (V)
14.517	14.665	0.148
14.662	14.812	0.15
14.809	14.953	0.144
14.949	15.095	0.146
Average		0.147 ± 0.004

Table 3.1: Threshold voltages of single circular gate MO*Skin*™ detector in solid water phantom to determine the calibration factor

The error for the average threshold difference value was determined using the Student's t-test and was calculated to 3 degrees of freedom at a 95% confidence level, giving a t value of 3.182. A 95% level of confidence is an accepted amount of error, giving a coverage factor of 2 (50). Using the TG43 formalisation, see equation 2.2, the dose of a Ir-192 source 15mm away from the detector was determined to be 56.1cGy for a 10 seconds irradiation time. The calibration factor was determined to be 2.62 ± 0.07 mV/cGy and was adjusted to be 2.45 ± 0.07 mV/cGy due to decrease in sensitivity drift over the detectors lifetime, described in chapter 5 through equation 5.1.

The results of the angular test using the gel prostate phantom are shown in table 3.2 and dose rate was determined from the adjusted calibration value. As the source was stepped away from the detector in the centre of the phantom the dwell times increased and the dose rate decreased at the two furthest ends of the catheter due to the inverse square law.

Position (mm)	Dwell Time (s)	Threshold Difference (V)	Experimental Dose Rate (cGy/s)	TG43 Dose Rate (cGy/s)
96	120	0.057	0.194±0.005	0.206
119	90	0.106	0.480±0.013	0.459
142	30	0.106	1.1440±0.040	1.413
165	10	0.096	3.922±0.109	3.896
188	30	0.106	1.440±0.040	1.413
211	90	0.099	0.448±0.013	0.459
234	120	0.060	0.204±0.006	0.206

Table 3.2: Angular dependence of single circular gate MO*Skin*$^{\text{TM}}$ detector in gelatine phantom

The predicted dose rate was calculated using TG43 formalisation and compared to the data collected from the gel phantom. The angular dose readout ranges for MO*Skin*$^{\text{TM}}$ Detectors are within ±60° from central axis; the results shown in figure 3.7 show a normalised dose response of 1.015±0.007 within the accepted range of ±5% of the treatment plan dose (50)(52).

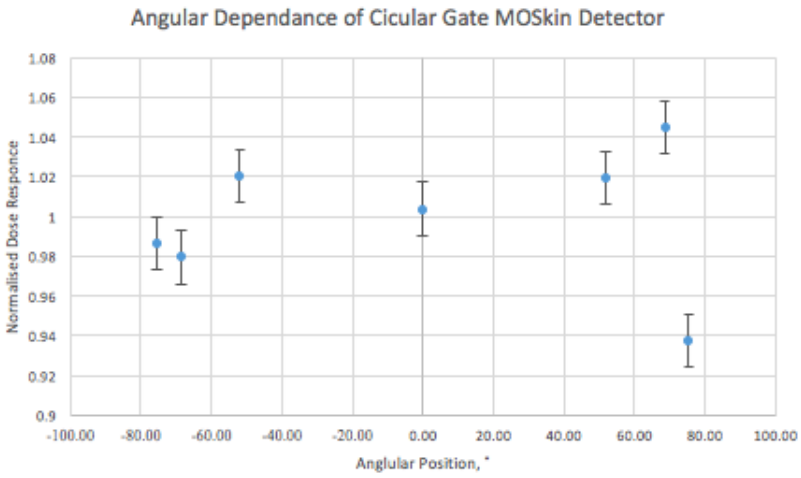

Figure 3.7: Comparison of agreement between experimental dose rate from circular gate MO*Skin*$^{\text{TM}}$ detector, normalised using the dose rate calculated using TG43 formalisation, in a gel phantom

In figure 3.8 the readout of the parallel gate MO*Skin*$^{\text{TM}}$ is shown from the One-Touch System over an irradiation dwell period of 900 seconds and a readout period of 1 second. The threshold differences are displayed over the treatment period with increasing readout dose. A slight decrease in response over the entire irradiation can be seen. The sensitivity drift of the readout system over this time was -0.0003±0.001mV/cGy.

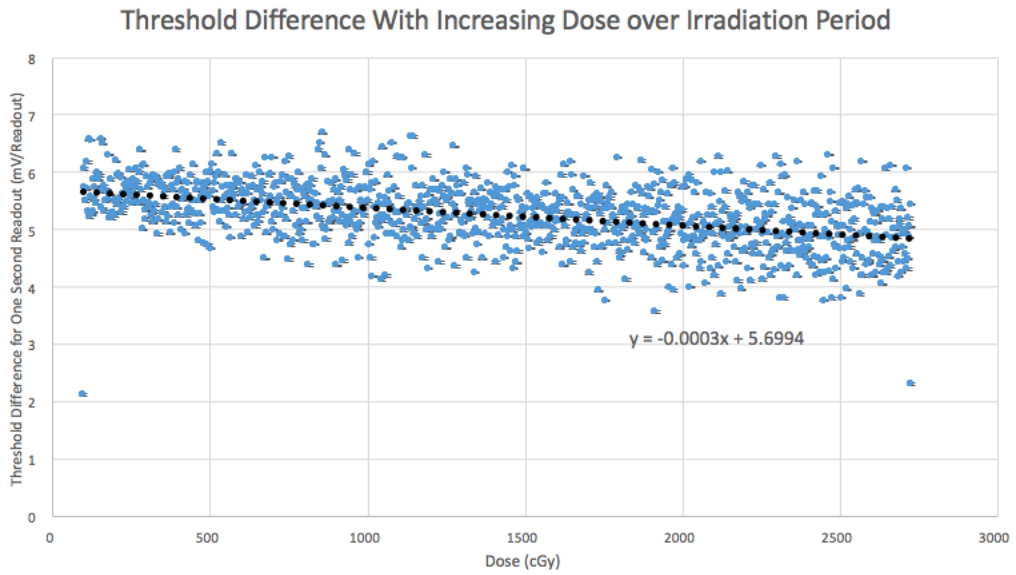

Figure 3.8: Threshold voltage difference over 900 second dwell time acquisition utilising the parallel gate MO*Skin*$^{\text{TM}}$ detector, readout every second

In figure 3.9 the data over an 800 dwell period with the newest model of detector, circular MO*Skin*$^{\text{TM}}$, is shown with a readout every 5 seconds design. The sensitivity drift of the detector was calculated to be -0.0012±0.005mV/cGy for every 5 readouts or -0.00025±0.002mV/cGy.

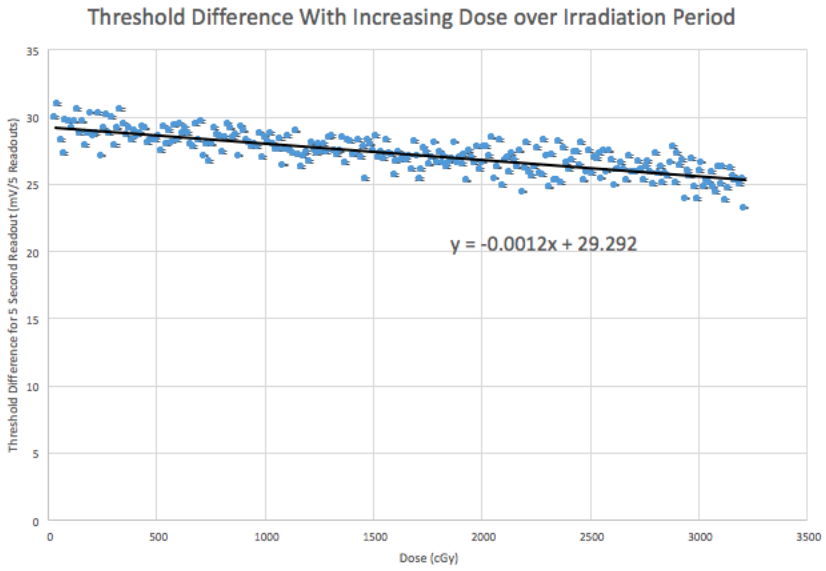

Figure 3.9: Threshold voltage difference over 800 second dwell time acquisition utilising the circular gate MO*Skin*$^{\text{TM}}$ detector, readout every 5 seconds

The total irradiation dose for each test was 3222.86cGy for 800 second dwell period and 2631.481cGy for 900 second dwell period, giving a sensitivity drift of -28.24±1.19% and -8.41±0.67% for the parallel and circular gate MO*Skin*™ respectively. Comparing the sensitivity drift response as well as the data from the angular testing, a comparison can be made between the parallel and circular versions of the MO*Skin*™ detector.

3.4.2 OneTouch Readout System Tests

The first section of experiments analysed the radiation creep and the available anti-annealing algorithms in the OneTouch Readout system. The first test was to display the anti-annealing phenomenon present in MO*Skin*™ detectors, which is shown in figure 3.10. The average decrease in dose readout was 2.51±0.21cGy within a 30 second period. A decrease was also seen between the final readout and the initial readout of the next irradiation test.

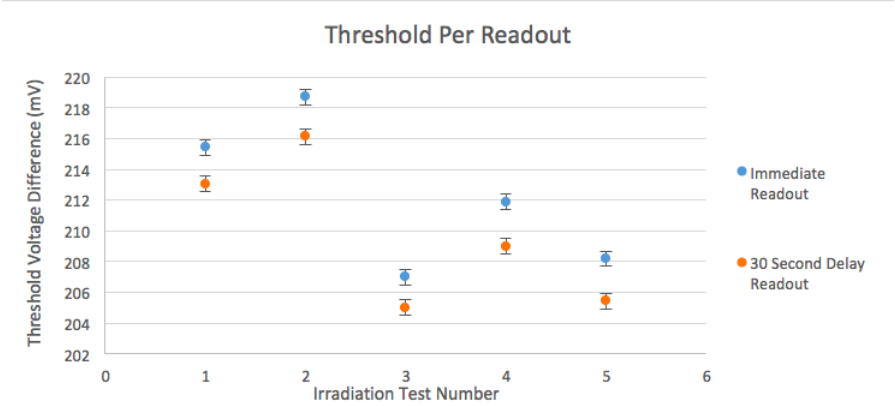

Figure 3.10: Demonstration of radiation creep or anti-annealing of MO*Skin*™ detectors

Using the four different algorithms available in the OneTouch system, two test were completed, one in air shown in figure 3.11 and one in a CIRS Plastic-Water ® phantom shown in figure 3.12.

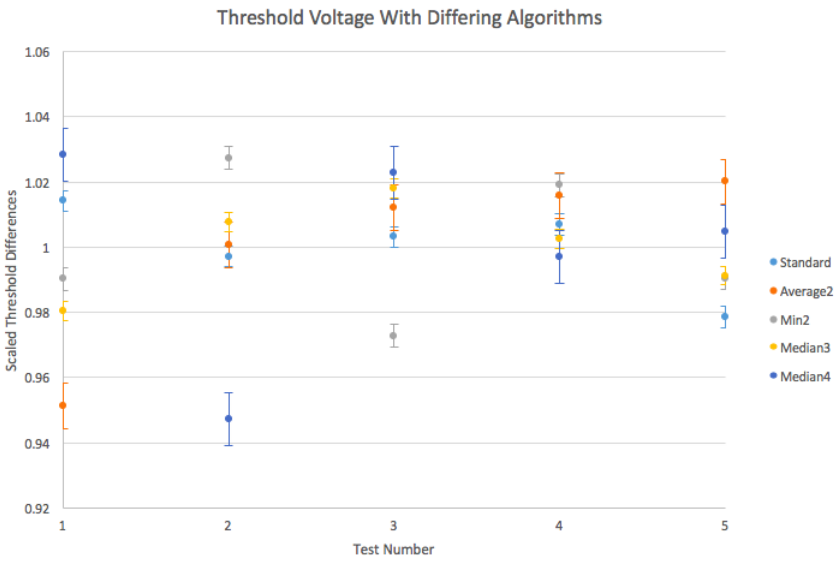

Figure 3.11: Comparison of the normalised threshold difference of anti-annealing algorithms when radiation dose measurement was completed in an open air environment

The threshold difference was recorded every two seconds and the data was analysed once the OneTouch system had stopped recording the irradiated dose. Each algorithm was normalised to the average of the three identical irradiations for each algorithm and were able to be compared to each other. The most ideal algorithm to be used in a clinical situation would be the algorithm that produces the most consistent readings during identical irradiations.

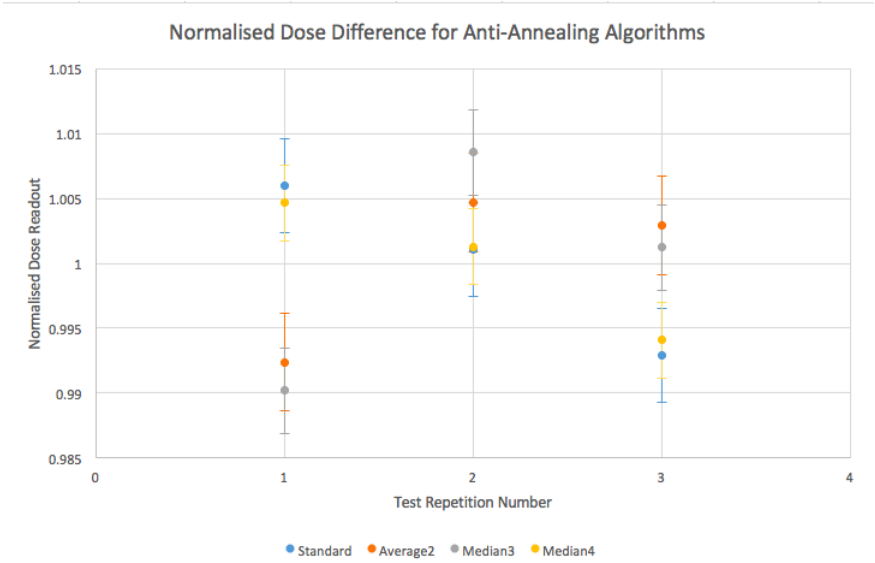

Figure 3.12: Comparison of the normalised dose readouts of anti-annealing when radiation dose measurement was completed in a solid plastic phantom

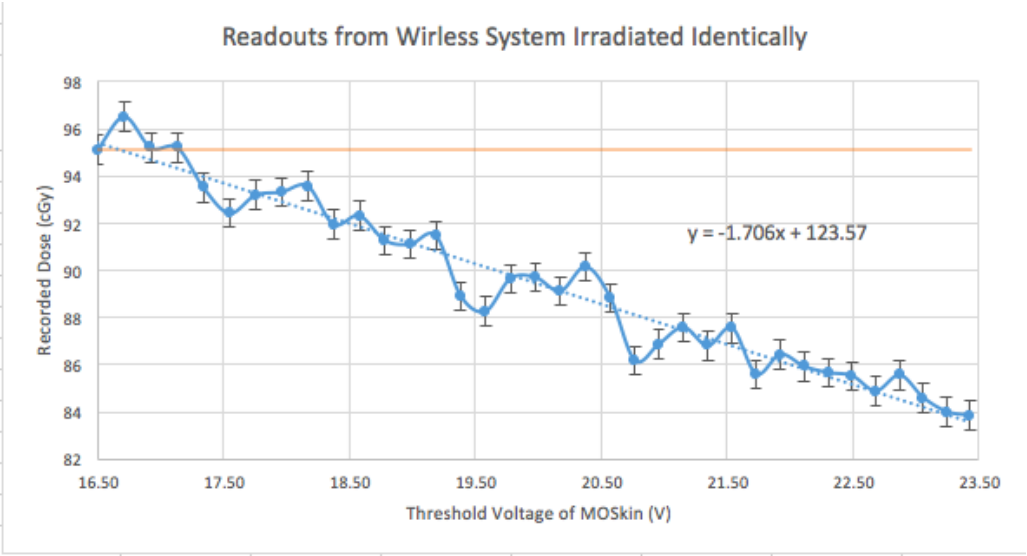

Figure 3.13: Measurement of sensitivity of OneTouch system over the lifetime of a MO*Skin*$^{\text{TM}}$ dosimeter

The sensitivity irradiation test completed by irradiating a single detector many times is displayed in figure 3.13, showing a slight decrease in response over the entire period. The orange line displayed the predicted dose value determined through TG43 (22) to be 95.1cGy and the blue line shows the 35 irradiations over the life

of the detector. The sensitivity drift of the readout system was determined to be -1.706±0.195cGy/V or -1.79±0.35%/V.

To accurately determine the validity of the temperature compensation factor, a TE Technology® Peltier Cooling Plate was used to manipulate the temperature of the MO*Skin*™ detector. In figure 3.14 the temperature response with increasing voltage is shown with an average increase of 0.52±0.05°C/ 0.1V. The dose response will be analysed in terms of voltage increase, rather than actual temperature, due to the OneTouch compensation calculation completed using voltage variations.

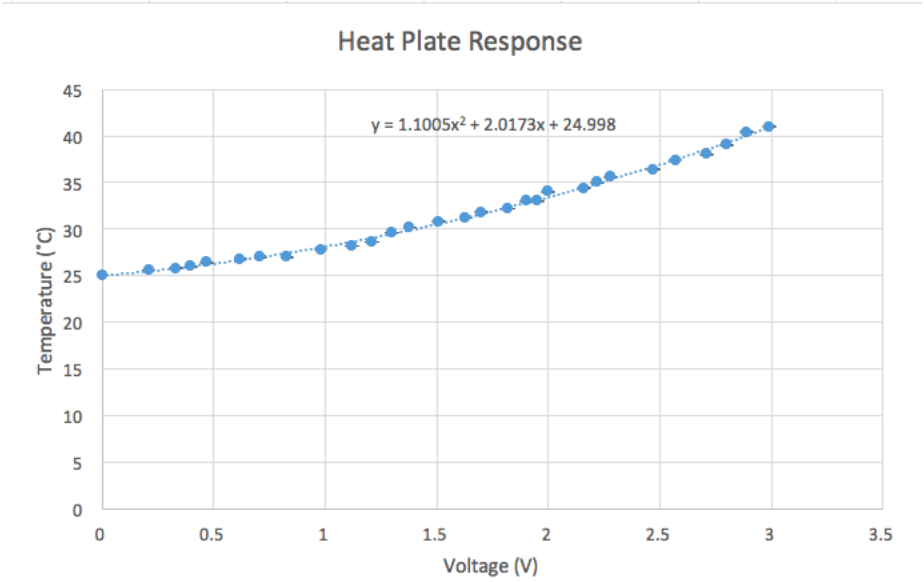

Figure 3.14: The temperature response of the TE Technology® Peltier Cooling Plate with varying input voltage to be used in future OneTouch temperature variation experiments

At St. George Hospital's Cancer Care Centre, identical irradiations were completed at varying temperatures and are shown in table 3.3, with the initial and final readouts completed at room temperature with no voltage applied to the heat plate. Due to sensitivity drift over the lifetime of the detector, the calibration value was adjusted for each irradiation using 4.1.

Temperature (°C)	Readout 1 (cGy)	Readout 2 (cGy)	Readout 3 (cGy)
19	227.06	229.32	229.65
40.4	221.43	219.98	217.82
36.5	218.45	218.70	217.74
29.8	213.42	212.40	212.40
24.4	213.45	209.11	209.28
18.4	206.26	209.63	210.57

Table 3.3: Adjusted dose readouts from varying temperatures applied by TE Technology® Peltier Cooling Plate to a MO*Skin*™ detector

The adjusted dose throughout the test is shown in figure 3.15, highlighting the decrease in MO*Skin*™ Detector sensitivity throughout its lifetime or sensitivity drift, identified through threshold voltage. The sensitivity drift with the varying temperature changes was determined to be -2.57±0.7cGy/V or 1.13±0.13%/V.

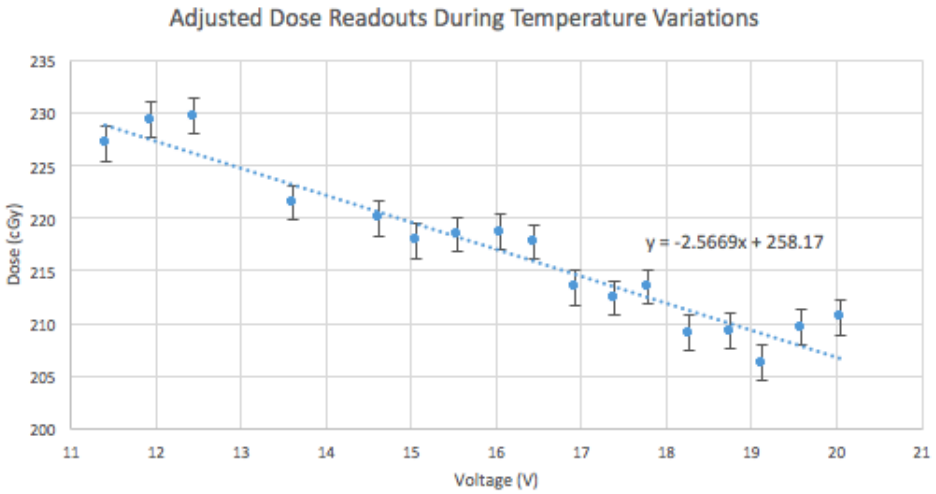

Figure 3.15: Increasing threshold voltage of MO*Skin*™ detector compared to adjusted dose readout during varying temperature changes with identical irradiations

The Vtavg and voltage from temperature change, V_{vt}-V_c, was also analysed for each test to determine if the temperature calibration factor was sufficient to account for any temperature change. In figure 3.16 this comparison is shown during an irradiation were the temperature was constantly increasing.

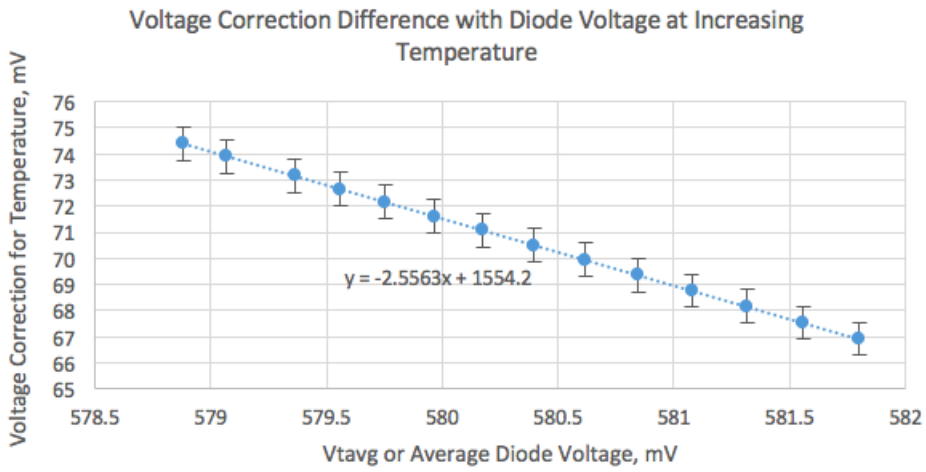

Figure 3.16: Voltage from temperature change only and diode voltage during an irradiation with increasing temperature from initial room temperature

Through these measurements, we are able to discuss the validity of the OneTouch Readout System to be used as a clinical *in-vivo* dosimetry system with MO*Skin*™ Detectors.

3.5 Discussion

Through the many experiments completed in this chapter, the characteristics of the OneTouch Readout System was understood and the circular gate MO*Skins*™ detectors were compared to previous versions. The response of the circular MO*Skin*™ with angular variation and sensitivity was shown to give better dose response compared to the parallel gate generation. It was determined that the circular generation detector was a superior dosimeter and utilised in further testing with readout systems. The OneTouch system, with single-irradiation calibration method and temperature compensation settings, was proved to effectually transmit dose information wirelessly throughout treatment to accurately verify the dose.

The dose response of different generations of MO*Skin*™ dosimeters was investigated through angular dependence and sensitivity tests. An understanding was also

gained into the equipment and methods available during clinical HDR brachytherapy, which will be applied in later tests for this thesis. A calibration factor is calculated for each individual MO*Skin*™ detector before clinical readout to determine the accurate dose value and to account for any dose dependence (24). The calibration factor for the detector used in the angular experiments was 2.45 ± 0.07 mV/cGy and is in agreement with previous MO*Skin*™ calibration values, such as Alnaghy, S. (2014) value of 2.45± 0.02 mV/cGy (47).For the calibration of the sensitivity tests, the value was calculated using the OneTouch Readout System. The calibration values for the parallel generation was 2.220±0.001mV/cGy and for the circular generation was 3.08±0.001mV/cGy.

A test was completed to investigate the angular dependence of the new circular MO*Skin*™ detector, which was designed to minimise the errors caused by differing angular position. The dose rate at different positions in a gel phantom is shown in figure 3.7, which compares the data obtained in the experiment to the dose distribution calculated using the Task Group Number 43 formalisation shown in equation 2.2. The response of the MO*Skin*™ detector is accurate within ±60° from central axis; outside of this range the dose response becomes non-linear (44) (42). The photon energy of Ir-192 is 400keV, which gives a very strong dose close to the source but is quickly attenuated within the medium. Due to the inverse square law the dose recorded away from source should decrease rapidly with a change in angular and geometric position of the source.(19). The normalised dose response shown in figure 3.7 displays an angle from from -75° - +75° as the source was moves across the length of the phantom. The overall normalised dose response of the circular gate MO*Skin*™ had a largest error -7%, however the dose response with the accepted angular range showed an error of ±1.5%. The previous angular response of the parallel MO*Skin*™ was within ±2.5% (44)(45), highlighting the improvement in dose with angular position with the newer version of detector. There

is also the possible affect of temperature on the detector; the phantom was placed in a refrigerator until use and was at a very different temperature than the room temperature of the previous solid water phantom. Temperature dependence with MO*Skin*™ and how to compensate for these variations will be investigated in the next chapter.

Radio-sensitivity drift is the change in readout capabilities of the detector over it's lifetime, specifically the threshold voltage compared to the dose recorded from the detector. With MOSFET detectors the sensitivity decreases over the detectors lifetime due to the build-up of hole traps within the silicon-silicon oxide insulator interface (7). The detector has an initial threshold voltage to allow the semiconductor within the MOSFET to be activated; the threshold voltage increases from the base voltage as the detector is irradiated but this however the sensitivity drift of the device (44). From the two long irradiation tests the sensitivity drift was determined to be -0.0003±0.001mV/cGy over a 900 second dwell period for the parallel gate generation and -0.0012±0.005mV/cGy for every 5 readouts or -0.00025±0.002mV/cGy over an 800 second dwell period for the circular generation, as seen in figure 3.9 and 3.8. The circular MO*Skin*™ detector was seen to have a slightly better sensitivity compared to the parallel MO*Skin*™, due to the different gate design shown in figure 3.1. With the larger sensitive volume in the gate due to the circular electrode layout, the sensitivity of readouts is greater than previous parallel gate layouts. The total irradiation dose for each test was 3222.86cGy for 800 second dwell period and 2631.481cGy for 900 second dwell period, giving a decrease in -28.24±1.19% for the parallel MO*Skin*™ and -8.41±0.67% for the circular MO*Skin*™ respectively over the entire irradiation period based on the average readout dose.

The first test OneTouch characterisation test analysed the radiation creep phenomenon present in MO*Skin*™ detectors and the compensation calculations available in the system. This phenomena, referred to as drift, annealing or 'creep-up' in

literature (8)(51), is caused by the decay of additional system perturbation from the current used to readout the threshold voltage. This initially increases the apparent dose directly after irradiation that decays after a period of time, usually leading to a 2% error with typical clinical radiation dose of around 2Gy (48). In an in depth study completed by Ramani et. al. MOSFET detectors showed an increase of 4mV after an apparent dose of 0.04Gy that decayed completely after a period of 60 seconds. Since this investigation, irradiation readouts with MOSFET detectors are typically completed 30-60 seconds post-irradiation to allow for the 'creep-up' to decay and plateau (8)(47). This wait period after each irradiation is a disadvantage when using MO*Skin*™ detectors clinically and the OneTouch system includes calculations that aims to compensate for this phenomenon.

In figure 3.10 the decrease in threshold voltage after an HDR irradiation was shown through manual readout, with an average change of -2.51±0.21cGy or -1.18±0.10% in total dose value 30 seconds after irradiation, which is what is expected from previous MO*Skin*™ studies (47). The five different compensation algorithms that are available in the OneTouch system are Standard, Min2, Average2, Median3 and Median4. The aim of the characterisation tests was to determine the most reliable calculation to remove creep from dose calculations shortly after irradiation. Two separate algorithm experiments were completed, one in an open air environment and the second in a solid water phantom. The open air experiment was completed with a 1mV/cGy calibration value, allowing the final dose output to be directly compared to the change in threshold voltage readout every second. For each algorithm 5 tests were completed and compared to each through normalising the results to the average threshold voltage increase, shown in figure 3.11. Based on the average threshold differences, the deviations for each of the creep-up compensation algorithms in open air were Standard is 0.97±0.32%, Average2 is 2.22±0.70%, Min2 is 1.86±0.35%, Median3 is 1.13±0.29% and Median4 is 2.23±0.81%. The most repeat-

able algorithms were found to be Min2 and Median3, however every algorithm was within the ±5% acceptance limit used for radiation readouts (50)(52). However, errors from being completed in open air environment could have affected the readout results, especially from additional air attenutation and movement of the catheter during source movement. The second algorithm experiment was completed in a solid water phantom, which limited the errors from air attenuation and variations in source to detector distance during source movement. In figure 3.12 the normalised dose readouts results from three irradiations using Min2, Average2, Median3 and Median4 are shown and compared. The average deviation from the average dose readout for each of the creep-up compensation algorithms were 0.471±0.002% for Standard algorithm, 0.508±0.002% for Average2, 0.653±0.005% for Median3 and 0.40±0.39% for Median4. These results were very similar to each other and each algorithm was able to eliminate annealing in the readout data with no ideal algorithm determined. In future tests, the Standard algorithm is used due to performing well during the algorithm characterisation tests and it is the default setting for the OneTouch device.

The sensitivity drift test was completed with the OneTouch system through a multiple irradiation test with the 2015 MO*Skin*™ detector. The OneTouch system showed a decrease in sensitivity over the lifetime of the MO*Skin*™ detector, which is consistent with previous studies into MO*Skin*™ and MOSFET detectors (44)(7)(32). It was seen that the initial threshold voltage for the OneTouch system was less than previous systems, averaging 12V compared to 15V in previous systems due to the more stable electronics of the OneTouch system. As this region reaches saturation, the response of the detector becomes non-linear and the sensitivity of the dose readout decreases (39). In previous studies it has been suggested to recalibrate the MO*Skin*™ detector often to reduce the impact of absorbed dose sensitivity, creating a more linear response (32). The sensitivity of the readout is also

due to the electronics of the readout system; the OneTouch system will be further compared to the previous readout system in the next chapter in a clinical setting. The multiple irradiation test shown in figure 3.13 highlighted the sensitivity drift, with the change in dose over the lifetime of the detector being -1.706±0.195cGy/V or -1.79±0.35%/V with the OneTouch Readout System. This value is similar to previous studies utilising MOSFET and MO*Skin*™ detectors with varies kinds of radiation treatments; Safari et. al. found with megavoltage radiation an equivalent sensitivity drift of -1.5%/V and Hardcastle et. al. found a reproducible sensitivity of MOSFETs with fractionated radiation treatments between 2-10Gy to be 1% (7) (44). The previous readout system, the Clinical Semiconductor Dosimetry System (CSDS), had an average sensitivity drift of -1%/V, which is very similar to the OneTouch readout sensitivity (47). With this sensitivity analysis, the OneTouch system has shown to accurately readout the radiation dose within acceptable limits and the sensitivity drift can be compensated through the recorded data.

For the temperature experiment, a current controlled heat plate was used to manipulate the temperature of the detector and determine if the temperature change was compensated the readout results. In figure 3.14 the heat plate was characterised to show the relationship between input voltage and temperature using the same temperature readout device used in future clinical experiments. It showed the average temperature increase with voltage from room temperature was 0.52±0.47°C. At the Cancer Care Centre at St. George Hospital three readouts were taken at 5 different temperatures and a single readout during a gradual temperature increase; the different readout temperatures were at 40±0.2°C, 36.5±0.2°C, 29.8±0.2°C, 24.4±0.2°C and two room temperature readings, one at the being of the tests, 19±0.2°C, and one at the end,18.4±0.2°C. The change dose readouts with increasing threshold voltage is shown in figure 3.15, with a sensitivity drift of -2.57±0.7cGy/V or 1.13±0.13%/V. Using the OneTouch data from each readout we could determine the effect temper-

ature variation has on the voltage output of the detector over an irradiation and compensate for this effect.

The temperature calibration factor, C_T, was used to analysed the OneTouch Readout Systems ability to compensate for changes in temperature during irradiation and changes from initial calibration. 'Vt Avg' is the average value recorded from the V_{diode}max and V_{diode}min and is determined through the diode voltage between the bulk and the gate of the MO*Skin*^{TM} detector. The Vt Avg value compensates for changes in detector temperature from initial calibration temperature. The initial Vt Avg value at 19±0.2°C was 607.13±0.50mV, at 40±0.2°C was 545±0.45mV, at 36.5±0.2°C was 556.60±0.45mV, at 29.8±0.2°C was 574.30±0.47mV, at 24.4±0.2°C was 587.74±0.48mV and finally at 18.4±0.2°C was 605.54±0.50mV. From the experimental data it was determined that the voltage compensation within increasing temperature was -2.85±0.24mV/°C.

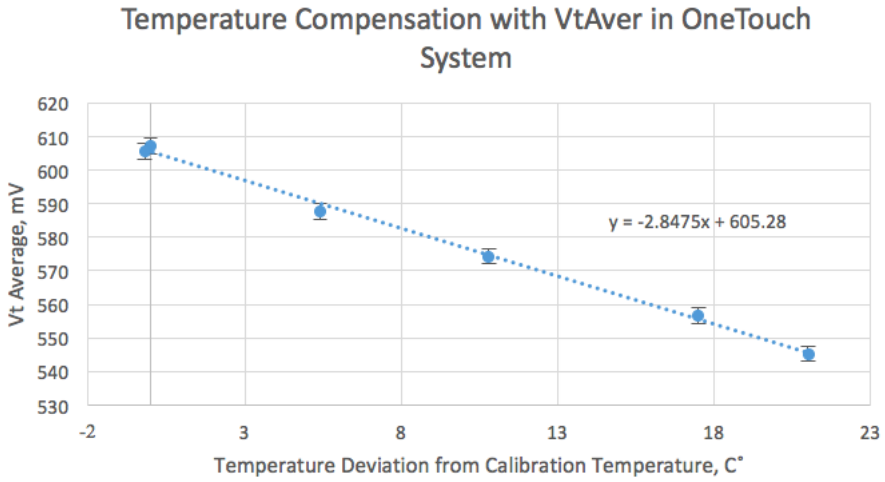

Figure 3.17: VtAvg values with temperature deviations from original calibration temperature

With a larger difference between the calibration and irradiated temperature, the Vt Avg value reduces to compensate for the increase in threshold voltage, which leads to a dose overestimation. To determine the accuracy of the temperature-only

voltage during each irradiation, the Vt Avg values and difference between original output and corrected voltage, V_{vt}-V_c, was analysed. The gradient of these changes was then compared to the temperature compensation factor determined at room temperature, -2.556, and the accuracy of the corrected voltage and dose outputs was analysed. Figure 3.18 shows the normalised agreement of the calibration factor at each temperature irradiation and the in depth comparison of temperature voltage with diode voltage is shown Section 7.2 of the Appendix.

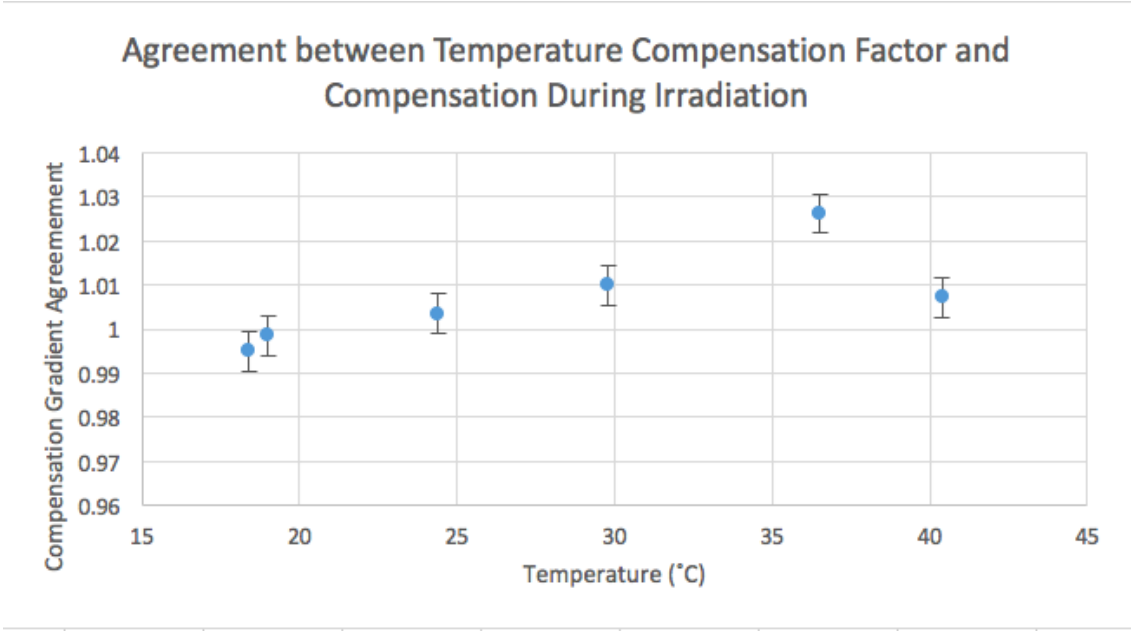

Figure 3.18: Comparison of temperature compensation at each temperature irradiation, determined through calculation of temperature voltage and diode Voltage, compared to original compensation factor

The average compensation gradient was 2.57±0.02 and the agreement over the temperature variation tests with this factor was 0.7±0.8%, showing the initial compensation factor as an acceptable value to limit the affect of temperature variation on dose readout. With the diode formed within the MO*Skin*$^{\text{TM}}$ detector, the voltage from temperature only can be calculated and account for in readout threshold voltage. Based on this analysis the OneTouch Readout System was successfully capable of compensating for MO*Skin*$^{\text{TM}}$ temperature changes.

From the above characterisation data, the OneTouch system and circular gate MO*Skin*™ detector was found to be a suitable readout equipment for clinical in vivo dosimetry for HDR brachytherapy, with acceptable sensitivity drift and temperature compensation capabilities. Further investigation between the previous readout system and the new wireless system as well as comparison between clinical dosimeters and MO*Skin*™ are discussed in the next chapter.

Chapter 4

In-Vivo Dosimetry for Clinical Use and Comparison Studies

4.1 Introduction

Through experimental research into the practical use of MO*Skin*$^{\text{TM}}$ dosimetry during brachytherapy treatments and the design of a new readout system, a clinical procedure was determined at St. George Hospital, Kogarah to integrate a brachytherapy dose verification system. In September/October 2016 St. George Hospital introduced Real-Time Ultrasound Planning, Oncentra Prostate (OCP) v4.2.2 (Elekta AB, Stockholm, Sweden), into HDR prostate brachytherapy treatments and an interest was also shown in integrating dosimetric verification with treatments. The HDR system used at St. George was HDR Nucleon remote afterloader (Nucletron, Veenendaal, The Netherlands). Several experiments were completed with the new equipment at St. George, along with the several kind of dosimeters and both generations of readout systems.

Two experiments were completed alongside St. George staff, one clinical simulation using the new treatment planning software as well as comparing readout systems,

and another to investigation dosimetric integration during treatment through a comparison between MO*Skin*™ detectors and other clinical dosimeters. The first phantom experiment was a comparison test between the new OneTouch Readout System and the previous system, the Clinical Semiconductor Dosimetry System (CSDS). CSDS is operated through a manual readout, needing a connection between the detector in the brachytherapy suite and the readout machine in the control room, and an associated computer program showing the dose recorded graphically in real time. The expected total dose from the ultrasound treatment plan was compared to the recorded dose from the OneTouch system and CSDS system. The second experiment utilised two types of dosimeters to compare the effectiveness of the in vivo dosimetry of radiochromic film and MO*Skin*™ detectors. The readout system used for the the MO*Skin*™ detectors was the OneTouch Readout System, while the dose from the film determined after the experiment.

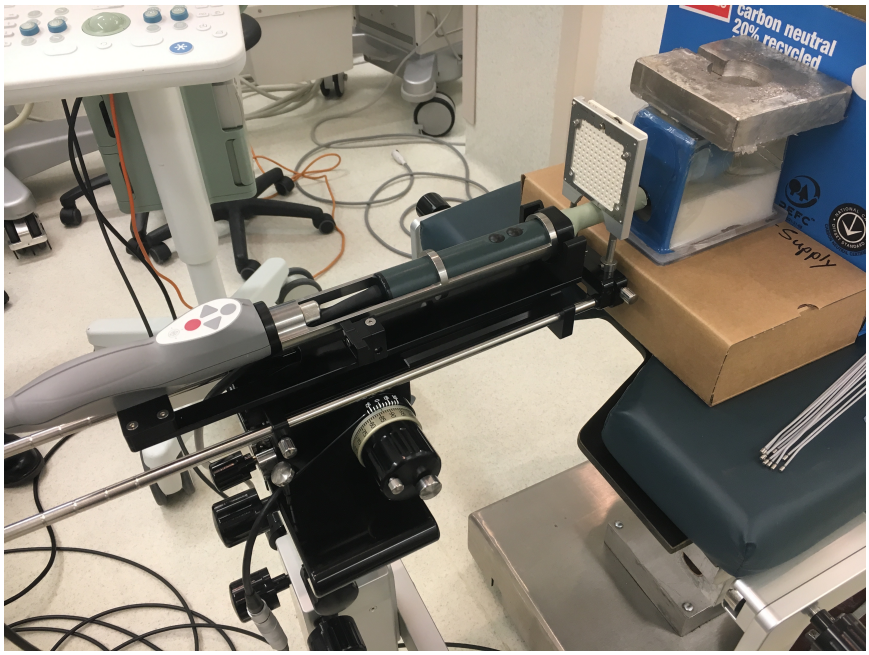

Figure 4.1: Real time ultrasound planning system with CIRS Ultrasound Prostate Phantom for quality assurance at St. George Hospital, Kogarah, before implantation of the phantom

was used during the both tests, which allowed the Medical Physicist to optimise the treatment plan using US images as the phantom was being implanted. A dual purpose probe was created by placing MO*Skin*^{TM} detectors and other detectors on top of the TRUS probe. The probe was placed in the rectum for the entire brachytherapy treatment to simulate the positioning within the patient during clinical treatment. After the completion of the initial experiment analysing the readout systems, an ethical write-up was requested to identify proper procedure and safety concerns of integrating the MO*Skin*^{TM} with the OneTouch Readout Program as a verification system for HDR prostate brachytherapy treatments. At the time of thesis submission, ethical approvals for patient trials at St. George Cancer Care Centre were still being completed.

4.1.1 CIRS Ultrasound Prostate Phantom

Computerised Imaging Reference System, Inc. developed a prostate phantom to be used specifically with ultrasound imaging, with the important structures created within the phantom such as seminal vesicles, urethra, prostate and rectum (53). This phantom was used at St. George Hospital to allow technicians and medical physicists to get used to the real time ultrasound planning system and during dose verification experiments.

The CIRS phantom is made out of Zerdine, a water-based polymer based off polyacrylamide, and was designed by CIRS specifically for imaging phantoms with MR, US and CT. The material was created based on characteristics of liver tissue and has changeable properties to reflect different organs within the body, such as speed of sound, acoustic attenuation and backscatter (54). Zerdine has similar density and atomic number to soft tissue, making it an ideal material for a prostate phantom (53). An ideal phantom must be water or tissue equivalent, meaning the substance must interact with radiation in the same way as a human patient does. An ad-

vantage of using a solid phantom compared to a water tank is organ contours can be created and analysed to determine any dosimetric affects that can be present in patients (55). The phantom must also be structurally strong to for different organs but flexible enough to allow for implantation of brachytherapy needles and mimic natural reactions of the implantation (56). The CIRS phantom, while expensive and can only be used during a single implantation, is very strong while malleable enough for needle implantation.

The radioactive brachytherapy isotope used at St. George Hospital is Ir^{192} and it interacts with the human body mainly through the Compton effect, which is dependent on the atomic mass of the material used in a phantom (4). Due to characteristics of Ir^{192} as a high energy source, the dose gradient is very steep and is diminished quickly due to the inverse square distance dependence of the source; therefore, the phantom needs to be able to mimic the radiation gradient in the human body in a reproducible manner (55).

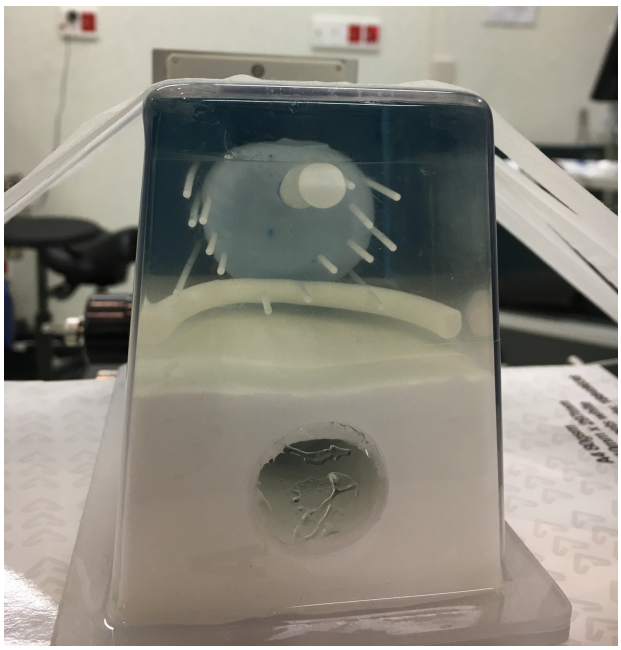

Figure 4.2: Implanted CIRS Ultrasound Prostate Phantom, Model 053

The phantom can simulate different soft tissues to allow for organ distinction

within different imaging modalities (56). The seminal vesicles and rectal wall have the same acoustic scattering properties and speed of sound, mimicking liver tissue, while the prostate is created to have high scattering. The urethra has low scattering and surrounding gel having similar properties to water (53). The CIRS phantom was determined to be ideal for the experimental tests that would be carried out during the setup of the new planning system and mock brachytherapy treatment.

4.2 Methodology

The experimental setup of the simulated prostate brachytherapy treatment was completed using a CIRS Ultrasound Prostate Phantom, Model 053, and real-time ultrasound system called Treatment Planning System (TPS) Oncentra Prostate (OCP) v4.2.2 (Elekta AB, Stockholm, Sweden) (57). The rectal ultrasound probe was transformed into a Dual Purpose Probe (DPP), similar to the probe used experimentally in Milan, Italy, by Carrara *et al.* (24) and Tenconi *et al.* (46), with three detectors placed on the ultrasound probe, shown in figure 4.3.

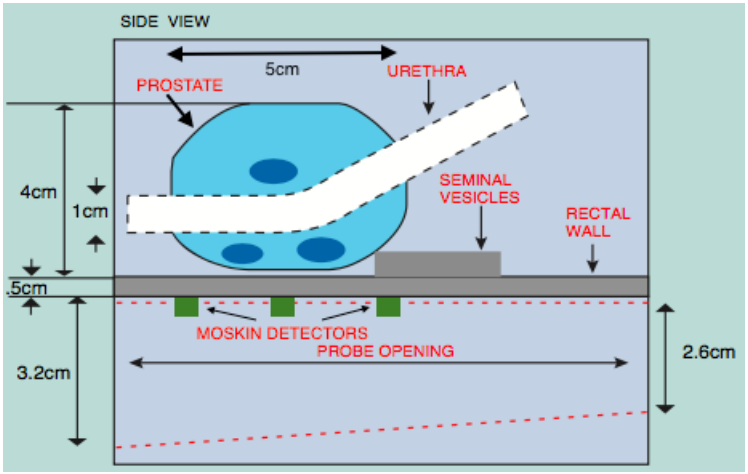

Figure 4.3: Simulated organs and dimensions of CIRS Prostate Phantom (58)

Using the treatment planning system, the total dose at the detector positions was calculated and was used as a point of comparison to the recorded doses by the

different readout systems and dosimeters. The prostate phantom was implanted by a medical physicist at St. George Hospital under ultrasound guidance and the treatment plan was optimised after each implantation. For the readout experiments, a condom was used to protect the detectors attached to the probe and for the dosimeter comparison experiments a rectal balloon was used, mimicking the clinical set-up for brachytherapy prostate treatments. The rectal probe was removed after implantation to attach the pre-calibrated detectors and was re-inserted in the prostate phantom, the same procedure that would be used in clinical situations.

4.2.1 Comparison of Two Readout Systems during Clinical Phantom Brachytherapy Experiment

4.2.1.1 MO*Skin*™ Calibration with Two Readout Systems

Before the readout systems could tested through a clinical HDR brachytherapy treatment, the detectors had to be checked for stability and calibration values had to be determine for both systems. Three MO*Skin*™ detectors were used during the simulated treatment but all available detectors had to be check for stability through determining that the voltage readout was stable for each detector. Each detector was connected to a readout system and a consistent threshold voltage was determined without irradiation. Each detector was then irradiated with Ir^{192} HDR brachytherapy source at St. George Cancer Care Centre, with the first irradiation ignored as a 'warm-up' as is typical practice with MO*Skin*™ dosimeters. To determine the calibration values and temperature compensation factor with the One-Touch System, the three detectors were irradiated separately for 20 seconds dwell time at 20±0.1mm away from the source in a CIRS Plastic-Water® phantom with the Standard algorithm to compensate for creep. The total dose for this irradiation calculated from TG43 Protocol was 63.397cGy, with a source strength of 40700U

and 3.5mm Ir^{192} source length (22). The Clinical Semiconductor Dosimetry System calibration value was determined from a single irradiation due to time constraints and was completed in the same set up as the OneTouch Readout System. In previous CSDS experiments the average of three manually readout irradiators were used to calculate the calibration value. Due to a miscalculation of needle position, the calibration values were adjusted for the second irradiation due to degradation of MO*Skin*™ dose readout response with use (44)(7)(32)(47).

$$C_{Eadj} = C_E - \frac{C_E \times S \times (V_{current} - V_{calibration})}{100} \tag{4.1}$$

The initial calibration values were adjusted due to the decrease in sensitivity of MO*Skin*™ detectors using equation 4.1. The adjusted value, C_{Eadj} was calculated from the original calibration value, C_E, using the previously determined sensitivity, S, of -1.79±0.35%/V as well as the threshold voltage before irradiation, $V_{current}$, and at calibration, $V_{calibration}$. The second, adjusted calibration values were used to accurately determine the total dose delivered to the three positions along the TRUS probe.

4.2.1.2 CSDS and OneTouch Readout Comparison Tests

After the calibration of each readout system and clinical treatment plan was completed, the DPP was re-inserted into the prostate phantom with a condom covering the probe to protect the three MO*Skin*™ attached. The detectors were placed along the probe in correspondence to the position of 0±0.5mm, 25±0.5mm and 50±0.5mm along the prostate length, with the apex of the prostate at 0mm shown in figure 4.4.

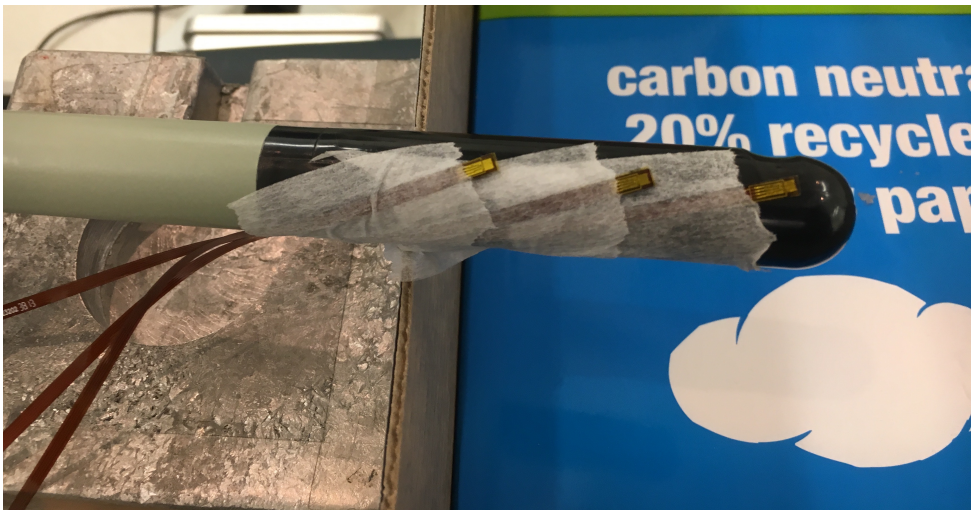

Figure 4.4: Transrectal ultrasound probe with three 2015 MO*Skin*^{TM} detectors attached for dose verification and real-time imaging

The experimental set up is shown below in figure 4.5 and the phantom was irradiated with a typical HDR brachytherapy treatment plan.

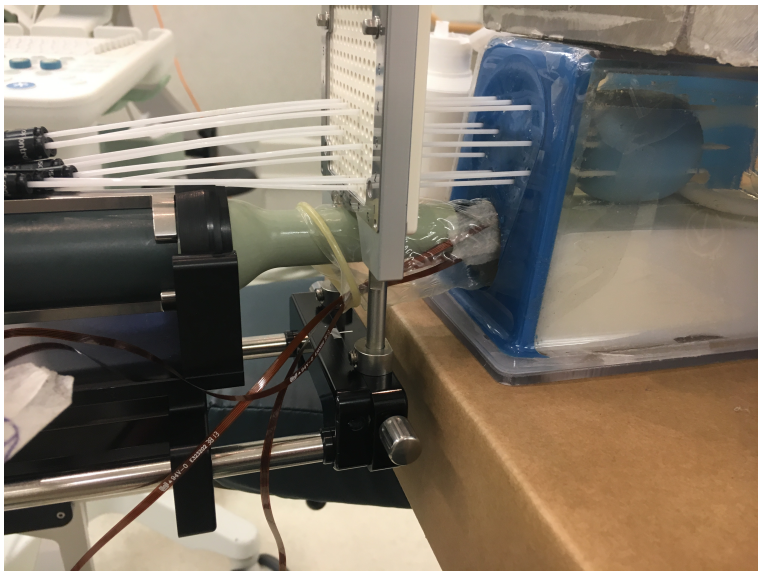

Figure 4.5: Ultrasound prostate phantom implanted with dual purpose probe and brachytherapy catheters

The treatment plan was the same for each readout system, Clinical Semiconductor Dosimetry System and OneTouch System. The older system needed to have the detectors connected directly to the readout system in the brachytherapy control

room, with three cords running directly from the room. The new OneTouch system required the transmitting unit to be within the room on the treatment bed while a USB receiver present in the treatment room was connected to a computer in the the brachytherapy control room.

The Clinical Semiconductor Dosimetry System required a manual readout of the threshold voltage for each detector and the dose recorded was calculated from the voltage increase and calibration value. Once the treatment was complete, the voltage reading was taken after a 30 second period, to compensate for 'creep-up' factors (8)(51). The OneTouch Readout System utilised it's computer program to determine the increase in dose and threshold voltage from treatment. The expected dose recorded by each detector was calculated by the Real-Time Ultrasound Planning System based on the ultrasound implantation images, optimised after the insertion of each needle.

4.2.2 Comparison of Three Dose Verification Dosimeters during Clinical Phantom Brachytherapy Experiment

4.2.2.1 Calibration of Dosimeters

Two types of detectors were used in the second experiment, Gafchromic EBT3 radiochromic film and MO*Skin*$^{\text{TM}}$ detectors. Film is very common in hospitals and are used verification purposes with many types of radiation treatments (35). Film is calibrated through irradiating film samples with known dose before treatment and the film used during simulation is compared of the calibrated samples after the experiment to determine dose. During each calibration test, the film and MO*Skin*$^{\text{TM}}$ detectors were placed in a solid water phantom with a 15±0.5mm source to detector distance. The dose was calculated through the TG43 Protocol with a source strength of 40700U and 3.5mm Ir^{192} source length for each calibration irradiation

(22). Three MO*Skin*™ detectors used in comparison tests were calibrated during a 10 second dwell time irradiation using the OneTouch Readout System with Standard algorithm. With a source strength of 40700U and 3.5mm Ir^{192} source length a dose of 56.13cGy dose was calculated through the TG43 formulation (22). The dose calibration value was repeated three times for each detector for accuracy. After the clinical experiments was completed, the calibration values were adjusted to compensate for decrease in sensitivity over the lifetime of the detector using equation 4.1 (44)(7)(32). The temperature compensation factor and initial compensation value for three MO*Skin*™ detectors were calculated to be -2.721 and 2.36±0.04mV/cGy, -3.047 and 2.24±0.03mV/cGy and -2.429 and 2.33±0.01mV/cGy. The film was calibration through irradiating nine separate samples of film with increasing dose from 1-9Gy in 1Gy increments using the Ir^{192} HDR brachytherapy source at St. George Cancer Care Centre. The film calibration and readout procedures were completed by the clinical staff at the hospital using clinical procedures; the results from the film as a comparison to the MO*Skin*™ detectors.

4.2.2.2 Film and MO*Skin*™ Comparison Tests

A single clinical treatment plan was completed using the Real-Time Ultrasound Planning system with 16 catheters and a rectal balloon filled with saline covered the TRUS probe and attached detectors. The treatment plan is shown in figure 4.6, with the planned dose percentages displayed over the ultrasound image of the prostate phantom.

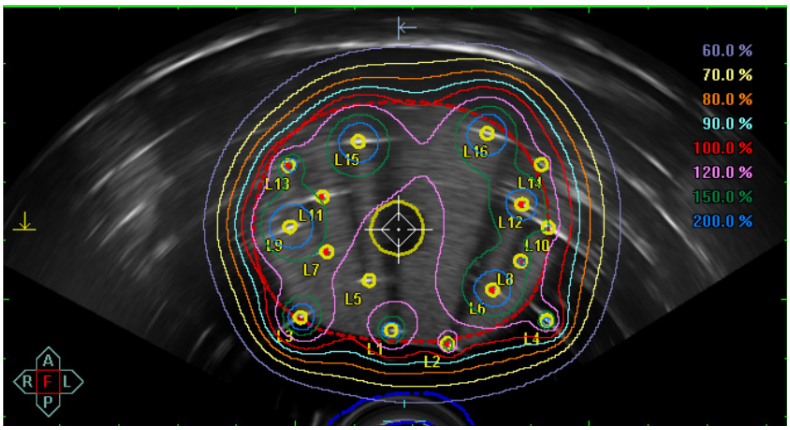

Figure 4.6: Real-time ultrasound treatment plan, Oncentra Prostate (OCP) v4.2.2 (Elekta AB, Stockholm, Sweden), used to compare irradiation doses from multiple dosimeters

Rectal balloons are used for all clinical HDR prostate brachytherapy treatments at St. George Cancer Care Centre to eliminate any air gaps around the rectal probe that could reduce the resolution of the ultrasound. The experimental set-up for the detector comparison tests is shown in figure 4.7.

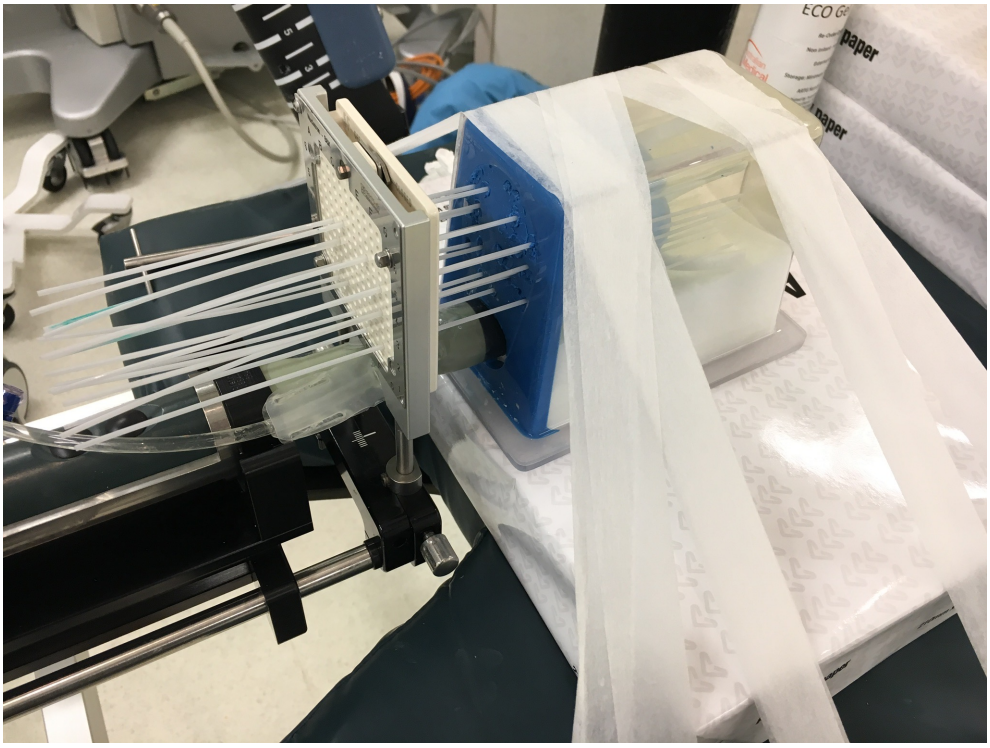

Figure 4.7: Experimental set-up of implanted phantom for HDR brachytherapy treatment with rectal balloon covering TRUS Probe

After all detectors were calibrated, the probe was removed from the phantom for attachment of detectors to create a dual purpose probe (DPP). The MO*Skin*™ detectors were attached to the probe in the same position as the readout comparison tests and were placed directly on top of the probe at 90°, using an indent in the rectal stepper as a guide. The first detector was positioned at apex of the prostate 0±0.5mm, the second in the middle at 25±0.5mm and third at the base of the prostate 50±0.5mm.

Once the probe was re-inserted into the simulation phantom and the plan was re-optimised, the MO*Skin*™ detectors were irradiated three times and the calibration values were adjusted with each irradiation. A piece of film of 10x80mm was wrapped around the TRUS probe and irradiated with a single treatment. This was repeated twice with separate film dosimeters and the dose at the three positions along the probe was analysed.

4.3 Results

4.3.1 Dosimetric Readout Comparison Experiments

The three MO*Skin*™ detectors were calibrated in a solid water phantom for each detector system, Clinical Semiconductor Dosimetry System and OneTouch System. The OneTouch System had an additional calibration value for temperature compensation, which are all shown in table 4.1. Two calibration values were determined, an initial value for the initial treatment plan and a second altered value for the second irradiation plan with an adjusted needle position.

	CSDS Calibration		OTRS Calibration		
	Initial	Adjusted	Temperature	Initial	Adjusted
Detector 1	2.57±0.02	2.52±0.02	-4.738	2.365±0.001	2.270±0.001
Detector 2	2.69±0.02	2.59±0.02	-3.027	2.426±0.001	2.195±0.001
Detector 3	2.73±0.02	2.63±0.02	-2.658	2.546±0.001	2.339±0.001

Table 4.1: Initial and adjusted dose calibration of clinical semiconductor dosimetry system (CSDS) and temperature compensation factor with initial and sensitivity altered dose calibration for OneTouch readout system (OTRS)

It was determined after the first two irradiations with each readout system that the positions of the needles were different to the outputted treatment plan, giving an under dose recorded by detector 1 and 2 and an over dose recorded by detector 3 for both systems. This indicated the catheters had shift positions to the posterior of the prostate after plan optimisation and before irradiation. The calculated treatment plan dose given to detector 1 was determined to be 289cGy, at detector 2 was 568cGy and at detector 3 was 379cGy. Because both readout systems displayed similar behavior from the three detectors, a second treatment plan was created through reoptimisation based on adjusted catheter positions and the detectors were irradiated again to investigate the irregular dose recordings.

	Detector One		Detector Two		Detector Three	
	CSDS	OTRS	CSDS	OTRS	CSDS	OTRS
Initial (V)	16.294	16.872	17.559	18.974	14.098	15.343
Final (V)	16.883	17.448	18.987	20.377	15.354	16.576
Difference (V)	0.589	0.576	1.428	1.403	1.256	1.233
Dose (cGy)	229.08 ±1.98	224.03 ±0.09	529.42 ±4.59	520.15 ±0.21	460.27 ±3.99	451.84 ±0.45
Agreement Comparison (%)	20.73 ±0.18	22.48 ±0.01	6.79 ±0.06	8.42 ±0.01	-21.44 ±0.19	-19.22 ±0.01

Table 4.2: Results from HDR brachytherapy treatment at position 1 of clinical semiconductor dosimetry system (CSDS) and OneTouch readout system (OTRS)

Each readout system was irradiated again and the calculated treatment plan dose at each detector was updated to 287cGy at detector 1, 554cGy at detector 2

and 395cGy at detector 3. The results from the readout systems are displayed in table 4.3 and were used to determine the ideal readout system to be used in clinical brachytherapy. For the OneTouch readout system two dose recording values were used, one for the dose recorded from the system interface shown in figure 3.3 and one calculated for the calibration value shown in table 4.1.

	Detector One		Detector Two		Detector Three	
	CSDS	OTRS	CSDS	OTRS	CSDS	OTRS
Initial (V)	17.705	18.195	20.929	22.201	17.265	18.033
Final (V)	18.43	18.827	22.341	23.410	18.237	18.889
Difference (V)	0.725	0.632	1.412	1.209	0.972	0.856
Dose (cGy)	287.28 ±2.49	278.41 ±0.12	543.35 ±4.71	550.75 ±0.23	369.02 ±3.20	366.01 ±0.14
Agreement Comparison (%)	0.09 ±0.01	-2.99 ±0.01	-1.87 ±0.02	-0.59 ±0.01	-6.86 ±0.06	-7.34 ±0.01

Table 4.3: Results from HDR Brachytherapy treatment at position 2 of clinical semiconductor dosimetry system (CSDS) and OneTouch readout system (OTRS)

Most of the dose recordings shown in table 4.3 were within the accepted percentage clinical value of ±5%, so the secondary treatment plan was deemed acceptable for a comparison between the two readout systems (50)(52). The agreement percentage between the readout and prescribed dose was -2.80±2.52% for the CSDS and -3.64±2.47% for the OTRS. The normalised agreement between the two readout systems and treatment plan dose is shown in figure 4.8 and was the average was calculated to be 0.97±0.03 for the CSDS and 0.96±0.02 for the OTRS.

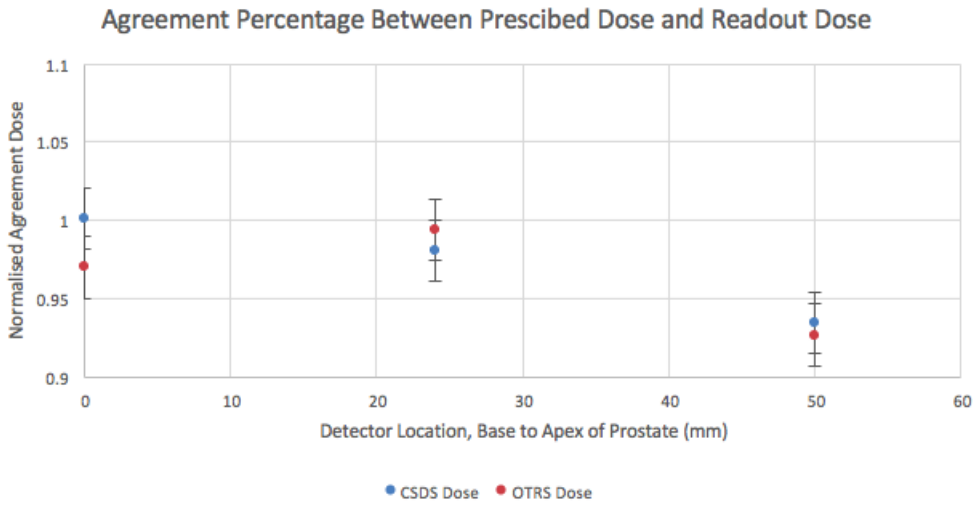

Figure 4.8: The agreement of clinical semiconductor dosimetry system (CSDS) Dose and OneTouch readout system (OTRS) dose compared with the Oncentra Prostate (OCP) treatment planning system

The OneTouch and CSDS showed similar and acceptable accuracy but some discrepancy could be possible due to slight movement of the probe during readout connection change. Due to the ease of use and acceptable results, the OneTouch system is capable of replacing the CSDS for clinical *in-vivo* dosimetry.

4.3.2 Dosimeters Comparison Experiments

For the second experiment, the CIRS phantom was re-implanted and a new treatment plan was created. Two dosimeters, radiochromic film and MO*Skins*^{TM}, were used for a dose response comparison from a clinical simulation treatment. The film was attached to the TRUS probe and two separate irradiations were completed. The dose was then determined at the three positions along the probe using the calibrated film samples and averaged to analyse the reliability of the dosimeter.

	Test 1 (cGy)	Test 2 (cGy)	Average Dose (cGy)
Detector 1	341.8	340.9	341.35±0.45
Detector 2	516.2	499.4	507.8±8.4
Detector 3	484.9	471.8	478.35±6.55

Table 4.4: Radiochromic film readouts from clinical HDR brachytherapy simulation

Three clinical treatment irradiations were completed with the MO*Skin*™ Detectors and the OneTouch Readout System. From the initial calibrations for the three detectors unique calibration values were calculated for each of the clinical irradiations using equation 4.1.

	Test 1 (cGy)	Test 2 (cGy)	Test 3 (cGy)
Detector 1	2.39±0.04	2.35±0.04	2.31±0.04
Detector 2	2.29±0.04	2.24±0.04	2.20±0.04
Detector 3	2.37±0.01	2.33±0.01	2.29±0.01

Table 4.5: Adjusted dose calibration for MO*Skin*™ detectors during each irradiation test to compensate for sensitivity drift

At the three positions along the DPP the dose was readout and averaged to determine the reliability of MO*Skin*™ detectors to be used as in vivo dosimeters.

	Location (mm)	Test 1 (cGy)	Test 2 (cGy)	Test 3 (cGy)	Average Dose (cGy)
Detector 1	0	409.2	407.2	403.8	406.7±2.9
Detector 2	25	509.9	512.5	508.6	510.3±2.4
Detector 3	50	431.7	436.4	433.0	433.7±2.4

Table 4.6: OneTouch Dose Readout from MO*Skin*™ Detectors Over Three Clinical Simulation Treatments

Using the ultrasound images from the Oncentra Prostate (OCP) system, the thickness of detectors was determined; the film was 0.15mm and the MO*Skin*™ was 1mm. The percentage dose relative to the prescription dose was then calculated using the treatment plan as well as the distance-to-agreement (DTA) for each point.

	Radiochromic Film			MO*Skin*™		
Dosimeter	1	2	3	1	2	3
Average Dose (Gy)	3.414 ± 0.045	5.078 ± 0.084	4.784 ± 0.066	4.046 ± 0.028	5.072 ± 0.023	4.313 ± 0.018
Relative Dose Percentage (%)	37.93 ± 0.05	56.42 ± 0.93	53.15 ± 0.73	44.96 ± 0.46	56.35 ± 0.40	47.92 ± 0.40
OCP Relative Dose Percentage (%) - 0.15mm for film and 1mm for MO*Skin*™	40.73	51.54	42.83	42.34	53.78	44.72
Distance to Agreement (mm)	1.5	1.75	3.9	1.3	0.9	1.3

Table 4.7: Comparison of radiochromic film and MO*Skin*™ detectors with the Ultrasound Planning Oncentra Prostate (OCP) relative dose and DTA

The response of the radiochromic film and MO*Skin*™ detectors analysed in terms of their agreement to the relative dose of the treatment plan, shown in figure 4.9. The normalised agreement based off the treatment planning dose of the film dosimeters was 1.10±0.01 and the agreement of the MO*Skin*™ detectors was 1.06±0.1.

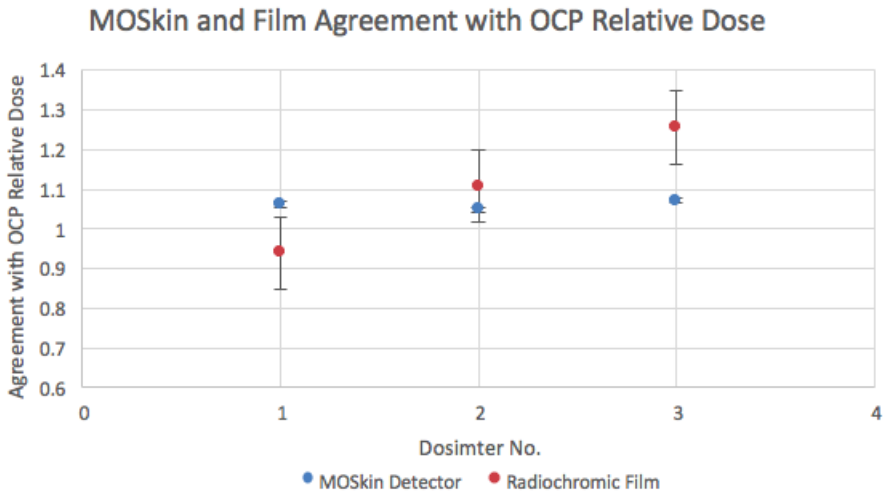

Figure 4.9: The Agreement of Radiochromic Film and MO*Skin*™ detectors with the Oncentra Prostate (OCP) Treatment Planning System

Based on the data from the two dosimeters used during the simulation treat-

ment, a direct comparison was made between two common clinical detectors and the MO*Skin*™ detector. The validity of using the MO*Skin*™ detectors for *in-vivo* dosimetry was then determined.

4.4 Discussion

High Dose Rate Brachytherapy currently has no routine *in vivo* system, leading to unknown errors and complications during treatment due to the high dose delivered in a very small region. A proposed verification system using MO*Skin*™ detectors have been researched previously, (46) (45) (24), however the calibration and readout methods have been problematic in clinical situations. MO*Skin*™ detectors themselves have many dependencies, such as temperature, that make them difficult to use for verification purposes. However, with a small sensitive volume and miniature size they are the most ideal detector to be used as an *in vivo* tool in a steep dose gradient region. The previous readout system utilised, Clinical Semiconductor Dosimetry System (CSDS), needed to be directly connected the detector, leading to many wires within the treatment room creating inconvenience for staff and a trip hazards. A new readout system, OneTouch, was developed by the University of Wollongong to correct for temperature and dose calibration in a single irradiation as well as transmitting the dose recordings wirelessly, limiting the disturbance within the treatment room. Two prostate treatment simulations were completed to compare the two treatment systems and investigate the reliability of the MO*Skin*™ detectors compared to other clinical detectors. These tests were able to determine if the OneTouch system and MO*Skins*™ were viable for treatment verification within a clinical setting. The simulation experiment was completed in combination with the St. George Cancer Care Centre staff to verify the new ultrasound TPS called Oncentra Prostate (OCP) v4.2.2.

The first experiment examined the readout capabilities of the new OneTouch System and the previous CSDS during clinical brachytherapy treatment. The dose recorded from the simulated treatment was completed twice due to noticeable errors from both readout systems. The expected treatment plan dose was calculated from ultrasound images taken with the OCP machine based on the geometrical position of anatomical landmarks. In table 4.2, the difference between the dose recorded and the treatment plan dose for detector 1 at position 0±0.5mm was 20.73±0.18% and 22.48±0.01%, detector 2 at position 25±0.5mm was 6.79±0.06% and 8.42±0.01% and detector 3 at position 50±0.5mm was -21.44±0.19% and -19.22±0.01% for the CSDS and OneTouch system respectively. Due to the similarity in errors the treatment plan was evaluated and re-calculated. It was determined that due to the implantation of the dual purpose probe after the treatment plan was calculated there was a shift in needle position, which affected the dose given to the detectors. The TPS OCP created a new expected treatment dose value from updated ultrasound images with the DPP implanted. Because of the time difference between the initial calibration calculation and the second simulation treatment irradiation, an adjusted calibration value was determined and used to calculate the recorded dose. The adjusted calibration values are shown in table 4.1 and the recorded data from the two readout systems is shown in table 4.3 and figure 4.8. The average difference between the treatment dose and recorded dose over all the detectors was 2.80±2.52%for the CSDS and 3.64±2.47% for the OneTouch system. The dose response from both systems were within acceptable limits, however the large error could be due to positional uncertainty during changing of readout connections. Because of the effect of inverse square distance on dose, a small positional difference could greatly effect the dose readout. The OneTouch system was more user-friendly with less interruptions to the clinical treatment room compared to the CSDS. The newer readout system also has accurate temperature compensation capabilities, which will be very

important in future patient studies.

The second experiment investigated the dosimetric potential of several detectors to be used for as an *in vivo* tool for clinical brachytherapy. Two detectors were analysed, one passive detector used commonly in radiotherapy treatments, radiochromic film, and one active detector, the MO*Skin*$^{\text{TM}}$ dosimeter. Film dosimeters require a lengthy calibration procedure to be completed before clinical testing, consisting of irradiating separate samples with known dose. Radiation dose can only be determined through a comparison of calibrated readouts after treatment. Radiochromic film uses radiosensitive dye that changes colour during irradiation and can be analysed through determination of optical density using a spectrophotometer (4). The film requires 24 hours to develop and dose to be readout (8). However, film is a very common type of detector, inexpensive and well understood in hospitals, making it a possible verification option for brachytherapy.

Before the clinical simulation tests were completed, the two types of detectors were calibrated in a solid water phantom. The MO*Skin*$^{\text{TM}}$ detectors were calibrated quickly using the OneTouch system, automatically determining the value after a single irradiation. The calibration values were adjusted for each irradiation test to account for the decrease in sensitivity through equation 4.1 and are shown in table 4.5. Each detector was then irradiated with the same clinical treatment plan determined using the OCP treatment planning system. The dosimeters were placed on the transrectual ultrasound (TRUS) probe, creating a dual purpose probe. A saline-filled rectal balloon was placed over the TRUS probe to mimic the clinical procedure during prostate brachytherapy. The small additional distance between the rectal wall and the dosimeters with this setup meant the rectal wall dose could not be analysed due to the steep dose gradient and the inverse square law. However, using the ultrasound images the thickness of the dosimeters was determined and the relative dose at the locations along the probe was calculated. The *in-vivo* dosimetric

capabilities of the detectors was directly compared to the expected relative dose and the DTA. The radiochromic film recorded average doses of 341.34±0.45cGy at position 1, 507.80±8.4cGy at position 2 and 478.35±6.55cGy at position 3. The average dose readout from the MO*Skin*™ detectors along the rectal probe was 406.7±2.9cGy at position 0±0.5mm, 510.3±2.4cGy at position 25±0.5mm and 433.7±2.4cGy at position 50±0.5mm. In table 4.7 the calculated relative dose percentage for each of the detectors is shown and was directly compared to the expected percentage from the OCP system. The DTA was also calculated and was within acceptable limits, <3mm, for both detectors; the average DTA for the radiochromic film was 2.4±1.0mm and for MO*Skin*™ was 1.2±0.2mm. The normalised agreement for the dosimeters was 1.10±0.01 for film and 1.06±0.1 for MO*Skin*™ detectors. With a closer agreement to the treatment plan relative dose and lower DTA, MO*Skin*™ detectors show superior *in vivo* dosimetry capabilities compared to traditional clinical dosimeters. The MO*Skin*™ detectors and OneTouch Readout System was utilised in an ethics proposal to implement a verification procedure during HDR prostate brachytherapy treatments.

Chapter 5

Conclusion

High dose rate (HDR) brachytherapy treatments utilise concentrated radiation dose using sources implanted directly into the tumour and currently there is no clinically accepted method to verify the treatment dose as the prescribed dose. This thesis focuses on investigating an accurate method for determining the in vivo treatment dose during prostate brachytherapy and evaluating the most equipment for real-time readout. The MO*Skin*$^{\text{TM}}$ detector and OneTouch Readout System, both designed by the Centre for Medical Radiation Physics at the University of Wollongong, were tested and utilised as a proposed verification method to be used during prostate brachytherapy treatments at the St. George Cancer Care Centre, Kogarah.

A new generation of MO*Skin*$^{\text{TM}}$ detectors was created in to account for angular dependence and improve sensitivity with circular electrodes. Angular and sensitivity testing was competed and compared to the previous parallel gate detector to determine ideal version to be used in verification testing. The average normalised agreement at the different angular positions the circular gate MO*Skin*$^{\text{TM}}$ dosimeter was calculated to be 1.015±0.007; the angular dose of MO*Skin*$^{\text{TM}}$ detectors produce a linear response within the range of ±60° from central axis. The parallel gate MO*Skin*$^{\text{TM}}$ detector was irradiated over an 800 second dwell period with a

-28.24±1.19% sensitivity drift. The circular MO*Skin*™ had a -8.41±0.67% sensitivity drift over a 900 second dwell period irradiation. With better sensitivity and acceptable angular dependence, the circular gate MO*Skin*™ was utilised to perform *in-vivo* dosimetry during brachytherapy simulations.

Characterisation testing of the new wireless OneTouch system was completed to determine the sensitivity of the system, the creep-up minimisation capabilities and the temperature compensation with readout dose. The 'creep-up' phenomenon was displayed through a decrease in dose of -2.51±0.21cGy over a 30 second period directly after radiation was stopped. The reliability of available anti-annealing algorithms was being calculated to be 0.471±0.002% for Standard algorithm, 0.508±0.002% for Average2, 0.653±0.005% for Median3 and 0.40±0.39% for Median4 algorithm. Due to the similarity in results there was no conclusive ideal algorithm and the factory standard was chosen to be used in future testing, Standard algorithm.

The sensitivity of the system was investigated over 35 identical irradiations and the response of the OneTouch Readout System was seen to be -1.706±0.195cGy/V or -1.79±0.35%/V. Sensitivity was also analysed during with the detector at different temperatures, showing a decrease of –2.57±0.7cGy/V or 1.13±0.13%/V. The sensitivity response of the MO*Skin*™through the OneTouch system was within acceptable limits and could be account for in future testing.

The temperature compensation capabilities of the system were also tested through dose readout at various temperatures. A diode voltage is determined within the MO*Skin*™ detector that changes solely with temperature and was used to determine the impact of temperature on voltage output during irradiation. The temperature-only voltage during irradiation was calculated and analysed to determine the successfulness in accounting for the temperature variations. The average normalised agreement of experimental calibration compensation value was calculated to be

1.007±0.008 and the diode voltage was seen to accurately account for additional voltage from temperature. Based on the data from the characterisation tests, the OneTouch Readout System was determined to be within acceptable limits to be used for clinical verification procedures.

Clinical simulation tests were completed with a prostate phantom to determine ideal readout system and dosimeter for brachytherapy dose verification. The OneTouch Readout System and previous Clinical Semiconductor Dosimetry System (CSDS) were compared during a HDR brachytherapy simulation treatment using the Real-Time Ultrasound Planning Oncentra Prostate (OCP) System. The average difference between the treatment dose and recorded dose was 2.80±2.52%for the CSDS and 3.64±2.47% for the OneTouch system. The results from both readout systems were within acceptable range but due to the ease-of-use and temperature compensation capabilities, the OneTouch Readout System was seen to be the superior model. MO*Skin*™ detector was compared to a common clinical detector, radiochromic film, using the OCP system and clinical prostate phantom. The normalised agreement with the relative treatment plan dose was 1.10±0.01 for film and 1.06±0.1 for MO*Skin*™ detectors. Through these clinical simulation test, the MO*Skin*™ detector was seen to be the superior dosimetry for *in-vivo* testing and the OneTouch system had a higher reliability with readout due to the lower error and dose recordings were within acceptable limits.

Due to the acceptable results from the MO*Skin*™ detector and OneTouch Readout System, an ethics proposal was submitted to the St. George Hospital, Kogarah. In the future patient testing will be completed to determine accuracy and feasibility to complete the verification procedure during HDR prostate brachytherapy treatments. A new software interface for the OneTouch system is also being designs as well producing a repeatable method for performing the temperature compensation without human contact.

Chapter 6

Future Studies

The clinical simulation results in Chapter 4 of this thesis were published as an abstract at the 26th Annual Scientific Meeting of the Australia Brachytherapy Group in February 2017 (57). The abstract was submitted by the St. George Cancer Care Centre Team to demonstrate the validity of the new treatment planning system, Oncentra Prostate (OCP) v4.2.2, as a real time TPS. The extensive quality assurance discussed was featured the OneTouch system results performed in the above tests to verify the geometrical accuracy of the OCP system as well any isodose distribution discrepancies. It stated the OCP TPS was safe for clinical use and is currently being used at St. George Hospital in prostate brachytherapy treatments.

To implement the OneTouch Readout System with MO*Skin*$^{\text{TM}}$ detectors as a dosimetric verification system for HDR brachytherapy treatments, an ethical write-up was completed and submitted to the St. George Hospital during mid 2017. The ethics approval of the proposed procedure is still being assessed at the time of thesis submission. Once approval patient trails will begin with performing dose verification during prostate brachytherapy treatments.

Bibliography

[1] R. Chen, Y. Horowitz, T. Kron, P.N. Mobit, P. Olko, A. Rosenfeld, G. Sandison, and M. Scholz. *Microdosimetric Response of Physical and Biological Systems to Low- and High-LET Radiations*. Elsevier B.V., Amsterdam, Netherlands, 2006.

[2] Australian Institute of Health and Welfare. Prostate Cancer Statistics, 2017.

[3] Olivier Chapet, Corina Udrescu, Marian Devonec, Ronan Tanguy, Marie Pierre Sotton, Ciprian Enachescu, Marc Colombel, David Azria, Patrice Jalade, and Alain Ruffion. Prostate hypofractionated radiation therapy: Injection of hyaluronic acid to better preserve the rectal wall. *International Journal of Radiation Oncology Biology Physics*, 86(1):72–76, 2013.

[4] Faiz.M Khan. *The Physics of Radiation Therapy*. John Wiley & Sons, Ltd, Philadelphia, Pennsylvania USA, 3rd edition, 2003.

[5] Peter Whelan, Ashutosh K. Tewari, and John D. Graham. *Prostate Cancer Diagnosis and Clinical Management*. John Wiley & Sons, Ltd, Somerset, NJ, USA, 2013.

[6] M Fatyga, J F Williamson, N Dogan, D Todor, J V Siebers, R George, I Barani, M Hagan, M Fatyga, J F Williamson, N Dogan, D Todor, J V Siebers, and R George. A comparison of HDR brachytherapy and IMRT techniques for dose escalation in prostate cancer : A radiobiological modeling study. *International Journal of Medical Physics Research and Practice*, 36(9):3995–4006, 2009.

[7] M J Safari, J H D Wong, K H Ng, W L Jong, D L Cutajar, and A B Rosenfeld. Characterization of a MOSkin detector for in vivo skin dose measurements during interventional radiology procedures. *International Journal of Medical Physics Research and Practice*, 42(5):2550, 2015.

[8] I S Kwan, D Wilkinson, D Cutajar, M Lerch, A Rosenfeld, A Howie, J Bucci, Y Chin, and V L Perevertaylo. The effect of rectal heterogeneity on wall dose in high dose rate brachytherapy. *International Journal of Medical Physics Research and Practice*, 36(1):224–232, 2009.

[9] Allen Chen, Srinivasan Vijayakumar, and Charles Thomas. *Prostate Cancer*. Demos Medical, New York, US, 2011.

[10] Byron Cannon and Richard Alder. Prostate Gland, 2013.

[11] Roger Kirby and Manish I Patel. *Fast Facts: Prostate Cancer*. Health Press Limited, Oxford, UK, 7 edition, 2012.

[12] Peter Metcalfe. Lecture Notes - Linear Quadratic Model: Radiotherapy Dose Fractionation. Technical report, CMRP, Faculty of Engineering and Informatics, University of Wollonong, 2014.

[13] David J B Benner and Eric J Hall. Fractionation and Protraction for Radiotherapy of Prostate Carcinoma. *International Journal of Radiation Oncology Biology Physics*, 43(5):1095–1101, 1999.

[14] Alan E. Nahum. The Radiobiology of Hypofractionation. *Clinical Oncology*, 27(5):260–269, 2015.

[15] David J. Brenner. Fractionation and late rectal toxicity. *International Journal of Radiation Oncology Biology Physics*, 60(4):1013–1015, 2004.

[16] Claudio Fiorino, Giuseppe Sanguineti, Riccardo Valdagni, and David J. Brenner. Fractionation and late rectal toxicity: No reliable estimates of α/β value for rectum can be derived from studies where different volumes of rectum are irradiated at different dose levels: In regard to Brenner [1] (multiple letters). *International Journal of Radiation Oncology Biology Physics*, 62(1):289–291, 2005.

[17] Simona Marzi, Biancamaria Saracino, Maria Petrongari, Stefano Arcangeli, Sara Gomellini, Giorgio Arcangeli, Marcello Benassi, and Valeria Landoni. Modeling of alpha/beta for late rectal toxicity from a randomized phase II study: conventional versus hypofractionated scheme for localized prostate cancer. *Journal of Experimental & Clinical Cancer Research*, 28(1):117, 2009.

[18] Susan L. Tucker, Howard D. Thames, Jeff M. Michalski, Walter R. Bosch, Radhe Mohan, Kathryn Winter, James D. Cox, James A. Purdy, and Lei Dong. Estimation of α/β for late rectal toxicity based on RTOG 94-06. *International Journal of Radiation Oncology Biology Physics*, 81(2):600–605, 2011.

[19] Piotr Wojcieszek and Brygida Białas. Prostate cancer brachytherapy: Guidelines overview. *Journal of Contemporary Brachytherapy*, 4(2):116–120, 2012.

[20] Adam P. Dicker, William Kevin Kelly, and Nicholas G. Zaorsky. *Prostate Cancer*. Demos Medical, New York, US, 2014.

[21] Ervin B. Podgorsak. *Radiation Physics for Medical Physicist*. Springer, Berlin, Germany, 1st edition, 2006.

[22] Mark J Rivard, Bert M Coursey, Larry A Dewerd, William F Hanson, M Saiful Huq, Geoffrey S Ibbott, Michael G Mitch, Ravinder Nath, Jeffrey F Williamson, and M Saiful Huq. Update of AAPM Task Group No. 43 Report: A revised

AAPM protocol for brachytherapy dose calculations. *International Journal of Medical Physics Research and Practice*, 31(3):2187–2205, 2004.

[23] W. R. Hendee, G. S. Ibbott, and E. G. Hendee. *Radiation Therapy Physics*. John Wiley & Sons, Ltd, Hoboken, New Jersey, 3 edition, 2005.

[24] Mauro Carrara, Chiara Tenconi, Giulio Rossi, Marta Borroni, Annamaria Cerrotta, Simone Grisotto, Davide Cusumano, Brigida Pappalardi, Dean Cutajar, Marco Petasecca, Michael Lerch, Grazia Gambarini, Carlo Fallai, Anatoly Rosenfeld, and Emanuele Pignoli. In vivo rectal wall measurements during HDR prostate brachytherapy with MOSkin dosimeters integrated on a trans-rectal US probe: Comparison with planned and reconstructed doses. *Radiotherapy and Oncology*, 118(1):148–153, 2016.

[25] Tania Simnor, Sonia Li, Gerry Lowe, Peter Ostler, Linda Bryant, Caroline Chapman, Dave Inchley, and Peter J Hoskin. Justification for inter-fraction correction of catheter movement in fractionated high dose-rate brachytherapy treatment of prostate cancer. *Radiotherapy and Oncology*, 93(2):253–258, 2009.

[26] Mira Keyes, Juanita Crook, W. James WJ Morris, Gerard Morton, Tom Pickles, Nawaid Usmani, and Eric Vigneault. Canadian prostate brachytherapy in 2012. *Canadian Urological Assosication Journal*, 7(February):51–58, 2013.

[27] Jesse N. Aronowitz. Afterloading: The technique that rescued brachytherapy. *International Journal of Radiation Oncology Biology Physics*, 92(3):479–487, 2015.

[28] Jesse N. Aronowitz. Introduction of transperineal image-guided prostate brachytherapy. *International Journal of Radiation Oncology Biology Physics*, 89(4):907–915, 2014.

[29] G. Kertzscher, A. Rosenfeld, S. Beddar, K. Tanderup, and J. E. Cygler. In vivo dosimetry: Trends and prospects for brachytherapy. *British Journal of Radiology*, 87(1041), 2014.

[30] Hossein Sadjadi, Keyvan Hashtrudi-Zaad, and Gabor Fichtinger. Needle deflection estimation: prostate brachytherapy phantom experiments. *International Journal of Computer Assisted Radiology and Surgery*, 9:921–29, 2014.

[31] N. Milickovic, I. Nikolova, N. Tselis, H. a. Azhari, N. Zamboglou, and D. Baltas. Influence of patient movement and anatomy alteration on the quality of 3D US-based prostate HDR brachytherapy treatment. *American Association of Physicists in Medicine*, 38(9):484–487, 2011.

[32] Kari Tanderup, Sam Beddar, Claus E Andersen, Gustavo Kertzscher, and Joanna E Cygler. In vivo dosimetry in brachytherapy. *International Journal of Medical Physics Research and Practice*, 40(7):070902, 2013.

[33] Wei Loong Jong, Jeannie Hsiu Ding Wong, Ngie Min Ung, Kwan Hoong Ng, Gwo Fuang Ho, Dean L. Cutajar, and Anatoly B. Rosenfeld. Characterization of MOSkin detector for in vivo skin dose measurement during megavoltage radiotherapy. *Journal of Applied Clinical Medical Physics*, 15(5):120–132, 2014.

[34] Peter J. Hoskin, Peter J. Bownes, Peter Ostler, Ken Walker, and Linda Bryant. High dose rate afterloading brachytherapy for prostate cancer: Catheter and gland movement between fractions. *Radiotherapy and Oncology*, 68(3):285–288, 2003.

[35] Valéry Olivier Zilio, Om Parkash Joneja, Youri Popowski, Anatoly Rosenfeld, and Rakesh Chawla. Absolute depth-dose-rate measurements for an 192Ir HDR brachytherapy source in water using MOSFET detectors. *International Journal of Medical Physics Research and Practice*, 33(6):1532–1539, 2006.

[36] G Knoll. *Radiation detection and measurement*. John Wiley & Sons, Ltd, United States of America, 3 edition, 2005.

[37] Ian Kwan, Bongsoo Lee, Wook Jae Yoo, Donghyun Cho, Kyoungwon Jang, Sanghun Shin, Martin Carolan, Michael Lerch, Vladimir Perevertaylo, Ian Kwan, Bongsoo Lee, Wook Jae Yoo, Donghyun Cho, Sanghun Shin, Martin Carolan, Michael Lerch, and Vladimir Perevertaylo. Comparison of the New MOSkin Detector and Fiber Optic Dosimetry System for Radiotherapy. *Journal of Nuclear Science and Technology*, 3131(February 2016):2–6, 2014.

[38] M. Garcia-Inza, S. Carbonetto, J. Lipovetzky, M. J. Carra, L. Sambuco Salomone, E. G. Redin, and A. Faigon. Switched bias differential MOSFET dosimeter. *IEEE Transactions on Nuclear Science*, 61(3):1407–1413, 2014.

[39] The MOSFET, 2006.

[40] S. O. Kasap. *Principles of Electronic Materials and Devices*. McGraw-Hill, New York, US, 3rd edition, 2006.

[41] Tony Enright. MOSKIN - MOSFET Dosimetry System. Number July. University of Wollongong, 2010.

[42] Ian S Kwan. *Characterization of the performance of the new MOSkin dosimeter as a quality assurance tool for pulsed dose-rate (PDR) prostate brachytherapy , and the effect of rectal heterogeneity on the dose delivered to the rectal wall*. PhD thesis, University of Wollongong, 2009.

[43] Zhen-yu Qi, Xiao-wu Deng, Shao-min Huang, Jie Lu, Michael Lerch, Dean Cutajar, and Anatoly Rosenfeld. Verification of the plan dosimetry for high dose rate brachytherapy using metal-oxide-semiconductor field effect transistor detectors. *International Journal of Medical Physics Research and Practice*, 34(6):2007–2013, 2007.

[44] Nicholas Hardcastle, Dean L Cutajar, Peter E Metcalfe, Michael L F Lerch, Vladimir L Perevertaylo, Wolfgang A Tomé, and Anatoly B Rosenfeld. In vivo real-time rectal wall dosimetry for prostate radiotherapy. *Physics in medicine and biology*, 55(13):3859–71, 2010.

[45] Sarah J Alnaghy, Shrikant Deshpande, Dean L Cutajar, Kemal Berk, Peter Metcalfe, and Anatoly B Rosenfeld. In vivo endorectal dosimetry of prostate tomotherapy using dual MO Skin detectors. *Journal of Applied Clincal Medical Physics*, 16(3):107–117, 2015.

[46] C. Tenconi, M. Carrara, M. Borroni, A. Cerrotta, D. Cutajar, M. Petasecca, M. Lerch, J. Bucci, G. Gambarini, E. Pignoli, and A. Rosenfeld. TRUS-probe integrated MOSkin detectors for rectal wall in vivo dosimetry in HDR brachytherapy: In phantom feasibility study. *Radiation Measurements Journal*, 71:379–383, 2014.

[47] Sarah Alnaghy. *In – vivo endorectal dosimetry of prostate high dose rate brachytherapy and TomoTherapy ® using MOSkinTM detectors*. PhD thesis, University of Wollongong, 2014.

[48] Ramaseshan Ramani, Stephen Russell, and Peter O'Brien. Clinical Dosimetry Using Mosfets. *International Journal of Radiation Oncology Biology Physics*, 37(4):959–964, 1997.

[49] TE Technology Inc. Peltier – Thermoelectric Cooler Modules, 2017.

[50] Larry a DeWerd, Geoffrey S Ibbott, Ali S Meigooni, Michael G Mitch, Mark J Rivard, Kurt E Stump, Bruce R Thomadsen, and Jack L M Venselaar. A dosimetric uncertainty analysis for photon-emitting brachytherapy sources: report of AAPM Task Group No. 138 and GEC-ESTRO. *International Journal of Medical Physics Research and Practice*, 38(2):782–801, 2011.

[51] Raelene Ann Nelligan. *Investigation into the Dosimetric Characteristics of MOSFETs for Use for In Vivo Dosimetry During External Beam Radiotherapy*. PhD thesis, University of Adelaide, 2009.

[52] R Nath, L L Anderson, J a Meli, a J Olch, J a Stitt, and J F Williamson. Code of practice for brachytherapy physics: report of the AAPM Radiation Therapy Committee Task Group No. 56. American Association of Physicists in Medicine. *International Journal of Medical Physics Research and Practice*, 24(10):1557–1598, 1997.

[53] Quality Control & Training Products for: Ultrasound Imaging Supertech. Prostate Ultrasound Training Phantom CIRS 053 Tissue Equivalent/Cryotherapy, 2016.

[54] Takashi Mizowaki and Marco Zaider. Functional Image Registration in Brachytherapy. In Adam P Dicker, G Merrick, Frank M Waterman, Leonard G

Gomella, and Richard K Valicenti, editors, *Basic and Advanced Techniques in Prostate Brachytherapy*, chapter 21, pages 304–318. Martin Dunitz Ltd., Taylor & Francis Group, Oxfordshire, UK, 1 edition, 2005.

[55] Andreas A Schoenfeld, Dietrich Harder, Björn Poppe, and Ndimofor Chofor. Water equivalent phantom materials for 192 Ir brachytherapy. *Physics in Medicine and Biology*, 60(24):9403–9420, 2015.

[56] Nikolai Hungr, Jean-Alexandre Long, Vincent Beix, and Jocelyne Troccaz. A realistic deformable prostate phantom for multimodal imaging and needle-insertion procedures. *American Association of Physicists in Medicine*, 39(4):2031–2041, 2012.

[57] Ryan Brown, Andrew Howie, Komiti Enari, Iliana Peters, Dean Cutajar, and Joseph Bucci. Implementation of a real-time prostate HDR brachytherapy system. In *26th Annual Scientific Meeting of the Australian Brachytherapy Group*, 2017.

[58] CIRS Inc. Tissue Equivalent Ultrasound Prostate Phantom Data Sheet [Model 053S, 053L & 053L-EF], 2013.

[59] Nicole Nesvacil, Kari Tanderup, Taran P. Hellebust, Astrid De Leeuw, Stefan Lang, Sandy Mohamed, Swamidas V. Jamema, Clare Anderson, Richard Pötter, and Christian Kirisits. A multicentre comparison of the dosimetric impact of inter- and intra-fractional anatomical variations in fractionated cervix cancer brachytherapy. *Radiotherapy and Oncology*, 107(1):20–25, 2013.

[60] Astrid A C De Leeuw, Marinus A. Moerland, Christel Nomden, Robert H A Tersteeg, Judith M. Roesink, and Ina M. Jurgenliemk-Schulz. Applicator reconstruction and applicator shifts in 3D MR-based PDR brachytherapy of cervical cancer. *Radiotherapy and Oncology*, 93(2):341–346, 2009.

[61] Felix Leborgne, Jack F. Fowler, Jose H. Leborgne, Eduardo Zubizarreta, and Rick Chappell. Biologically effective doses in medium dose rate brachytherapy of cancer of the cervix. *Radiation Oncology Investigations*, 5(6):289–299, 1997.

[62] Antony Palmer, David Bradley, and Andrew Nisbet. Physics-aspects of dose accuracy in high dose rate (HDR) brachytherapy: Source dosimetry, treatment planning, equipment performance and in vivo verification techniques. *Journal of Contemporary Brachytherapy*, 4(2):81–91, 2012.

[63] D Granero, J Pérez-Calatayud, E Casal, F Ballester, and J Venselaar. A dosimetric study on the Ir-192 high dose rate flexisource. *International Journal of Medical Physics Research and Practice*, 33(12):4578–4582, 2006.

[64] P Grimm, I Billiet, D Bostwick, a P Dicker, S Frank, J Immerzeel, M Keyes, P Kupelian, W R Lee, S Machtens, J Mayadev, B J Moran, G Merrick, J Millar, M Roach, R Stock, K Shinohara, M Scholz, E Weber, A Zietman, M Zelefsky, J Wong, S Wentworth, R Vera, and S Langley. Comparative analysis of

prostate-specific antigen free survival outcomes for patients with low, intermediate and high risk prostate cancer treatment by radical therapy. Results from the Prostate Cancer Results Study Group. *British Journal of Urology International*, 109 Suppl:22–29, 2012.

[65] Computerized Imaging Reference Inc. Systems. Tissue Equivalent Prostate Phantom: Model 053S, 053L & 053L-EF, 2016.

[66] Felix Leborgne and Jack Fowler. Late Outcomes Following Hypofractionated Conformal Radiotherapy vs. Standard Fractionation for Localized Prostate Cancer: A Nonrandomized Contemporary Comparison. *International Journal of Radiation Oncology Biology Physics*, 74(5):1441–1446, 2009.

[67] Marion Essers and Ben J. Mijnheer. In vivo dosimetry during external photon beam radiotherapy. *International Journal of Radiation Oncology Biology Physics*, 43(2):245–259, 1999.

[68] M.J. Berger, J.S. Coursey, M.A. Zucker, and J. Chang. Composition of Tissue, Soft (ICRU Four Component), 2005.

[69] May Whitaker, George Hruby, Aimee Lovett, and Nitya Patanjali. Prostate HDR brachytherapy catheter displacement between planning and treatment delivery. *Radiotherapy and Oncology*, 101(3):490–494, 2011.

[70] P. Metcalfe, P., Kron, T. and Hoban. *The Physics of Radiotherapy, X-Rays and Electrons*. Medical Physics Publishing, Madision, Wisconson, 1 edition, 2007.

[71] Erin L. Seymour, Simon J. Downes, Gerald B. Fogarty, Michael a. Izard, and Peter Metcalfe. In vivo real-time dosimetric verification in high dose rate prostate brachytherapy. *International Journal of Medical Physics Research and Practice*, 38(8):4785, 2011.

[72] Anna M. Dinkla, Bradley R. Pieters, Kees Koedooder, Philip Meijnen, Niek Van Wieringen, Rob Van Der Laarse, Johan N. Van Der Grient, Coen R N Rasch, and Arjan Bel. Deviations from the planned dose during 48 hours of stepping source prostate brachytherapy caused by anatomical variations. *Radiotherapy and Oncology*, 107(1):106–111, 2013.

[73] G. Gambarini, M. Carrara, C. Tenconi, N. Mantaut, M. Borroni, D. Cutajar, M. Petasecca, I. Fuduli, M. Lerch, E. Pignoli, and A. Rosenfeld. Online in vivo dosimetry in high dose rate prostate brchytherapy with MOSkin detectors: In phantom feasibility study. *Applied Radiation and Isotopes*, 83:222–226, 2014.

[74] B. J. Van Zeghbroeck. The MOSFET - Introduction, 2011.

[75] P J Hoskin and A Rembowska. Dosimetry Rules for Brachytherapy Using High Dose Rate Remote Afterloading Implants. *Clinical Oncology*, 10:226–230, 1998.

[76] I. Chow Hsu, Kyounghwa Bae, Katsuto Shinohara, Jean Pouliot, James Purdy, Geoffrey Ibbott, Joycelyn Speight, Eric Vigneault, Robert Ivker, and Howard Sandler. Phase II trial of combined high-dose-rate brachytherapy and external beam radiotherapy for adenocarcinoma of the prostate: Preliminary results of RTOG 0321. *International Journal of Radiation Oncology Biology Physics*, 78(3):751–758, 2010.

[77] Facundo Ballester, Åsa Carlsson Tedgren, Domingo Granero, Annette Haworth, Firas Mourtada, Gabriel Paiva Fonseca, Kyveli Zourari, Panagiotis Papagiannis, Mark J. Rivard, Frank-André Siebert, Ron S. Sloboda, Ryan L. Smith, Rowan M. Thomson, Frank Verhaegen, Javier Vijande, Yunzhi Ma, and Luc Beaulieu. A generic high-dose rate 192Ir brachytherapy source for evaluation of model-based dose calculations beyond the TG-43 formalism. *International Journal of Medical Physics Research and Practice*, 42(6):3048–3062, 2015.

[78] I. S. Kwan, A. B. Rosenfeld, Z. Y. Qi, D. Wilkinson, M. L F Lerch, D. L. Cutajar, M. Safavi-Naeni, M. Butson, J. A. Bucci, Y. Chin, and V. L. Perevertaylo. Skin dosimetry with new MOSFET detectors. *Radiation Measurements*, 43(2-6):929–932, 2008.

[79] Alvaro A Martinez, Jeffrey Demanes, Carlos Vargas, Lionel Schour, Michel Ghilezan, and Gary S Gustafson. High-Dose-Rate Prostate Brachytherapy An Excellent Accelerated-Hypofractionated Treatment for Favorable Prostate Cancer. *American Journal of Clinical Oncology*, 33(5):481–488, 2010.

[80] International Commission on Radiological Protection. Adult Reference Computational Phantoms. *International Commission on Radiological Protection Publication*, 39(2):48–51, 2009.

[81] Prabhjot Juneja, Andrew Kneebone, Jeremy T Booth, David I Thwaites, Ramandeep Kaur, Emma Colvill, Jin A Ng, Paul J Keall, and Thomas Eade. Prostate motion during radiotherapy of prostate cancer patients with and without application of a hydrogel spacer : a comparative study. *Radiation Oncology*, 10(215):1–7, 2015.

[82] T Cheung, Martin J Butson, and P K N Yu. Energy dependence corrections to MOSFET dosimetric sensitivity. *Australasian Physical and Engineering Sciences in Medicine*, 32(1):16–20, 2009.

[83] Alex F Bielajew. Fundamentals of Radiation Dosimetry and Radiological Physics. page 131, 2005.

[84] T P Loftus. Standardization of Iridium-192 Gamma-Ray Sources in Terms of Exposure. *Jounral of Research of the Bureau of Standards*, 85(1):19–25, 1980.

[85] A.A. Martinez, I. Pataki, G. Edmundson, E. Sebastian, D. Brabbins, and G. Gustafson. Phase II Prospective Study of the Use of Conformal High-Dose-Rate Brachytherapy as Monotherapy for the Treatment of Favorable Stage

Prostate Cancer: A Feasibility Report. *International Journal of Radiation Oncology Biology Physics*, 49(1):61–69, 2001.

[86] Aswin L Hoffmann and Alan E Nahum. Fractionation in normal tissues: the (α/β) concept can account for dose heterogeneity and volume effects. *Physics in medicine and biology*, 58(19):6897–6914, 2013.

[87] Richard Shaffer, Tom Pickles, Richard Lee, and Vitali Moiseenko. Deriving prostate alpha-beta ratio using carefully matched groups, long follow-up and the phoenix definition of biochemical failure. *International Journal of Radiation Oncology Biology Physics*, 79(4):1029–1036, 2011.

[88] Cancer Research UK. Internal Radiotherapy (Brachytherapy) for Prostate Cancer, 2014.

[89] G. Gambarini, M. Carrara, C. Tenconi, N. Mantaut, M. Borroni, D. Cutajar, M. Petasecca, I. Fuduli, M. Lerch, E. Pignoli, and A. Rosenfeld. Online in vivo dosimetry in high dose rate prostate brchytherapy with MOSkin detectors: In phantom feasibility study. *Applied Radiation and Isotopes*, 83(2014):222–226, 2014.

[90] Carlos Bravo-Miranda, Amanda Burg Rech, Harley Francisco Oliveira, Edenyse Bertucci, Teodoro Cordova-Fraga, and Oswaldo Baffa. Measurement of rectum dose by in vivo alanine/ESR dosimetry in gynecological 192Ir HDR brachytherapy. *Radiation Measurements Journal*, 75:45–52, 2015.

[91] Tom Brett. Prostate Specific Antigen. *Australian Family Physician*, 40(7):497–500, 2011.

[92] A B Rosenfeld. Mosfet dosimetry on modern radiation oncology modalities. *Solid State Dosimetry, Pts 1 and 2, Proceedings*, 101:A393–A398, 2002.

[93] Mark J Rivard, Wayne M Butler, Larry a DeWerd, M Saiful Huq, Geoffrey S Ibbott, Ali S Meigooni, Christopher S Melhus, Michael G Mitch, Ravinder Nath, and Jeffrey F Williamson. Supplement to the 2004 update of the AAPM Task Group No. 43 Report. *International Journal of Medical Physics Research and Practice*, 34(6):2187–2205, 2007.

[94] RV Griffith. Polyurethane as a base for a family of tissue equivalent materials. In International Radiation Protection Assosiation, editor, *Radiation Protection : A Systematic Approach To Safety*, pages 380–383. Pergamon Press, Oxford, UK, 1st edition, 1980.

[95] Jack F Fowler. The radiobiology of prostate cancer including new aspects of fractionated radiotherapy. *Acta oncologica (Stockholm, Sweden)*, 44(3):265–276, 2005.

[96] Georgios Koukourakis, Nikolaos Kelekis, Vassilios Armonis, and Vassilios Kouloulias. Review Article Brachytherapy for Prostate Cancer : A Systematic Review. *Advances in Urology*, 2009:11, 2009.

[97] Gustavo Kertzscher, Claus E. Andersen, and Kari Tanderup. Adaptive error detection for HDR/PDR brachytherapy: Guidance for decision making during real-time in vivo point dosimetry. *International Journal of Medical Physics Research and Practice*, 41(5):052102, 2014.

[98] T Hijal, A A Al Hamad, T Niazi, K Sultanem, B Bahoric, T Vuong, and T Muanza. Hypofractionated radiotherapy and adjuvant chemotherapy do not increase radiation-induced dermatitis in breast cancer patients. *Current Oncology*, 17(5):22–27, 2010.

[99] Koh Ichi Sakata, Hisayasu Nagakura, Atushi Oouchi, Masanori Someya, Kensei Nakata, Mitsuo Shido, Kazumitsu Koito, Satoru Sagae, Ryuichi Kudo, and Masato Hareyama. High-dose-rate intracavitary brachytherapy: Results of analyses of late rectal complications. *International Journal of Radiation Oncology Biology Physics*, 54(5):1369–1376, 2002.

Chapter 7

Appendix

7.1 Additional Data from OneTouch Characterisation

During the OneTouch characterisation experiments the five available algorithms were tested in an open air experiment set-up over five irradiations. The detectors were irradiated for 10 second source dwell time at a distance of 10±1mm, with results shown below as readout by the new readout system.

Compensation Algorithm	Test 1 (mV)	Test 2 (mV)	Test 3 (mV)	Test 4 (mV)	Test 5 (mV)
Standard	220.42	216.69	218	218.83	212.67
Average2	212.92	223.96	226.52	227.33	228.3
Min2	276.1	286.46	271.24	284.12	276.17
Median3	273.15	280.72	283.62	279.25	276.15
Median4	285.26	262.79	283.75	276.56	278.73

Table 7.1: Results from Anti-Annealing Algorithm Tests Completed in Open Air with MO*Skin*$^{\text{TM}}$ Detectors Irradiated at a 10 Second Dwell Time

A single MO*Skin*$^{\text{TM}}$ detector was irradiated three times for the four creep-compensation algorithms, as Standard and Min2 used the same calculation. In a solid water phantom the threshold voltage difference was a 60 second irradiation was analysed and the dose was calculated, with results shown below.

Compensation Algorithm	Test One		Test Two		Test Three	
	Threshold Difference (mV)	Dose (cGy)	Threshold Difference (mV)	Dose (cGy)	Threshold Difference (mV)	Dose (cGy)
Standard	140.6	60.9	139.0	60.6	138.2	60.1
Average2	136.6	59.6	139.2	60.4	139.1	60.3
Median3	139.4	59.2	135.9	60.3	138.4	59.9
Median4	135.9	59.4	134.8	59.81	135.6	59.8

Table 7.2: Results from Anti-Annealing Algorithm Tests Completed in Solid Water Phantom with MO*Skin*™ Detectors Irradiated at a 60 Second Dwell Time

The figure 7.1 to figure 7.7 the response of a MO*Skin*™ using the OneTouch Readout System was analysed during at temperatures to characterise the temperature composition feature. The detector was irradiated at initial room temperature 19°, increasing temperature to 40°, at 40.4°, at 36.5° or body tempertaure, at 29.8°, at 24.4° and at final room temperature or 18.4°.

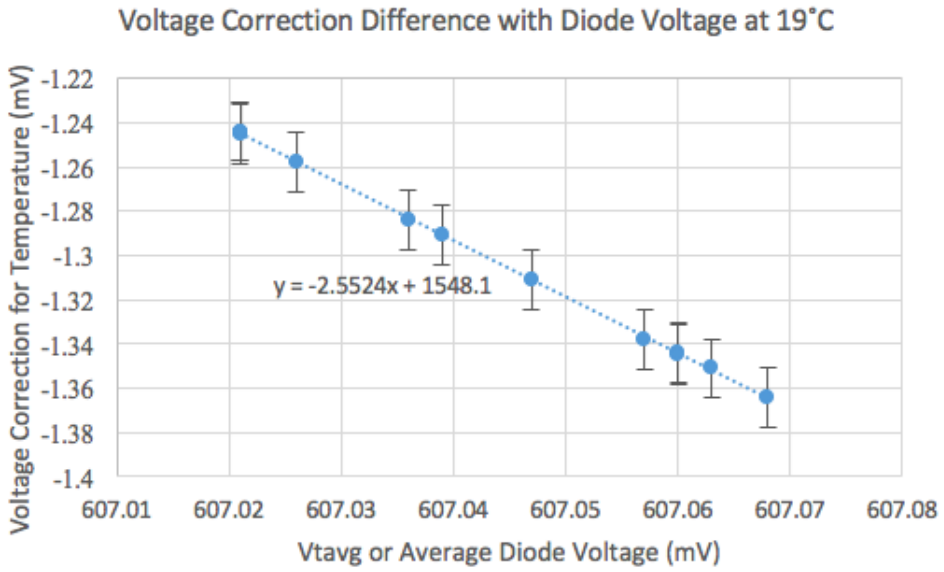

Figure 7.1: Voltage from Temperature Change Only and Diode Voltage During an Irradiation at Initial Room Temperature or 19°

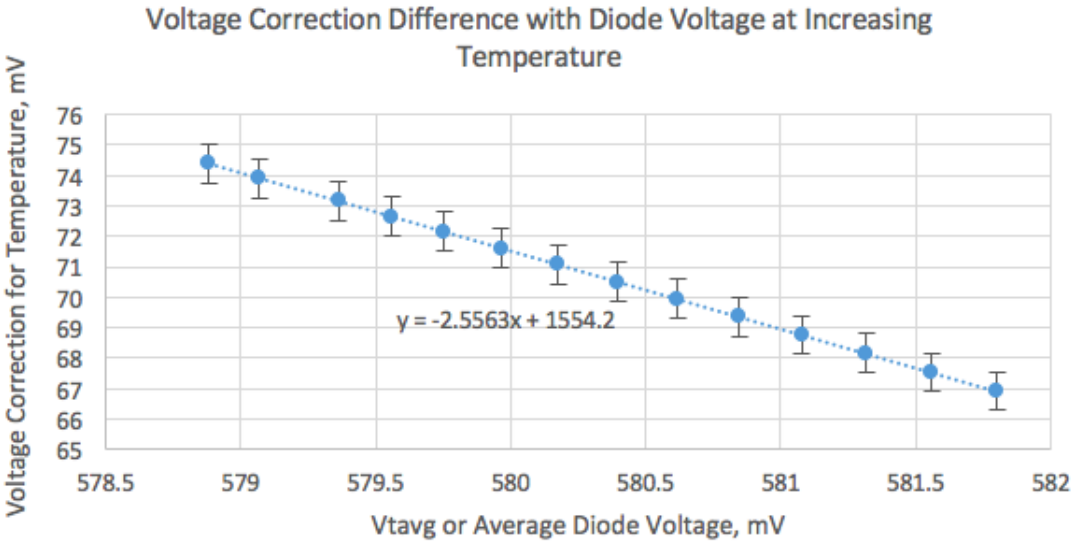

Figure 7.2: Voltage from Temperature Change Only and Diode Voltage During an Irradiation a with Gradual Increasing Temperature

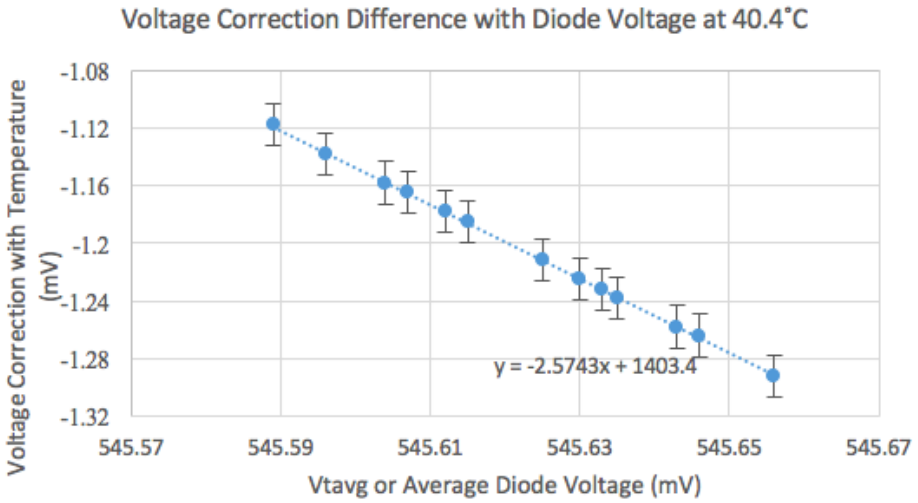

Figure 7.3: Voltage from Temperature Change Only and Diode Voltage During an Irradiation at 40.4°C

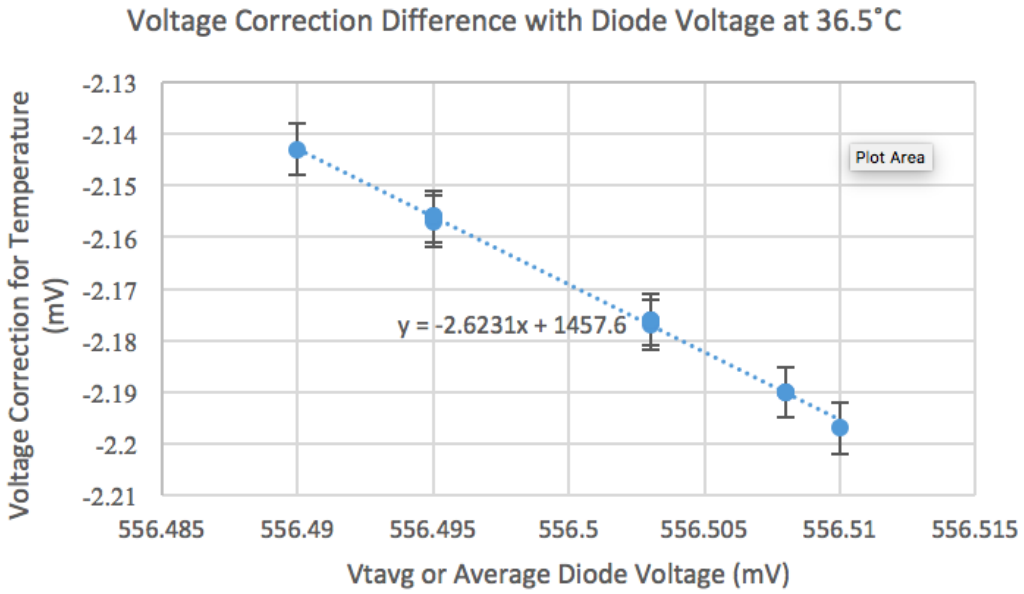

Figure 7.4: Voltage from Temperature Change Only and Diode Voltage During an Irradiation at 35.6°

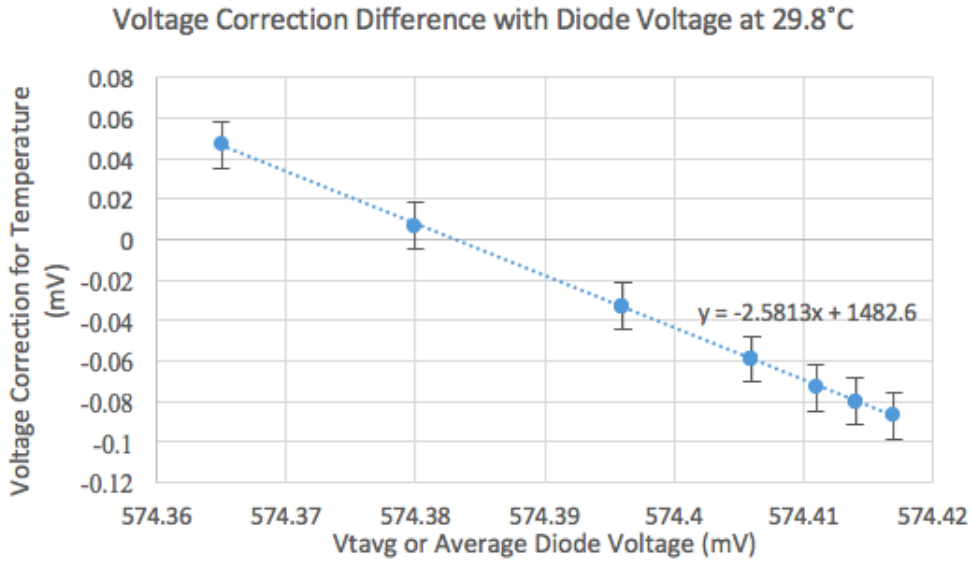

Figure 7.5: Voltage from Temperature Change Only and Diode Voltage During an Irradiation 29.8°

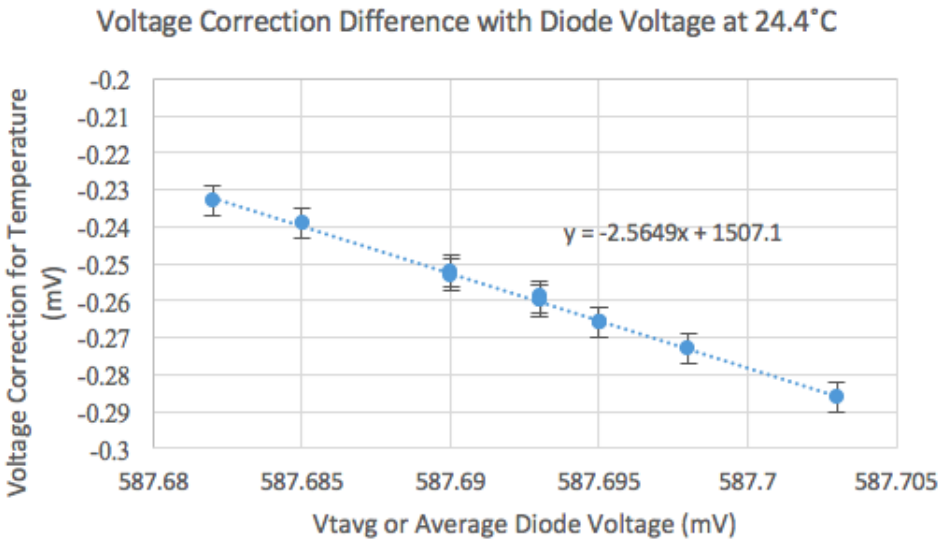

Figure 7.6: Voltage from Temperature Change Only and Diode Voltage During an Irradiation at 24.4°

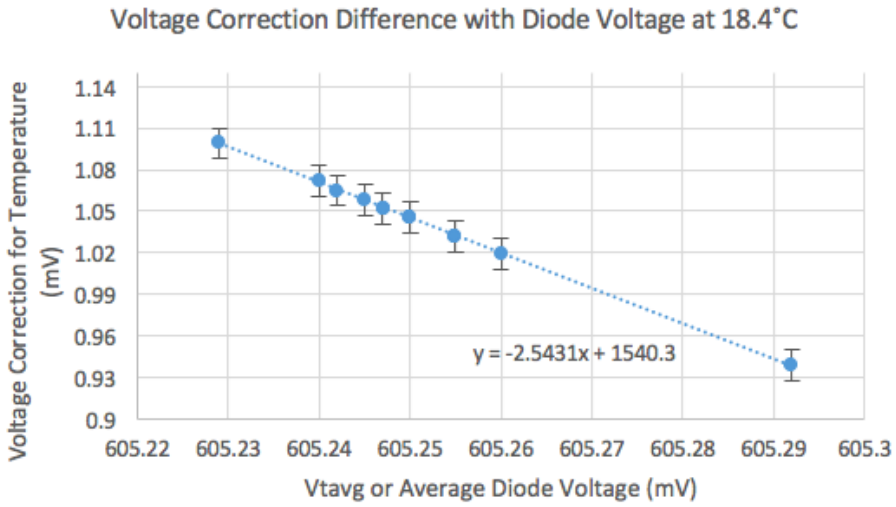

Figure 7.7: Voltage from Temperature Change Only and Diode Voltage During an Irradiation at Finial Room Temperature or 18.4°